INSTITUTE OF AEROPHYSICS

UNIVERSITY OF TORONTO

DRAG MEASUREMENTS ON CIRCULAR CYLINDERS AND SPHERES IN THE TRANSITION REGIME AT A MACH NUMBER OF 2

by

A. K. Sreekanth

APRIL, 1961

UTIA REPORT NO. 74
ARL - 53

DRAG MEASUREMENTS ON CIRCULAR CYLINDERS AND SPHERES IN THE TRANSITION REGIME AT A MACH NUMBER OF 2

by

A. K. Sreekanth

APRIL, 1961

UTIA REPORT NO. 74
ARL - 53

ACKNOWLEDGEMENTS

The author wishes to express his sincere gratitude to Dr. G. N. Patterson, for having given him the opportunity to do graduate work at the Institute of Aerophysics under his guidance and for his steady interest and encouragement during the course of this work.

The author is indebted to Dr. J. H. deLeeuw for his friendly interest in the reported work and his valuable advice.

Thanks also go to Mr. B. G. Dawson of the Institute's Shop Staff for making the probes and models used in this investigation.

The co-operation of the low density group at the Institute of Engineering Research, University of California (Berkeley) who furnished the design for the drag balance used is gratefully acknowledged.

This investigation was made possible through the financial assistance rendered by the Wright Air Development Division, United States Air Force (Contract AF 33(616)-6990) and the Defence Research Board of Canada.

SUMMARY

Measurements of the drag of circular cylinders placed transverse to the flow and spheres at a Mach number of 2 in air were obtained in the UTIA low density wind tunnel. The mean free path of the air in the test flow was 0.049" and the model sizes were such that Knudsen numbers in the range 0.2 to 6 for the cylinders and 0.1 to 0.8 for the spheres were covered.

The drag coefficient of circular cylinders calculated from the measured forces was found to increase with increasing Knudsen number and to reach a value of 3.02 at Kn = 3. There was no apparent increase as the Knudsen number was further increased. In contrast, the theoretical value for free molecule flow conditions is 3.7 if completely diffuse reflection and complete temperature accommodation are assumed and 3.35 if complete specular reflection occurs. This shows that at a Knudsen number of approximately 5 the drag coefficient is still significantly lower than the free molecule flow value. On the other hand the experimental results on sphere drag in the same flow indicate that the theory and experiment are essentially in agreement. It is suggested that the discrepancy between the theoretical and measured values for the case of circular cylinders is associated with the fact that in this case not all dimensions are smaller than the mean free path. This contention was supported by additional experiments conducted in subsonic flow; pressure readings taken by means of an orifice on the side of a cylinder normal to the flow proved to be dependent on the cylinder's length. From these findings it was concluded that the validity of the conventional assumption that the free molecule flow conditions should be applicable at a Knudsen number of approximately 5 is in doubt for the case of cylinders transverse to the flow.

TABLE OF CONTENTS

NOTATION

A	projected area of cylinder or sphere
c_1, c_2	constants in the Sutherland's formula (see Appendix D).
C_D	drag coefficient = $\frac{\text{drag force}}{\frac{1}{2} \rho V^2 A}$
D	drag force
K	a factor which accounts for interference and end effects
Kn	Knudsen number
l	length of cylinder model
M	mach number
p	static pressure
p_o	stagnation pressure
$p'_{o\,meas.}$	measured impact pressure
$p'_{o\,ideal}$	impact pressure in the absence of viscous effects
R	Gas constant
Re	Reynolds number
T_o	stagnation temperature
T_1	free-stream temperature
V	free-stream velocity
w	force per unit length on the cylinder model.
W	force on the supporting sting
x_1, y_1, y_2	lever arm lengths
γ	ratio of specific heats
λ	mean free path

ρ	density
μ	viscosity

I. INTRODUCTION

Interest in the field of high-speed, high-altitude aerodynamics has increased in recent years with the advent of missiles and satellites. In order to fully understand the flow phenomena occuring at the high altitudes one has to resort to either the kinetic theory of gases or continuum fluid mechanics, depending upon the degree of rarefaction of the gas medium in which the vehicle is moving. The basic parameter that indicates the degree of rarefaction of a gas is the Knudsen number, Kn, defined as

$$Kn = \frac{\lambda}{L}$$

where λ is the molecular mean free path (i.e., the average distance traversed by molecules between collisions) and L is some significant dimension in the flow field. The Knudsen number can also be expressed in terms of the Mach number, M and the Reynolds number, Re (the two basic parameters used in continuum mechanics) by the relation

$$Kn = 1.26\sqrt{\gamma}\,\frac{M}{Re} \qquad (\gamma = \text{ratio of specific heats})$$

where both Kn and Re are based on the same characteristic length.

Gasdynamics can be divided roughly in to the following regimes according to the degree of rarefaction measured by the Knudsen number based on the free stream value of λ and a characteristic body length

Continuum flow	$Kn < 0.01$
Slip flow	$0.01 < Kn < 0.1$
Transition flow	$0.1 < Kn < 5$
Free molecule flow	$Kn > 5$

However, this rough division is no longer considered adequate at hypersonic speeds or in cases where there exists a large temperature difference between the adiabatic body temperature and actual body temperature. It has been found that at such conditions the local value of the mean free path, rather than the free-stream value, must be used for determining the Knudsen number and classifying the flow. At speeds with a Mach number smaller than 5, on the other hand, the classification given proves quite useful.

The analyses of transition and free molecule flows are based on the kinetic theory of gases, whereas the continuum and slip flows are characterized by the Navier-Stokes equations of motion with the appropriate

boundary conditions, dervived essentially on the basis of continuum fluid mechanics.

In free molecule flow (Kn > 5) collisions between molecules themselves can be neglected compared to the collisions between gas particles and the body. In such a case the fluxes of incident and reflected streams of molecules may be treated separately. This allows the incident molecules to have a Maxwellian (equilibrium) velocity distribution, and the transport of mass, momentum, and energy is governed only by the molecule-surface interaction.

In the transition regime in which the mean free path is of the same order of magnitude as the characteristic body dimension , both inter-molecular collisions and molecule-surface interactions must be considered and the flow is quite complicated. Except for very limited theoretical work, the knowledge of the flow in the transition region is in the form of empirical or semi-empirical relations. From a practical standpoint, the accurate knowledge or the determination of the aerodynamic forces on bodies of various geometric shapes placed in a low density flow is of utmost importance. Extensive experimental work especially in the slip flow regime has been done by the low density research group at the University of California (Ref. 1 and 2).

The first experimental work on force measurements in a high speed free molecule flow was done by Stalder and his co-workers (Ref. 3) who measured the drag of a circular cylinder transverse to the gas stream in free molecule flow. Apart from this, as far as the author is aware, no experimental work on the force measurements in free molecule or near-free molecule flows have been reported to this date.

Recently Baker and Char wat (Ref. 4) have theoretically investigated the transitional drag of a sphere in a near-free molecule flow. In their analyses they neglect the thermal motion of the molecules in relation to the mass motion and their results are therefore strictly valid only for very high flow speeds (M > 10). The present measurements of drag forces on circular cylinders and spheres were undertaken because of the very limited theoretical approaches and complete absence of experimental work in near-free molecule flow. All the experiments were performed in a Mach 2 flow of air.

II. EXPERIMENTAL APPARATUS

1. Low Density Wind Tunnel

The experiments were performed in the UTIA low density wind tunnel, a complete description of which including its instrumentation is given in Ref. 5. The tunnel is of the continuous, open circuit type with a vacuum pump drive designed to operate at Mach numbers up to 5, over a

static pressure range from 1 to 70 microns Hg. A side view of the tunnel is shown in Plate 1.

An axially symmetric open jet nozzle designed to give a Mach number of 2 at a static pressure of about 20 microns Hg was used in the present experiments. Details of the performance and the characteristics of the Mach 2 nozzle can be found in Ref. 5. The nozzle has an exit diameter of 5.82" but the uniform core of Mach 2 flow was only 1" in diameter at the center of the nozzle, the remaining portion of the jet being filled with boundary layer.

Atmospheric air passes through a dryer in to a needle valve which is used to regulate the mass flow rate by throttling the air down to low pressure before it enters the stagnation chamber of the tunnel. In this chamber any desired value of stagnation temperature up to 150°F could be set by means of a heated liner. A series of six booster pumps on the downstream side of the nozzle maintain a continuous flow of air through the test section. A butterfly -type flap on one of the booster pumps allows fine control of the test chamber static pressure by changing the pumping speed slightly. The desired flow conditions are set by proper manipulation of both the needle valve and the pumping speed.

2. Force Balance

A single component microbalance similar to one designed by Latz (Ref. 6) with slight modifications was used. Schematic diagrams of the balance are given in Figs. 1 and 2, and a photograph is shown in Plate 2. It is a remote control, beam-type, null balance with crossed flexural pivots. The flexure pivots consist of two pairs of crossed wires rigidly attached to two jaws. The upper jaw is fastened to a base plate and the lower is free to rotate about a flexural point. A $\frac{1}{4}$" diameter brass shaft is attached to the lower jaw and is passed through holes cut in the base plate and the upper jaw. A small platform of about 1" x 3/4" size with two pins for positioning the base that supports the model is attached to the top of the brass rod. A beam is attached to the lower jaw. The core of a LVDT (linear variable differential transformer) is attached to one end of the beam and serves to detect deviations from the null position; a helical quartz spring is attached to the other end. The other attachment point of this spring can be moved by means of a motor-driven lead screw. The extension of the spring is indicated by a Veeder-Root counter.

Referring to the Fig. 2 application of a force on the model in the flow direction will produce a counter-clockwise moment on the flexure pivots. This moment will cause the lower jaw to rotate. The resulting displacement of the core of the LVDT from its initial position will change the circuit current which is indicated by a galvanometer, see the circuit diagram in Fig. 3. Null balancing is achieved by extending the quartz spring until the galvanometer again indicates the null position.

The spring extension is a measure of the spring force, and the actual force on the model is determined by the spring constant and lever arm lengths. For the purpose of determining the constant of the spring, a weight pan is attached to the beam.

For damping the oscillations of the balance suspension, an aluminum vane is attached to the lower jaw and is made to move in a magnetic field produced by two horseshoe shaped Alinco permanent magnets. The damping factor is varied by simply changing the distance of the magnets to the vane.

The balance is designed to measure a force accurate to 0.1 mg. and has an angular null sensitivity of 0.001 degrees rotation.

3. Models

a) Cylinder Models

A sketch of the models used to determine the drag of the cylinder is shown in Fig. 4. Stainless-steel hypodermic tubing was used for making these models. The diameters of the cylinders tested varied between 0.008" and 0.180". Since the uniform core of the Mach 2 flow in the jet was only 1" in diameter, the maximum length of the cylinders were restricted to about 0.8". The core of the cylinder was filled with solf solder.

b) Sphere Models

Brass and steel bearing balls were used as models in the sphere drag experiments. Two types of models were tested. They differ in the manner in which they are supported. (see Fig. 5). A small hole was drilled in the sphere and it was attached to the model support by a push fit. The sphere support piece consisted of a fine, tapered sewing needle. The diameters of the spheres tested varied between 1/16" and 7/16". The sizes of the spheres and support rods are given in Table I.

For the case of the 1/16" diameter models, the spheres used were steel bearing balls and these were welded on to the supporting rod. The spheres were separated from their supporting rods for the purpose of determining the tare drag by just breaking the weld.

A photograph of typical cylinder and sphere models is shown in Plate. 3.

c) Shields

As mentioned previously the diameter of the uniform Mach 2 core was only about an inch, the remaining portion of the nozzle being

filled with boundary layer. The model which was about 0.8" in length has to be supported by a rod from the balance. Since the exit diameter of the nozzle is 5.82", the model requires a supporting rod with a minimum length of 2.91" or 2.51" depending whether it is exposed to the flow horizontally and supported from behind or vertically and supported at one end. Under these conditions the force on the supporting sting will be many times that on the model itself. One method to minimize the support force, by making it extremely thin, could not be used as there were some vibrations present in the tunnel introduced by the pumping units.

In order to know the force on the model, the force on the supporting sting has to be subtracted from the total force. Even a slight experimental scatter in the total measured forces on the model and its support may then appear as a large error in the force on the model itself. To improve this situation,use of a shield for the supporting sting as another method of minimizing the support force has been made. Care then has to be taken to ensure that the shield has no interference effect on the model. Extensive experiments were conducted to determine the best position of the shield with respect to the model to minimize interference effects. The effect of the shield on the flow is discussed in Section III, 4, and also in Appendix A. The dimensions of the shield used are shown in Fig. 6.

d) Pressure Probe

The dimensions of the pressure probe that was used in subsonic flow to determine the effect of the length of the probe on the pressure readings is given in Fig. 7. It was mounted transverse to the flow on a specially designed rotating mechanism by means of which the angular position of the orifice with respect to the mass flow direction could be varied. The pressures were recorded by a thermistor gauge, which is described in detail in Ref. 10.

III. DESCRIPTION OF EXPERIMENTS

1. Flow Calibration

All the cylinder and sphere drag measurements were done in a Mach 2 air flow. The nozzle that provided this flow is designed to operate at a stagnation pressure of 156.6 microns Hg and a test chamber static pressure of 20 microns Hg. An impact probe of 0.184" dia. with 10^{o} external chamfer was used to calibrate the flow. The calibrations were performed with the drag models removed from the balance but leaving the shield in the flow. First the stagnation pressure was set at the designed value by means of the air inlet valve. The test chamber pressure was set at the design value of 20 microns Hg by manipulating the booster pump valves. The impact probe readings were taken on the nozzle center line at the nozzle exit and 3/4" downstream. The pressure in the test

chamber was varied slightly by changing the pumping speed of one of the booster pumps by means of a flap until the difference in impact probe readings at these two positions was less than $\frac{1}{2}$ percent. The absence of fluctuations in these impact pressure readings with time and the constancy of pressure reading at all point along the nozzle centerline for a distance of 3/4" from the nozzle exit indicated that the jet was smooth and well balanced and that there were no axial gradients in the flow field at the center of the jet. A mercury McLeod gauge was used to measure the impact and stagnation pressures. To get continuous readings, a thermistor gauge was connected to the impact probe while balancing the jet and checking for fluctuations in the flow. Pressure probe traverses were made along the nozzle centerline and across the jet at distances of $\frac{1}{4}$" and $\frac{1}{2}$" from nozzle exit.

At the very low Reynolds numbers of the flow at which these experiments were done the measured impact pressures ($p'_{o\ meas.}$) depart radically from the ideal values owing to viscous effects. The viscous correction to the measured pressure can be expressed in the following form.

Supersonic flow: $\dfrac{p'_{o\ ideal}}{p'_{o\ meas.}}$ = f (Mach No., Reynolds No. based on probe diameter, and probe shape).

Subsonic flow: $\dfrac{p'_{o\ meas.} - p'_{o\ ideal}}{\frac{1}{2}\rho V^2}$ = f (Mach No., Reynolds No., and probe shape)

where ρ and V are free stream density and velocity respectively.

The relation between the impact pressure and stagnation pressure (p_o) in a supersonic isentropic flow is given by

$$\frac{p'_{o\ ideal}}{p_o} = \left[\frac{(\gamma+1)M^2}{2+(\gamma-1)M^2}\right]^{\frac{\gamma}{\gamma-1}} \left[\frac{\gamma+1}{2\gamma M^2-(\gamma-1)}\right]^{\frac{1}{\gamma-1}}$$

$p'_{o\ ideal}$ was calculated from measured impact pressure by using the viscous correction chart given in Ref. 7. The centerline Mach number was calculated by the ratio of $p'_{o\ ideal}$ to p_o assuming isentropic flow, which is appropriate because the presence of a uniform core is indicated by the measurements. As the true Mach number and the Reynolds number are both unknown, an iterative procedure was applied, starting by assuming the viscous correction to be zero and using successively more accurate values of M and Re until convergence was obtained. From

the calculated Mach number and the value of $p'_{o\,ideal}$, the static pressure (p) at the point on the centerline was determined by the Rayleigh supersonic pitot formula

$$\frac{p'_{o\,ideal}}{p} = \left[\frac{\gamma+1}{2} M^2\right]^{\frac{\gamma}{\gamma-1}} \left[\frac{\gamma+1}{2\gamma M^2-(\gamma-1)}\right]^{\frac{1}{\gamma-1}}$$

This calculated static pressure was used to provide a check on the calculated values of M by comparing it with the wall tap pressure near the nozzle exit. These two pressures agreed within a fraction of a micron of Hg. From this it was inferred that the static pressure across the jet was essentially constant and the evaluation of the Mach number for points away from the centerline, for which the isentropic relation to the stagnation conditions is no longer valid owing to the viscous effects, is based on the ratio of impact pressure and the constant static pressure. The viscous effect on the probe readings was again eliminated by an iterative procedure. The Mach number profile across the jet at a station $\frac{1}{4}$" from the nozzle exit plane is shown in Fig. 8.

In all the drag force tests the center of the model was placed $\frac{1}{4}$" downstream from the nozzle exit. As there were no axial gradients in the flow for a distance of 3/4" from nozzle exit, the whole model was subjected to the same flow conditions. A complete calibration of the flow field was done periodically but the centerline Mach number at $\frac{1}{4}$" from nozzle exit was checked before the start and at the end of each experiment. During the drag force measurements the maintainence of the calibrated flow was checked by measuring the stagnation, wall tap static, and test chamber pressures.

2. Alignment of Balance and Model

It was necessary to determine the plane of motion allowed by the balance suspension. To do this, a long pointer was attached to the suspension which was then allowed to oscillate. The tip of the pointer thus described a line in the plane of oscillation. The orientation of this line was then marked on the balance base plate. This line was further checked by optical means. When the optical axis of a telescope was exactly aligned with the plane of motion there was no apparent lateral movement of the image of the pointer with respect to the telescope cross-hair. Having located the plane of motion it was then possible to check the correspondence with the line previously drawn on the base plate. It was concluded from observations that the deviation of the line marked on the balance from being parallel to the plane of oscillation of the model suspension was within $\pm$ 0.2°.

The balance was placed on a circular turntable inside the tunnel test section. The model to be tested was put on the balance and was rigidly attached to it by means of a special spring clip. The position of the model and the balance with respect to the nozzle was set approximately to the desired position by eye. A circular steel plate $6\frac{1}{2}$" diameter and

3/16" thick having a 4" long, $\frac{1}{4}$" square steel bar attached to it at its center and perpendicular to it was held tightly against the nozzle exit. The steel bar was found to be perpendicular to its base within 1/10 of a degree. For the final adjustment, the balance was then rotated by means of the turntable until the line marked on the balance was set parallel to the steel bar. It was estimated that the force measuring direction of the balance was parallel within $\frac{1}{2}$ degree to the nozzle centerline (i.e., the direction of mass flow) thereby ensuring that the balance was measuring the drag force. This drag force position was double-checked by rotating the turntable and measuring the force on a model set vertical to the flow direction. The measured force was quite symmetrical about this position, decreasing in either direction of rotation. These measurements indicated that the balance was aligned to the flow direction within 0.5 degrees.

A mirror having two thin crossed lines marked on it was held tight against the nozzle exit so that one of the lines was horizontal and passed through the center of the nozzle. The cylinder model was aligned with the help of this mirror so that it was horizontal and normal to the flow direction. For the case of spheres, the center of the sphere was set at the center of the jet.

The lever arm lengths of the suspension system were measured by means of an optical comparator and a cathetometer before the balance was put in the tunnel.

After having aligned the balance and the model, the sensitivity of the balance was adjusted. This was done by moving the vertical counter weight (see Fig. 2) until placing a weight of $\approx$ 2 mg. in the weight pan produced a galvanometer deflection of 6 divisions from its null position. This corresponded to a force of less than 0.1 mg on the model for one galvanometer division deflection from its null position, i.e. the balance was able to sense a force difference of 0.1 mg on the model.

3. Static Calibration of the Balance

Having adjusted the sensitivity of the balance, the galvanometer needle was set at zero by means of the helipot connected in the LVDT circuit. The reading of the Veeder-root indicator which was connected to the quartz spring actuating mechanism was recorded. A known weight was placed in the calibrating pan. The quartz spring was elongated until the galvanometer indicated the zero position. The extension of the spring as indicated by the Veeder-root counter was noted. The weight was then removed and the tension on the quartz spring was released until the galvanometer came back to the original position. The reading of the counter was checked against the initially recorded reading. In most cases the initial and final readings were the same but in few cases they differed slightly. This might have been due to the hysteresis effect in flexures and possible backlash in the gear mechanism. The calibration was repeated for these

cases until the initial and final counter readings were the same. The procedure was repeated for different weights in the pan. A typical calibration curve is shown in Fig. 9.

The static calibration was performed before and after each experiment. The variations in these calibrations were negligible.

4. Determination of the Method of Model Support and the Best Postion of the Shield with Respect to the Model

a) Cylinder Models

There are various ways of supporting a cylinder model to measure its drag in a wind tunnel. The following set of figures indicate the most commonly used methods.

(a)

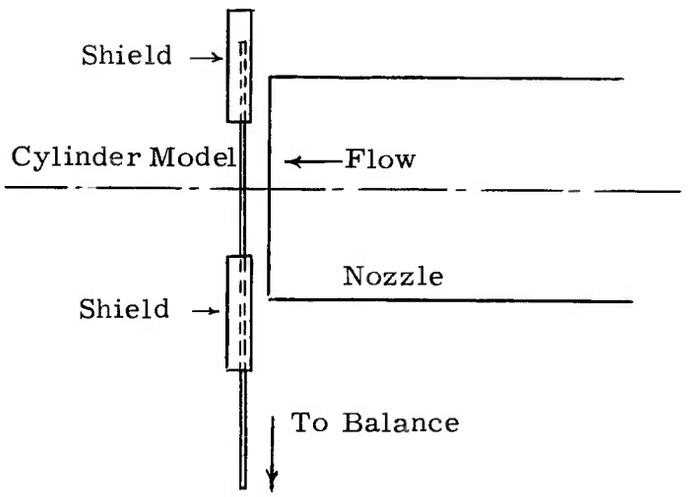

Model and shields can be either horizontal or vertical. If the shields are not disturbing the flow around the model, then the measured force coefficient is equal to that of a two dimensional model as the end effects are eliminated by the presence of shields.

(b)

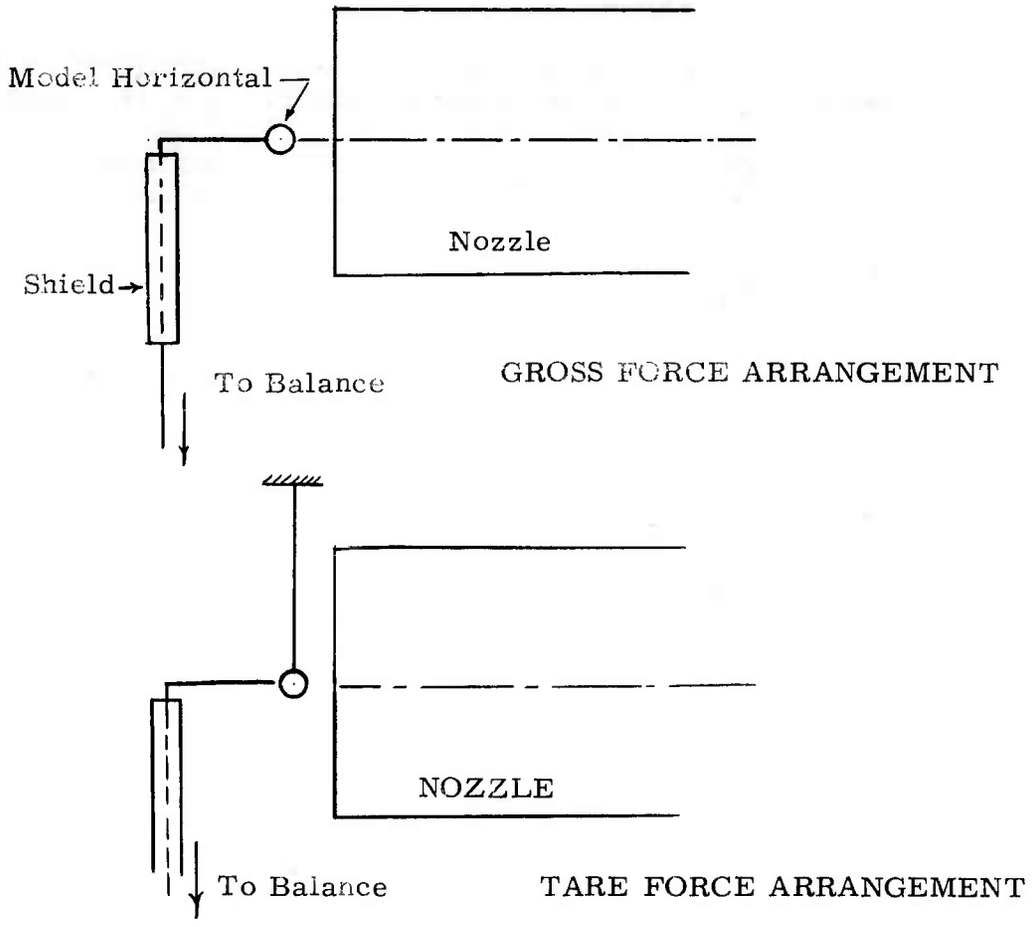

The measured net force on the model in the above arrangement is influenced by end effects and therefore is a function of the model's aspect-ratio

(c)

(i)

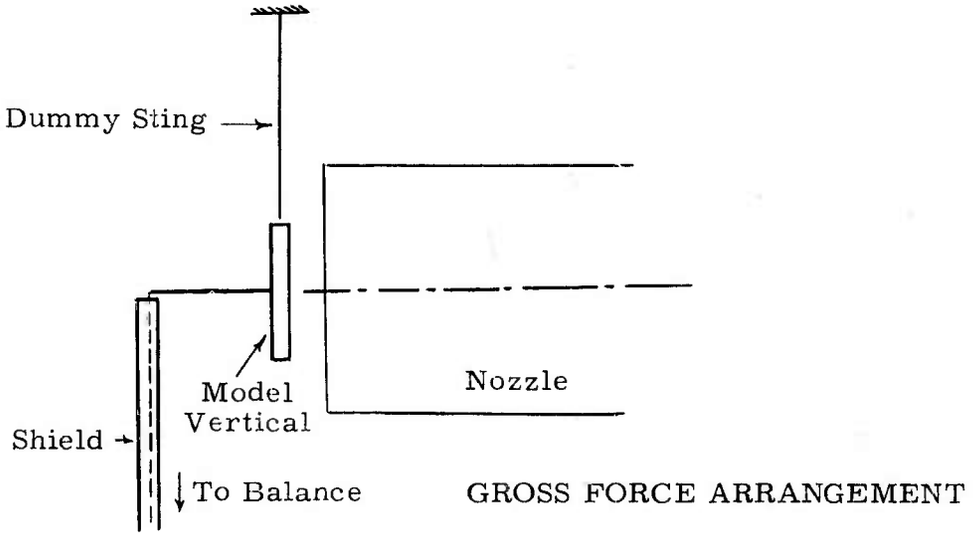

(ii)

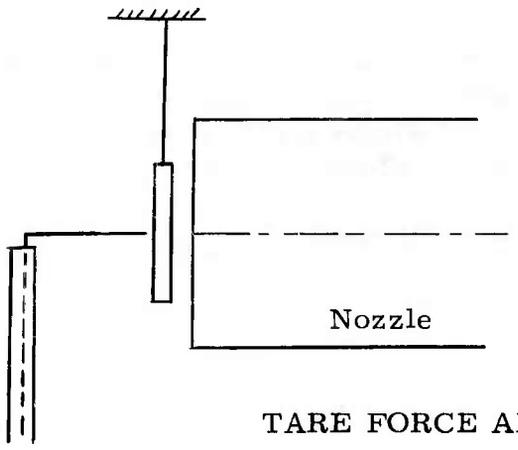

TARE FORCE ARRANGEMENT

In this arrangement the force on the model is again a function of its aspect-ratio.

The above arrangements of the models show some of the methods to measure the drag on cylinders in conventional wind tunnels.

In the course of some preliminary work done in the UTIA low density wind tunnel it was noticed that the shield used to cover the supporting rod was disturbing the flow field slightly. The shield extended from the center of the jet to the outer edge and the disturbance caused by it was propagated upstream through the subsonic portion of the boundary layer to affect the flow in the supersonic core of the jet. It was observed from the impact probe survey that the shield was causing a disturbance in the supersonic region of the flow for a distance of about $\frac{1}{2}$" upstream from its leading edge. Consequently, it was decided to place the model at a distance of at least 1" upstream from the leading edge of the shield so that the model was free from any interference from the shield.

Some experiments were done in which the cylinder models were placed just downstream of the shield as shown in Fig. (a) above, where the shields covered parts of the model itself, so that the cylinders were actually in the disturbed flow. A complete description of these tests and their results are given in Appendix A.

The mean free path in the flow in which the experiments were performed was approximately 0.049". The diameter of the cylinder models varied from 0.008" to 0.180". As mentioned previously in Section II, 3, the length of the models was restricted to 0.8" because the Mach 2 flow was uniform only over a diameter of 1". Since the model had to be upstream of the shield it was placed horizontal and transverse to the flow and supported from behind, with the shield covering the vertical portion of the sting. A schematic diagram of this type of support and the postion of the model with respect to the shield is shown in Fig. 10. A photograph of the actual arrangement is shown in Plate 4.

The model support and the shield used in the sphere drag experiments were similar and are referred to in the text as tailsting supports. Plate 5 shows a photograph of this set up and Fig. 11 gives a schematic diagram of the arrangement used to measure the sphere drag.

5. Force Measurements

(a) Cylinder Models

Having determined the method of model support and the position of the shield with respect to the model, the problem left was to isolate the tare or the supporting rod force from gross force. The conventional method of separating the model from the support rod and suspending it by a dummy rod and then measuring the tare force will not work in the present case because the sizes of the supporting rod and the models happen to be of the same order of magnitude. The net force on the cylinder obtained by taking the difference between the measured gross force and the tare force will not be the same as that on an isolated cylinder (i.e., a cylinder not supported by any stings) as no account is taken of the interference effects between the supporting rod and the model. Moreover, it was desired to correct for the aspect ratio effects on the force readings so that the final result could be extrapolated to a two dimensional cylinder. It was therefore decided to measure the drag of the cylinder by a new technique in which the length of the cylinder was successively diminished and the gross force was measured in each case.

After placing the model in position and making a static calibration of the balance, the tunnel was evacuated and kept under vacuum for some hours for out-gassing purposes. The galvanometer needle was brought to the zero position and the reading of the counter was noted. As the recovery temperature of a model is always higher than the stagnation temperature in free molecule flow or near-free molecule flow and as the drag force is a function of this temperature, a period of 10 to 15 minutes was allowed after starting the flow for the model to reach an equilibrium temperature, before the drag force was measured. After this, the flow was shut off and the null position of the balance was checked. A minimum of three force readings were recorded for each experiment to make sure that the measured forces were correct. The variations between these measured forces were within $\pm \frac{1}{2}\%$.

First the model having about 0.8" length was put in the flow and the force on it and on the supporting rod was measured. The tunnel was then let to atmosphere and the balance suspension was rigidly held by means of clamps provided on the balance base plate to protect the fragile suspension. The position of the model was measured with a telescope placed outside the tunnel. The model and its supporting base was very carefully removed from the balance and it was placed on a specially designed jig in which the length of it was reduced to about 0.6" by shortening its ends by 0.1". The model was then put back on the balance, the whole

operation being carried out without bending or distorting the model support. The position of the model was checked to see whether it had gone back to its original position. (In cases in which thetelescope indicated that the model did not return to its original position, because of some distortions caused while shortening its length, the experiment was abandoned and a new one was started). The force on the shortened model was then measured. The experiment was repeated for various different lengths of the model ranging from 0.8" to 0.15". Forces on a minimum of four different lengths of the model were measured for all the models except the 0.008" diameter one. For the latter, forces on only 3 different lengths were measured as it was desired to have an appreciable difference between their readings.

(b) Sphere Models

Experiments performed by Sherman and Kane, on the sphere drag in a low density flow, Ref. 8, indicated that the model support had an influence on the measured drag. The interference caused by the cross-stream support was much greater than that due to the tail-sting arrangement. The same two types of support were used in the present experiments, see Fig. 5. First the gross force was measured. During this run, a dummy sting (of a size equal to that of the model support) which later became the model support during the tare force measurements, was attached to the traversing mechanism and was placed vertically on top of the model center so that it was almost touching the surface. The effect on the measured force of the presence or absence of this sting near the model was observed. It served to indicate the magnitude of the interference between the sting and the model and its support. The model was then separated from the support and subsequently suspended by the dummy sting, and the tare drag was measured. Schematic diagrams of this arrangement for both types of model support are shown in Figs. 11 and 12. Photographs of the arrangement during a run are shown in Plates 5 and 6. It should be noted that for cross-stream supported models no shield was used for covering part of the support. The difference between the gross and tare forces gave the force on the sphere. In the absence of any interference effects due to the supports this force becomes the true net drag on the sphere. The procedure for measuring the forces was the same as that for the cylinders, and a minimum number of three force readings were taken in each experiment.

IV. REDUCTION OF THE DATA

a) Cylinder Models

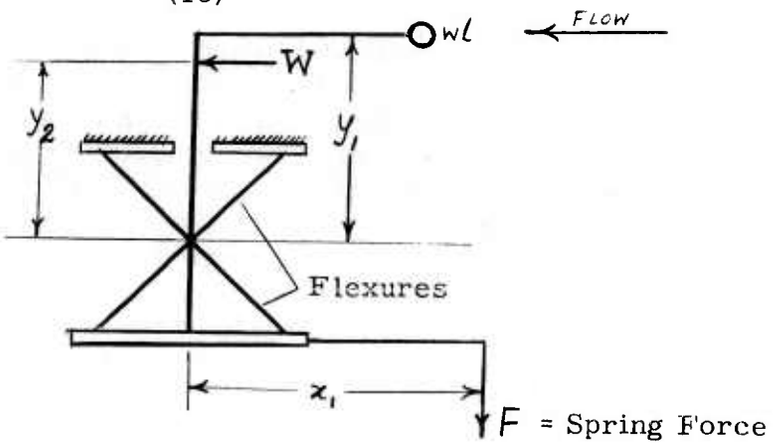

Let w = force per unit length on the cylinder model

l length of the cylinder

W net force on the model support acting at a center of pressure situated at a distance of y_2 from the flexural point

F spring force

K a factor which accounts for both the interference of the supporting sting on the model and the cylinder end effects.

Taking moments about the flexural point, for equilibrium

$$wly_1 + Wy_2 + K = Fx_1$$

In the experiments only l was varied

So $$\frac{d}{dl}\left(wly_1 + Wy_2 + K - Fx_1\right) = 0$$

or $$w = \frac{dF}{dl}\,\frac{x_1}{y_1}$$ if it is assumed that the factor Wy_2 and K are independent of l.

K will be independent of l if the supporting sting influences only a very short length of the cylinder at its center and if the end effects are confined to a short length adjacent to the ends. This is because any disturbances produced in the free molecule or near-free molecule flows are felt mostly within a radius of one mean free path. Since the mean free path in the test flow was 0.049" and the first model length was about 0.8", there is an appreciable part of this length (about 0.6") which is

unaffected by support interferences or end effects. The assumption that the disturbance effects are confined to a very small portion of the length of the cylinder and that it is constant as the model length is varied was justified by the following fact. The drag coefficient values derived from the slope of the force-vs-length curve agree closely with the drag measured in another experiment in which the cylinder model was placed downstream of two shields. This is further discussed in Appendix A.

The derived expression for w, the force acting on unit length of the cylinder is also based on the assumption that Wy_2 (moment about flexural point due to forces acting on model support) is independent of the length of the cylinder model. This was justified by conducting an additional experiment in which the support rod sizes were varied. Appendix B gives details of this experiment and the results. The expression $w = (dF/dl)(x_1/y_1)$ indicates that the graph of F vs l should be a straight line. Knowing the slope dF/dl one can determine w, since the lever arm lengths x_1 and y_1 are known (measured).

In all the experiments the graph of F vs l was plotted and the value of w determined from the slope. In every case the graphs of F vs l were straight lines in that portion of the curve where l was greater than 0.2". In some experiments in which the length of the model was reduced to less than 0.2" the curve deviated from this straight line below the point indicating that the supporting sting interference contribution to K became dependent on the length of the model or that the end effects started to merge for this length. Hence the slope of the curve between 0.2" and 0.8" was expected to give the force per unit length.

A typical graph of F vs l is shown in Fig. 13. The effect of shortening the model to a length less than 0.2" is shown in Fig. 14.

b) Sphere Models

The force on the sphere was obtained directly by calculating the difference between the gross drag force and the tare force. The experiments described in Section III, 5b, in which a dummy rod was brought close to the sphere model during a gross force run, gave the following results. Except for the case of the 1/16" diameter sphere model, there was no noticeable change in the force when the dummy rod was in position as compared with that when the rod was absent, indicating the negligible influence of the dummy rod on the model. However, there was quite an appreciable change in the force on the 1/16" dia. sphere model when this dummy rod was brought near the sphere.

The measured drag forces on cylinders and spheres are listed in Tables II and III respectively.

V. DISCUSSION OF THE RESULTS

(a) Cylinder Models

Let D be the drag force on the cylinder of length L. The drag coefficient is defined as

$$C_D = \frac{D}{\frac{1}{2} \rho V^2 A}$$

where ρ and V are free stream values of density and velocity respectively and A is the projected area of the cylinder and equal to L. d (d = dia. of cylinder).

The value of w is the force per unit length of the cylinder. This was reduced to the drag coefficient by dividing it by $\frac{1}{2} \rho V^2 d$. The plot of C_D as a function of Knudsen number based on cylinder diameter is shown in Fig. 15.

The theoretical free molecule values of C_D for the case of complete diffuse reflection, no net heat transfer from the cylinder (adiabatic model) and for complete specular reflection are also indicated on the same figure. It can be seen that the measured drag coefficient curve levels off to a value of about 3.02 at a Knudsen number of about 3 and that there is no appreciable change in this value for a further increase in the Knudsen number from 3 to 6. Experiments performed by Stalder et all (Ref. 3) on the drag of a cylinder at a Kn = 15 gave the same value of approximately 3 for C_D. The theoretical values of C_D for a cylinder in free molecule flow at a Mach number of 2 is 3.7 for complete diffuse reflection, no net heat transfer from the model and 3.34 for complete specular reflection. Experiments with rotating cylinders and molecular beams have shown that the reflection of molecules from most surfaces of engineering interest is diffuse, i.e., the momentum accommodation coefficient is equal to one. Consequently there is a discrepany of about 20% between the experimental and theoretical values assuming diffuse reflection to be valid. This could be explained by the fact that the length of the cylinder is considerably longer than the mean free path so that free molecule conditions are not attained at the Knudsen numbers of the experiments.

In an extremely simplified physical model one could see the the effect of the length as follows.

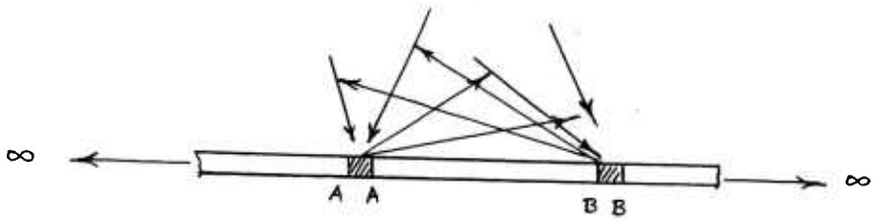

Let AA and BB be two infinitesimal portions of the cylinder situated a little less than one mean free path apart. . Molecules rebounding from the portion AA will not significantly influence the flux of particles striking AA because the collisions take place many diameters ahead of AA, but the rebounding molecules will collide after travelling one mean free path with some of the molecules directed to BB just in front of it and hence will be prevented from reaching it. Similarly some molecules that would not have struck BB will strike it due to these collisions. The case of reflected molecules from BB is similar. The basic postulate of free molecule flow (no collisions between reflected and incident molecules close to the body) is thereby violated and problem becomes one similar to that of transition or near-free molecule flow in which collisions between reflected and incident molecules have to be taken into account.

(b) Sphere Models

The drag coefficient of the spheres as a function of Knudsen number based on sphere diameter is plotted in Fig. 16. A comparison is made in Fig. 17 of the present sphere drag results with those measured by Kane and Sherman (Ref. 8) and Jensen (Ref. 9).

Except for the case of 1/16" dia. sphere the drag coefficients of the spheres were the same for both types of supports thereby indicating that the model support rod had a negligible effect on the drag coefficient. Since the dimensions of a sphere are the same in all the directions there should be a better correlation between experiment and theory for the case of spheres in free molecule flow. Unfortunately, it was not possible to measure the drag of a sphere at a Knudsen number larger than one because of size limitations. However, the present tests indicate a trend that shows for the case of spheres the drag coefficient at larger Knudsen numbers will not be seriously lower than the theoretical free molecule value.

VI. PRESSURE MEASUREMENTS TO DETERMINE THE EFFECT OF THE LENGTH OF A CIRCULAR CYLINDER TRANSVERSE TO THE FLOW

The large difference between the experimental drag coefficient of a two dimensional cylinder and its theoretical free molecule flow value (based on diffuse reflection) called for further investigations to find out the effect of the length. Hence it was decided to make pressure measurements around a cylinder transverse to the flow. Since the diameter of the pressure probe had to be considerably larger than the diameter of the drag models, the desired values of the Knudsen numbers could only be obtained in the low density wind tunnel at lower pressures and low speed ratios, a subsonic nozzle was used in these pressure probe experiments.

An orifice probe similar to the one tested and used by Enkenhus (Ref. 7) was used to calibrate the flow. An 0.008" diameter orifice was drilled through a thin sheet (0.00025" thick) of aluminum foil

and cemented over a 0.030" dia. hole drilled in the side of a 0.049" dia stainless steel tubing, with the orifice carefully positioned at the exact center of the hole. The pressure readings at three specific angular positions of the orifice (0^{o}, 90^{o} and 180^{o} to the flow directions) will give the speed ratio (Ref. 11). In particular the 90^{o} pressure reading will give the stream static pressure when thermal transpiration is taken into account.

After having calibrated the flow, the orifice probe was removed and another cylindrical probe with a diameter of 0.049" was put in the flow. This probe was almost identical to the orifice probe except that instead of having an orifice through an aluminum foil, an 0.008" dia. hole was drilled in the tubing itself (see Fig. 7). This hole had a length of 0.008" so that the ratio of length to diameter was one and hence a short tube probe resulted rather than an orifice probe. Efforts were made to have this hole drilled as close to the free end of the tube as possible, the end being plugged by soft solder. Pressure readings were taken at various angular positions of the orifice. A second set of measurements was made with another cylinder of the same diameter as that of the probe attached to the traversing mechanism and positioned vertically above the orifice probe and almost touching it. This combination gave the effect of a pressure hole essentially in the middle of a long tube. A photograph of this arrangement is shown in Plate 7. Pressure readings were taken with this configuration at the same angular positions as before. The results obtained are shown in Fig. 18 in which the pressure ratios with and without the added length is shown at various angular positions of the hole to the flow direction (0^{o} corresponds to the position of the hole at the stagnation point). From this it can be seen that at Knudsen number of about 5 and a speed ratio of 0.96 the difference in the two readings is approximately 4.3%. Since this 4.3% represents the contribution from only one half of an infinite cylinder and since an equal contribution may be expected from the probe (because its construction makes it essentially the other half of the infinite cylinder) the total error introduced by an infinite cylinder would probably be 8.6%. It can also be seen in the figure that at Knudsen number as high as 14 there is still a significant effect due to cylinder length and free molecule conditions have not been reached yet. As these experiments were done only to prove that there is an effect of the length (or two dimensionality of the objects) on force and pressure readings, no effort was made to investigate any functional relationship between the length effect and speed ratio.

It should be noted that since the pressure probe experiments indicated that the length of the probe had an effect on pressure readings the speed ratios of the flow as calibrated by the orifice probe may be in error.

VII. EXPERIMENTAL ERRORS

It is difficult to give an accurate estimate about the errors of the present experiments but the probable magnitude of the errors are as follows.

The flow parameters, Mach Number and static pressure were accurate to $\pm$ 1%. The lever arm lengths were measured with an optical comparator and a cathetometer and the error in this is less than 0.1%. The quartz spring calibration varied by $\pm$ 1% due to hysteresis of the flexures and the backlash in the gear mechanism. The error in the alignment of the balance with respect to the flow direction was estimated to be less than $\pm$ 0.5°.

In the sphere drag results significant errors may occur as a result of taking the difference of two large numbers to get the drag. In two sets of experiments carried out in which the spheres were supported by two different methods viz the cross-stream support and the tailsting support the force on the models were the same in both cases but the forces on the supporting sting in one case was many times larger than that in the other. The closeness of the final results indicate that the error were within reasonable limits except for the 1/16" dia. model.

The drag force on the cylinders was calculated by the slope of the total force vs the model length which the discussion in Section IVa, and experiment showed to be a straight line. Hence the error in these results should come mainly from the spring calibration error which would be no more than about $\pm$ 1%. Since the slope had an error of only $\pm$ 1% the total error on the force measurements is $\pm$ 2%. The drag coefficient was obtained by dividing the measured force by $\frac{1}{2} \rho V^2 A$. The variation in the flow Mach number will vary the static pressure and at a Mach number of 2 at which these experiments were performed, a 1% error in Mach number introduces about 2% maximum error in the value of $\frac{1}{2} \rho V^2$. The total maximum error that can occur will be $\pm$ 4% but the absence of scatter in the final results show that actual error was well below this value.

Repeatability of the Experiments

Two experiments on the drag of a 0.0203" dia. cylinder were perfomred at an interval of about 10 weeks using two different quartz springs. The results were as follows

Dia.	Kn	C_D
0.0203	2.37	2.92
0.0203"	2.397	2.95

This shows that the experiments were quite repeatable.

VIII. CONCLUSIONS

Drag forces of spheres and cylinders were measured in air at a Mach number M = 2 in the Knudsen number range of $0.1 < Kn < 1$ for spheres and $0.2 < Kn < 7$ for cylinders.

There is no theory available at present that will predict the aerodynamic forces on bodies in transition or near-free molecule flows at moderate Mach numbers where thermal motion of the incident stream is not negligible. Consequently it was not possible to compare the experimental data with relevant theories.

The drag results for the cylinders show that free molecule flow is not reached at a Knudsen number of 5 based on cylinder diameter in contrast to statements by previous workers (Ref. 15). The measured drag coefficient at this value of the Knudsen number was about 20% lower than the theoretical free molecule flow values for the case of complete diffuse reflection and 10% lower for specular reflection. On the other hand the available experimental results on the sphere drag indicate that the free molecule flow theory and experiment will most likely agree at Knudsen numbers only slightly larger than unity since at a Knudsen number of about 0.6 the measured drag was already higher than the theoretical free molecule flow value based on specular reflection.

It is suggested that the discrepancy between the theoretical and measured values for the case of circular cylinders is associated with the fact that in this case not all dimensions are smaller than the mean free path. This contention was supported by additional experiments conducted in subsonic flow. Pressure readings taken by an orifice probe indicated that there is an appreciable effect of the length of the cylinder on pressure readings at Knudsen numbers as high as 9. On the basis of these results, it is suggested that for flows over cylindrical bodies normal to the stream the value of the Knudsen number based on the cylinder diameter is inadequate to classify the type of flow over the body. Perhaps this conventional Knudsen number based on cylinder diameter could be suitablly modified by a model aspect-ratio term to show its appropriate free molecule flow limit.

The theoretical work done by Lunc and Lubonski (Ref. 16) on the aerodynamic force on an infinite strip in a high speed flow shows that at a Knudsen number of 5 based on the width of the strip, the theoretical value of the drag is about 7.5% lower than the corresponding free molecule flow value. Their calculations also show that as the Knudsen number is further increased, this difference decreases. This is consistent with the physical reasoning because, for an infinitely long model normal to the flow, the free molecule force values should be asymptotically reached as the Knudsen number based on model's width is increased. Contrary to this, the present results show that a drag coefficient value of 3.02 is reached at a Knudsen number of 3 and that there was no apparent further increase as the Knudsen number was further increased. A possible explanation for

this, is that the range of Knudsen numbers (viz. 3. to 6) covered in the present experiments may not be large enough to positively indicate that the drag coefficient values become independent of Knudsen number. In addition, the experimental accuracy might have been lower in these regions due to a low magnitude of the forces measured as compared to the neighbouring points.

Finally it is suggested that further work should be done with a different nozzle to permit the use of a wider range of high Knudsen numbers than was possible in the present work in order to resolve some of these uncertanties.

REFERENCES

1. Schaaf, S. A. Chambre, P. L. — Flow of Rarefied Gases, Section H, Fundamentals of Gas Dynamics, Vol. III, High Speed Aerodynamics and Jet Propulsion. Princeton University Press, 1958.

2. Schaaf, S. A. Talbot, L. — Mechanics of Rarefied Gases, Section 16, Handbook of Supersonic Aerodynamics, NAVORD Report 1488 (Vol. 5), 1959.

3. Stalder, J. R. Goodwin, G. Creager, M.O. — A comparison of Theory and Experiment for High Speed Free Molecule Flow. NACA Tech. Note. 2244, 1950.

4. Baker, R.M.L. Charwat, A.F. — Transitional Correction to the Drag of a Sphere in Free Molecule Flow. Physics of Fluids, Vol. 1, March-April 1958.

5. Enkenhus, K.R. — The Design, Instrumentation and Operation of the UTIA Low Density Wind Tunnel. UTIA Rep. No. 44, June 1957.

6. Latz, R. N. — Design of a Two Component Microbalance for Low Density Wind Tunnels. University of California Engineering Project. Report HE-150-124, Aug., 1954.

7. Enkenhus, K.R. — Pressure Probes at Very Low Density. UTIA Rep. No. 43, Jan. 1957.

8. Sherman, F. S. Kane, E.D. — Supplementary Data on Sphere Drag Tests. University of California Engineering Project Report HE-150-71, August 1950.

9. Jensen, N. A. — Supplementary Data on Sphere Drag Tests - Part 2 - University of California Engineering Project Report HE-150-92, Sept., 1951.

10. Harris, E. L. — Investigation of Free Molecule and Transition Flows Near the Leading Edge of a Flat Plate. UTIA Rep. No. 53, Nov. 1958.

11. Patterson, G. N. — Theory of Free Molecule, Orifice Type Pressure Probes in Isentropic and Non-Isentropic Flows. UTIA Report No. 41 (Revised) May, 1959.

12. Gowen, F. E.
Perkins, E. W.
Drag of Circular Cylinders for a Wide Range of Reynolds numbers and Mach Number. NACA TN 2960, July, 1953.

13. Patterson, G.N.
Molecular Flow of Gases.
John Wiley and Sons Inc., 1956.

14. Stalder, J. R.
Zurick, V. J.
Theoretical Aerodynamic Characteristics of Bodies in a Free-Molecule Flow Field.
NACA TN 2423, July, 1951.

15. Stalder, J. R.
Goodwin, G
Creager, M. O.
Heat Transfer to Bodies in a High Speed Rarefied Gas Stream. NACA Rep. 1093, 1952.

16. Lunc, M.
Lubonski, J.
Sur Une Solution Approchee Du Probleme De L'e coulement D'un Gaz Rarefie Autour D'un Obstacle.
Nadbitka Z Archiwum
Mechaniki Stosowanej
Tom VIII Zeszyt 4, Warsaw, 1956.

APPENDIX A

Drag Measurements Using Movable Shields

In order to know the Mach number at any point in the flow one has to know the impact and static pressures at that point. Due to the very low magnitude of the Reynolds number of the flow, probe readings are subject to high viscous corrections. At the Reynolds and Mach numbers at which the UTIA low density wind tunnel operates only viscous corrections to the impact probe readings are known. Hence the flow has to be calibrated using impact probes alone. The usual assumption which is experimentally verified is made that the flow is isentropic at the centre of the jet and the static pressure is constant across it. When a shield is placed in the flow the accurate determination of the Mach number downstream of the leading edge of the shield is difficult and there is an uncertainty of the flow Mach number close to the shield as the flow may not be isentropic in these regions.

At the beginning of this research project it was decided to make drag measurements by mounting a model 5" in length vertically on the balance and exposing only 0.8" of the cylinder at the nozzle centre to the flow by covering the remaining length by two shields. These shields were mounted on a specially designed traversing mechanism by means of which they could be moved in or out relative to the nozzle centreline. This permitted the length of the cylinder exposed to the Mach 2 flow to be varied remotely while the flow was on (Plate 8). An impact probe survey made on the nozzle centreline with the model removed but shields left on is shown in Fig. (19). Referring to this figure it can be seen that shields disturb the flow quite appreciably even upstream. There is a significant change in the impact probe readings at the nozzle exit plane with and without the shields when they are placed so that their leading edges are 0.116" from the exit plane. There is also a sudden change in the flow immediately downstream of the shields. (It is worthwhile to mention it here that when only one shield was placed in the flow about 1-1/8" from the nozzle exit to cover the supporting sting for the experiments described in the main part of this report, there was no change in the flow Mach number at the nozzle exit). The impact probe reading alone will not give the Mach number in this region as the flow may not be isentropic. Because of the uncertainty of the flow velocity immediately downstream of the shields the idea of keeping the model downstream of them had to be given up. However, for comparison purposes some experiments were performed with the model placed downstream of the shield. Care was taken to place the model as close to the leading edge as practicable without touching it. First about 0.8" of the model was exposed to the flow and the force on it measured. The length was then reduced in steps of 0.1" and force measured in each case. From the slope of the force vs length graph (a typical curve is shown in Fig. 20) the drag was evaluated assuming that any influence of the shields on the cylinder would be confined to a very short length adjacent to the shields. The curve would be a straight line whose slope gives the drag per unit

length. Results thus obtained on cylinders of different diameters are shown in Fig. (21). The Mach number was calculated by measuring the impact probe pressure on the nozzle centreline at a distance of 0.034" downstream of the leading edge of the shield assuming isentropic flow. (This is the approximate position at which the models were placed). On the same figure the two sets of drag coefficients measured by placing cylinders downstream of the shield and far upstream of it (as reported in the main section of this report) are shown.

Some significant conclusions can be drawn from the comparison of these two experimental data. For the case in which the cylinder model was placed downstream of the shields, the drag coefficient value obtained was essentially that of a cylinder of infinite aspect ratio. Any influence of the shields on the model was assumed to be confined to a very short region and to be constant as the model length was varied. On the other hand the experiments with the model far upstream of the shield were performed on a model of finite length. Again if one assumes that the end effects (or the aspect-ratio effects) were constant as the model length was varied, then the slope of the force vs length curve gives the drag on a two-dimensional cylinder.

In these two experiments the "end-effects" were due to two different causes. In one case, the effect was due to the presence of the shields, in the other it was due to the finite aspect ratio. In either case, however, these effects were eliminated mathematically by taking measurements on different lengths. The close agreement of the final results indicates that the technique used was quite satisfactory and correct, thereby justifying assumptions originally made on physical reasoning.

APPENDIX B

Effect of the Supporting Sting on the Cylinder Model

All the cylinder models were supported by a stainless steel tubular sting 0.020" diameter and 1.1" long (Fig. 4). In computing the drag force from the data it was assumed that the interference effect of the supporting sting was confined to a very small portion of the length of the model at the center where the model was soldered to the sting and that the force on the support remained constant as the model length varied. To check these assumptions an experiment was conducted in which the diameter and the length of the support rod were increased to 0.049" and 2.1" respectively, see Figure below.

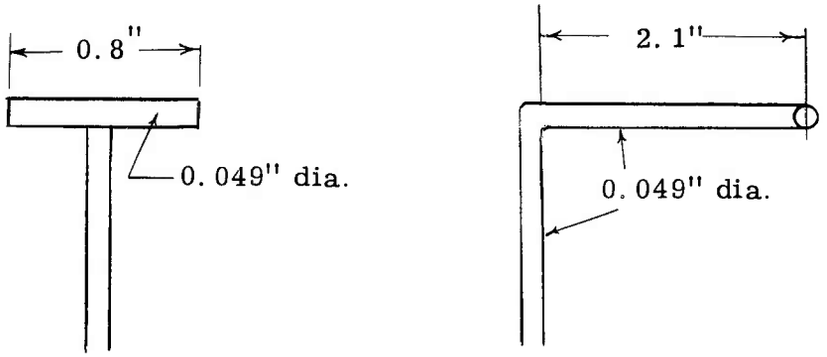

The results were as follows.

Diameter of the model	Length of the Supporting Sting	Dia. of the Supporting Sting	C_D	Kn
0.049"	1.1"	0.020"	2.51	1.004
0.049"	2.1"	0.049"	2.49	1.007

The close agreement of the values found for the final drag coefficient justifies the above assumptions.

APPENDIX C

Temperature Measurements

In the absence of a net heat transfer the equilibrium temperature of a thermally conductive body will be higher than the free-stream stagnation temperature. If the body is not thermally conductive, its temperature would also be higher but vary with position on the surface. The drag coefficient of the body in free molecule flow is a function of this equilibrium temperature (see Appendix E). At the speeds and free-stream temperatures at which the drag force experiments were conducted, the theoretically calculated values of the drag coefficient of an adiabatic cylinder are as follows:

C_{D_i} = drag coefficient due to incident molecules = 2.51

C_{D_r} = drag coefficient due to reflected molecules = 1.18

T_o = stagnation temperature = $545^{o}R$

T_1 = free stream static temp = $302.8^{o}R$ at M = 2

It was not practicable to thermally insulate the model from its support and hence there was some heat transfer. A 0.003" dia. copper-constantan thermo-couple was used to measure the model temperature. Two sets of readings were taken, one with the thermocouple welded on to the model and the other with the thermocouple inserted inside the hollow models. Both gave almost identical readings. The results are tabulated in Table IV.

When this experimentally determined value of temperature (about $125^{o}F$ for $Kn > 2$) is inserted in Equation (A29) the theoretical value of the drag coefficient is 3.66 which is less than 1% lower than that of the adiabatic model value. (It should be noted that variation in body temperature will affect only that part of the drag coefficient due to reflected molecules and in this particular case this value is changed from 1.18 to 1.15). This shows that the effect of heat transfer cannot explain the discrepancy between experimental and theoretical values of cylinder drag coefficient.

APPENDIX D

Calculation of the Mean Free Path

In order to calculate the Knudsen number, it is necessary to know the value of the molecular mean free path in the flow.

In Ref. 13, it is shown that the molecular mean free path is given by

$$\lambda = \frac{16}{5\sqrt{2\pi}} \frac{\mu}{\rho} \frac{1}{\sqrt{RT_1}}$$

where μ = coefficient of viscosity

ρ = density

T_1 = temperature

Substituting for ρ in terms of p(pressure) and RT_1, the above expression reduces to

$$\lambda = \frac{16}{5\sqrt{2\pi}} \frac{\mu}{p} \sqrt{RT_1}$$

The viscosity is a function of temperature only and may be represented adequately by Sutherland's relation

$$\mu = \frac{C_1 T_1^{3/2}}{T_1 + C_2}$$

where C_1 and C_2 are constants for a particular gas.

The formula for air is

$$\lambda = \frac{5.328 \times 10^{-3}}{p} \frac{T_1^2}{T_1 + 210.6}$$

where λ is in inches, p is in microns Hg., and T_1 is in degrees Rankine.

The value of T_1 was found from the flow Mach number and the stagnation temperature assuming adiabatic flow.

APPENDIX E

Theoretical Aerodynamic Characteristics of Bodies in a Free Molecule Flow Field

NOTATION

C_D	drag coefficient , Drag force/ $\frac{1}{2} \rho V^2 A$
C_L	lift coefficient, Lift force/$\frac{1}{2} \rho V^2 A$
c_m	most probable molecular speed
E	internal energy flux, energy/ unit time x unit area
erf(s)	error function $= \frac{2}{\sqrt{\pi}} \int_0^s e^{-x^2} dx$
f	molecular distribution function
$I_o\left(\frac{s^2}{2}\right)$, $I_1\left(\frac{s^2}{2}\right)$	modified Bessel functions of the first kind
j	number of molecular degrees of freedom
m	molecular mass.
N	number flux
p	normal momentum
R	gas constant
s	speed ratio $V/\sqrt{2RT}$
T	temperature, absolute
T_w	wall temperature
$T_{w\,equi}$	adiabatic wall temp.
u_i	components of molecular velocity
V	mass velocity
θ	local angle of attack
α	thermal accommodation coefficient
γ	ratio of specific heats

If the gas through which a body is moving is sufficiently rarefied, the motion of the molecules impinging on the body will be essentially unaltered by collisions with reflected molecules. Under these conditions the total force and energy imparted to the body by the molecules can be broken down into two components; one arising from the impingement of incident molecules and the other from the re-emission of the molecules from the surface. The velocity distribution of the gas molecules until they strike the body will therefore be that of a gas at rest, namely the Maxwellian velocity distribution. In order to compute the forces imparted to the surface by the reflected molecules, it is necessary to make some assumptions regarding the nature of the molecular interactions with the surface.

The concepts of specular and diffuse reflection have been recognized since the early studies of Knudsen and others. If the walls are perfectly smooth, specular reflection will occur in which the component of the molecular velocity tangent to the surface remains unchanged while the component normal to the surface, on contact with the wall reverses its direction with no change in magnitude. However a real surface is more or less rough and the molecules are reflected quite randomly so that all traces of their past history become entirely or almost entirely lost. This type of reflection is called diffuse. If the reflection is completely diffuse, all directions of emission about the normal to the surface are equally probable; they then obey a cosine law similar to that of a surface emitting radiant energy. In the case of completely diffuse reflection the velocity distribution of the re-emitted particles is Maxwellian and is consistent with the surface temperature. For most surfaces of interest in engineering the re-emission process deviates slightly from completely diffuse reflection. It is then possible to characterize the reflection process from a given surface material by defining a quantity representing the average "diffuseness" of the re-emission, or, what amounts to the same, the degree of accommodation to the wall conditions of the re-emitted molecules. This quantity takes the form of a coefficient ranging from 0 to 1 as the re-emission changes from completely specular to completely diffuse. Such "accommodation coefficients" are defined separately for energy (thermal accommodation) and for the two components of momentum (tangential and normal to the surface).

Thus, the thermal accommodation coefficient is defined as

$$\alpha = \frac{dE_i - dE_r}{dE_i - dE_w} \qquad \text{(A-1)}$$

where dE_i = incident energy flux (per unit time and area)

dE_r = re-emitted energy flux from the surface

dE_w = the re-emitted energy flux for complete diffuse reflection.

For the tangential momentum exchange the accommodation coefficient is defined as

$$\sigma_T = \frac{\tau_i - \tau_r}{\tau_i} \qquad \text{(A-2)}$$

where τ_i = incident tangential momentum flux

τ_r = re-emitted tangential momentum flux

Similarly for the normal momentum exchange we have

$$\sigma_N = \frac{p_i - p_r}{p_i - p_w} \qquad \text{(A-3)}$$

where p_i and p_r are the incident and reflected fluxes of normal momentum respectively and p_w = emitted normal momentum for complete diffuse reflection.

It can be seen that for complete diffuse reflection $\alpha = \sigma_N = \sigma_T = 1$ whereas for specular reflection $\alpha = \sigma_N = \sigma_T = 0$

Analysis

Let (c_1, c_2, c_3) be the components of the random (thermal) molecular velocity $\vec{c}$ with respect to an orthogonal co-ordinate system fixed in space. Then Maxwell's distribution law states that the fraction of molecules having velocity components lying in an element of velocity space $dc_1\, dc_2\, dc_3$ centered at (c_1, c_2, c_3) is

$$f(c_1, c_2, c_3)\, dc_1\, dc_2\, dc_3 = \frac{1}{(\sqrt{\pi}\, c_m)^3}\, e^{-\frac{1}{c_m^2}(c_1^2 + c_2^2 + c_3^2)}\, dc_1\, dc_2\, dc_3 \qquad \text{(A-4)}$$

where $c_m = \sqrt{2RT}$ = the most probable molecular speed.

The motion of a body with velocity $-\vec{V}$ having components $(-u_1, -u_2, -u_3)$ along the co-ordinate axes (x_1, x_2, x_3) may be transformed into an equivalent dynamical problem by considering the body to be at rest, and the total molecular velocity components having the values

$$\xi_1 = u_1 + c_1 ,$$

$$\xi_2 = u_2 + c_2 ,$$

$$\xi_3 = u_3 + c_3 .$$

The velocity distribution function referred to axes fixed in the body then becomes

$$f = \frac{1}{(\sqrt{\pi}\, c_m)^3}\; e^{-\frac{1}{c_m^2}\left[(\xi_1-u_1)^2+(\xi_2-u_2)^2+(\xi_3-u_3)^2\right]}$$

We shall first derive expressions for the forces and the heat transfer arising from collisions of the molecules with a surface element of the body. The aerodynamic quantities for the whole body are then found by integration over all surface elements.

Let us consider a surface element of area dA and choose a co-ordinate system such that the element lies in the (x_2, x_3) plane so that x_1 is normal to dA (see Fig. A-1).

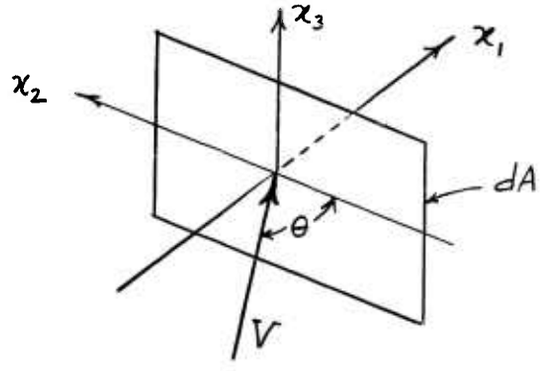

FIG. A-1

If the incident velocity $\vec{V}$ lies in the (x_1, x_2) plane and is at an angle θ with the plane of the element, then

$$u_1 = V\sin\theta \;; \quad u_2 = V\cos\theta \;; \quad u_3 = 0$$

The number of molecules with velocities in the range ξ and $\xi + d\xi$ striking an element of area dA on the front side of the surface, in unit time will lie in a cylinder of base dA and length ξ_1, with its axis in the direction of ξ; the volume of this cylinder is $\xi_1\, dA$. If n_i is the number density of the incident stream, then the number of molecules striking dA per unit time is

$$(N_i)_F = \int_{\xi_1=0}^{\infty}\int_{-\infty}^{+\infty}\int_{-\infty}^{+\infty} n_i \xi_1 f(\xi_1,\xi_2,\xi_3)\, d\xi_1\, d\xi_2\, d\xi_3\, dA$$

$$= \frac{n_i\, dA}{(\sqrt{\pi}\, c_{m_i})^3}\left[\frac{u_1 \pi^{3/2} c_{m_i}^3}{2}\left(1+\operatorname{erf}\frac{u_1}{c_{m_i}}\right)+\frac{\pi c_{m_i}^4}{2}\, e^{-\frac{u_1^2}{c_{m_i}^2}}\right]$$

We now define the speed ratio $s = V/c_{m_i}$ and recall that $u_1 = V\sin\theta$. Then $u_1 = c_{m_i}\sin\theta\, s$.

Thus
$$(N_i)_F = \frac{n_i c_{mi}}{2\sqrt{\pi}} \left[\chi \right] dA \qquad \text{(A-5)}$$

where
$$\chi = e^{-s^2 \sin^2\theta} + \sqrt{\pi}\, s \sin\theta \,(1 + \operatorname{erf} s \sin\theta)$$

The number of molecules striking the rear side of the element may be found by the same method, except that the limits of integration for ξ_1 become $-\infty \leq \xi_1 \leq 0$. The result is

$$(N_i)_R = \frac{n_i c_{mi}}{2\sqrt{\pi}} \left[\chi' \right] dA \qquad \text{(A-6)}$$

where
$$\chi' = e^{-s^2 \sin^2\theta} - \sqrt{\pi}\, s \sin\theta \,(1 - \operatorname{erf} s \sin\theta)$$

Normal Momentum

Each molecule striking a surface element carries a momentum component normal to the surface of magnitude $m\xi_1$ where m is the mass of the gas molecule. The number of molecules with velocities in the range $\vec{\xi}$ to $\vec{\xi} + d\vec{\xi}$ which strike the front surface will impart to the surface element a momentum equal to

$$m n_i f(\xi_1, \xi_2, \xi_3)\, d\xi_1 d\xi_2 d\xi_3\, \xi_1^2\, dA$$

The total momentum imparted to the front surface by incident molecules is obtained by integrating the above expression over all possible velocities. The result is

$$(p_i)_F = \frac{\rho_i V^2 \sin^2\theta\, dA}{2} \left[\frac{e^{-s^2 \sin^2\theta}}{\sqrt{\pi}\, s \sin\theta} + (1 + \operatorname{erf} s \sin\theta)\left(1 + \frac{1}{2 s^2 \sin^2\theta}\right) \right] \qquad \text{(A-7)}$$

where $\rho_i = m n_i$ = density of the incident molecules.

Similarly, the incident normal momentum due to molecules striking the rear surface can be calculated as

$$(p_i)_R = \frac{\rho_i V^2 \sin^2\theta\, dA}{2} \left[\frac{e^{-s^2 \sin^2\theta}}{\sqrt{\pi}\, s \sin\theta} - (1 - \operatorname{erf} s \sin\theta)\left(1 + \frac{1}{2 s^2 \sin^2\theta}\right) \right] \qquad \text{(A-8)}$$

Tangential Momentum

Each molecule carries a tangential momentum of $m\xi_2$. The total tangential momentum imparted to the element by the incident molecules striking the front side is

$$(\tau_i)_F = m n_i dA \int_0^{\infty} \int_{-\infty}^{+\infty} \int_{-\infty}^{+\infty} \xi_1 \xi_2 f \, d\xi_1 d\xi_2 d\xi_3$$

$$= \frac{\rho_i V^2 \cos\theta \sin\theta}{2} dA \left[\frac{e^{-s^2 \sin^2\theta}}{\sqrt{\pi}\, s \sin\theta} + (1 + \operatorname{erf} s \sin\theta) \right] \quad \text{(A-9)}$$

Similarly for the rear side the tangential momentum is

$$(\tau_i)_R = \frac{\rho_i V^2 \cos\theta \sin\theta}{2} dA \left[\frac{e^{-s^2 \sin^2\theta}}{\sqrt{\pi}\, s \sin\theta} - (1 - \operatorname{erf} s \sin\theta) \right] \quad \text{(A-10)}$$

Momentum due to Molecular Emission from a Surface

It is assumed that the emitted stream has a Maxwellian velocity distribution corresponding to a gas in equilibrium at an unspecified temperature T_w. Since the reflection is diffuse the molecules can be considered as though coming from a ficticious gas on the rear side of the surface at a most probable molecular velocity c_{m_w} corresponding to the temperature T_w.

Let n_w be the number density of the reflected molecules. The normal momentum imparted to the front surface by the molecules rebounding from it is

$$(p_w)_F = \frac{m n_{wF}}{(\sqrt{\pi}\, c_{m_{wF}})^3} \int_{-\infty}^{0} \int_{-\infty}^{+\infty} \int_{-\infty}^{+\infty} c_1^2 \, e^{-\frac{1}{c_{m_{wF}}^2}(c_1^2 + c_2^2 + c_3^2)} \, dc_1 dc_2 dc_3 \, dA$$

$$= \frac{\rho_{wF} R (T_w)_F}{2} dA$$

Similarly the normal momentum imparted to the element due to molecules reflected from the rear side of the element is

$$(p_w)_R = - \frac{\rho_{wR} R (T_w)_R}{2} dA \quad \text{(A-12)}$$

If the front surface is thermally insulated from the rear, then $(T_w)_F$ and $(T_w)_R$ will differ. ρ_{wF} and ρ_{wR} also differ.

In order to obtain values for ρ_{wF} and ρ_{wR} in terms of known quantities the conservation laws are applied. The number of molecules reflected from the surface N_w is equated to the number of molecules striking the surface (N_i).

$$(N_w)_F = \frac{n_{wF}}{2\sqrt{\pi}} c_{m_{wF}} dA = (N_i)_F \quad \text{(A-13)}$$

$$\therefore \rho_{wF} = \rho_i \chi \sqrt{\frac{T_i}{(T_w)_F}}$$

$$(N_\omega)_R = \frac{(n_\omega)_R}{2\sqrt{\pi}} (c_{mw})_R \, dA = (N_i)_R$$

$$\therefore \quad (\rho_w)_R = \rho_i \chi' \sqrt{\frac{T_i}{(T_w)_R}}$$

Substituting this value in equations (A-11) and (A-12) we have

$$(P_w)_F = \frac{\rho_i V^2}{4s^2} \sqrt{\frac{(T_w)_F}{T_i}} \, \chi \, dA \qquad \text{(A-14)}$$

and

$$(P_w)_R = -\frac{\rho_i V^2}{4s^2} \sqrt{\frac{(T_w)_R}{T_i}} \, \chi' \, dA \qquad \text{(A-15)}$$

By symmetry considerations $(\tau_w)_{front}$ and $(\tau_w)_{rear}$ are zero. i.e., the net tangential momentum from diffusely reflected molecules is zero.

The values of $(T_w)_{front}$ and $(T_w)_{rear}$ depend on the energy exchange. By equating the total incident energy to the energy carried by the reflected molecules plus the heat loss from the body in the form of conduction and radiation, one could determine $(T_w)_{front}$ and $(T_w)_{rear}$.

We have calculated the momentum imparted to the element by the reflected molecules assuming that they are in a Maxwellian distribution at the respective temperatures $(T_w)_F$ and $(T_w)_R$ for the front and rear surface. We are now in a position to calculate the actual forces on the body by the use of accommodation coefficients defined previously.

Normal momentum:

$$p = p_i + p_r = (2 - \sigma_N) p_i + \sigma_N p_w$$

Tangential momentum:

$$\tau = \tau_i - \tau_r = \sigma_T \tau_i$$

Substituting the values for p_i, p_r and τ_i in the above relations, the final expression for normal and tangential momentum imparted to a surface element in free molecule flow are thus

$$p_{front} = \frac{\rho_i V^2}{2} dA \left\{ \sin^2\theta \,(2-\sigma_N)\left[(1+\mathrm{erf}\, s\sin\theta)\left(1+\frac{1}{2s^2\sin^2\theta}\right) + \frac{e^{-s^2\sin^2\theta}}{\sqrt{\pi}\, s\sin\theta} \right] \right.$$
$$\left. + \frac{\sigma_N}{2s^2}\sqrt{\frac{T_{WF}}{T_i}}\left[e^{-s^2\sin^2\theta} + \sqrt{\pi}\, s\sin\theta\,(1+\mathrm{erf}\, s\sin\theta) \right] \right\} \qquad \text{(A-16a)}$$

$$p_{rear} = \frac{\rho_i V^2}{2} dA \left\{ \sin^2\theta \,(2-\sigma_N)\left[\frac{e^{-s^2\sin^2\theta}}{\sqrt{\pi}\, s\sin\theta} - (1-\mathrm{erf}\, s\sin\theta)\left(1+\frac{1}{2s^2\sin^2\theta}\right) \right] \right.$$
$$\left. - \frac{\sigma_N}{2s^2}\sqrt{\frac{T_{WR}}{T_i}}\left[e^{-s^2\sin^2\theta} - \sqrt{\pi}\, s\sin\theta\,(1-\mathrm{erf}\, s\sin\theta) \right] \right\} \qquad \text{(A-16b)}$$

$$\tau_{front} = \frac{\rho_i V^2}{2} dA \left\{ \sigma_T \cos\theta \sin\theta \left[\frac{e^{-s^2\sin^2\theta}}{\sqrt{\pi}\, s\sin\theta} + (1+\mathrm{erf}\, s\sin\theta) \right] \right\} \qquad \text{(A-17a)}$$

$$\tau_{rear} = \frac{\rho_i V^2}{2} dA \left\{ \sigma_T \cos\theta \sin\theta \left[\frac{e^{-s^2\sin^2\theta}}{\sqrt{\pi}\, s\sin\theta} - (1-\mathrm{erf}\, s\sin\theta) \right] \right\} \qquad \text{(A-17b)}$$

If the front and rear surfaces are in perfect thermal contact, then $(T_w)_{front} = (T_w)_{rear}$. The total normal momentum imparted to the surface element as a whole is

$$p = p_{front} + p_{rear}$$

$$\therefore \quad p = \frac{\rho_i V^2}{2} dA \left\{ \frac{2(2-\sigma_N) e^{-s^2 \sin^2\theta}}{\sqrt{\pi}\, s} \sin\theta + 2(2-\sigma_N)\, erf.\, s.\sin\theta \left(\sin\theta + \frac{1}{2s^2}\right) + \frac{\sqrt{\pi}\sin\theta}{s} \sqrt{\frac{T_w}{T_i}}\, \sigma_N \right\} \quad (A-18)$$

Similarly

$$\tau = \tau_{front} + \tau_{rear}$$

$$\therefore \quad \tau = \frac{\rho_i V^2}{2} dA \left\{ 2\sigma_T \cos\theta \sin\theta \left[\frac{e^{-s^2\sin^2\theta}}{\sqrt{\pi}\, s \sin\theta} + erf\, s.\sin\theta \right] \right\} \quad (A-19)$$

The normal and tangential momentum on the surface element can now be resolved into components along the flow direction and normal to it to obtain drag and lift forces respectively. In non-dimensional form (through division by $\frac{1}{2}\rho_i V^2 dA$) the results become as follows,

Lift coefficient

$$C_{L_{front}} = \left\{ e^{-s^2\sin^2\theta} \cos\theta \left[\frac{(2-\sigma_N-\sigma_T)\sin\theta}{\sqrt{\pi}\, s} + \frac{\sigma_N}{2s^2} \sqrt{\frac{T_{WF}}{T_i}} \right] + (1 + erf\, s.\sin\theta) \cos\theta \left[\sin^2\theta (2-\sigma_N-\sigma_T) + \frac{(2-\sigma_N)}{2s^2} + \frac{\sqrt{\pi}}{2s} \sigma_N \sqrt{\frac{T_{WF}}{T_i}} \cdot \sin\theta \right] \right\} \quad (A-20a)$$

$$C_{L_{rear}} = \left\{ e^{-s^2\sin^2\theta} \cos\theta \left[\frac{(2-\sigma_N-\sigma_T)\sin\theta}{\sqrt{\pi}\, s} - \frac{\sigma_N}{2s^2}\sqrt{\frac{T_{N_{rear}}}{T_i}} \right] - \right.$$

$$\left. (1-\operatorname{erf} s\sin\theta)\cos\theta \left[\sin^2\theta\,(2-\sigma_N-\sigma_T) + \frac{2-\sigma_N}{2s^2} - \frac{\sigma_N}{2s}\sqrt{\pi}\sqrt{\frac{T_{N_{rear}}}{T_i}}\sin\theta \right] \right\} \quad \text{(A-20b)}$$

$$C_L = C_{L_{front}} + C_{L_{rear}}$$

$$C_L = \left\{ \frac{\sin\theta\cos\theta\, e^{-s^2\sin^2\theta}}{\sqrt{\pi}\, s} 2\,(2-\sigma_N-\sigma_T) + \frac{\sigma_N}{s}\cos\theta\sin\theta\sqrt{\pi}\sqrt{\frac{T_N}{T_i}} \right.$$

$$\left. + \cos\theta \left[2\sin^2\theta\,(2-\sigma_N-\sigma_T) + \frac{2-\sigma_N}{s^2} \right] \operatorname{erf} s\sin\theta \right\} \quad \text{(A-21)}$$

Drag Coefficient

$$C_{D_{front}} = \left\{ \frac{e^{-s^2\sin^2\theta}}{\sqrt{\pi}\, s} \left[(2-\sigma_N)\sin^2\theta + \frac{\sigma_N}{2s}\sin\theta\sqrt{\pi}\sqrt{\frac{T_{N_{front}}}{T_i}} + \sigma_T\cos^2\theta \right] \right.$$

$$+ (1+\operatorname{erf} s\sin\theta)\sin\theta \left[(2-\sigma_N)\left(\sin^2\theta + \frac{1}{2s^2}\right) + \frac{\sigma_N}{2s}\sqrt{\pi}\sin\theta\sqrt{\frac{T_{N_{front}}}{T_i}} \right.$$

$$\left. \left. + \sigma_T\cos^2\theta \right] \right\} \quad \text{(A-22a)}$$

$$C_{D_{rear}} = \left\{ \frac{e^{-s^2\sin^2\theta}}{\sqrt{\pi}\, s} \left[(2-\sigma_N)\sin^2\theta - \frac{\sigma_N}{2s}\sin\theta\sqrt{\pi}\sqrt{\frac{T_{N_{rear}}}{T_i}} + \sigma_T\cos^2\theta \right] \right.$$

$$\left. - (1-\operatorname{erf} s\sin\theta)\sin\theta \left[(2-\sigma_N)\left(\sin^2\theta + \frac{1}{2s^2}\right) - \frac{\sigma_N}{2s}\sqrt{\pi}\sin\theta\sqrt{\frac{T_{N_{rear}}}{T_i}} + \sigma_T\cos^2\theta \right] \right\} \quad \text{(A-22b)}$$

$$C_D = C_{D_{Front}} + C_{D_{rear}}$$

$$\therefore \quad C_D = \frac{e^{-s^2\sin^2\theta}}{\sqrt{\pi}\, s}\left[2(2-\sigma_N)\sin^2\theta + 2\sigma_T\cos^2\theta\right] + \frac{\sigma_N}{s}\sqrt{\pi}\sin^2\theta\sqrt{\frac{T_w}{T_i}}$$

$$+\left[\operatorname{erf}(s\sin\theta)\right]\sin\theta\left[2(2-\sigma_N)\left(\sin^2\theta + \frac{1}{2s^2}\right) + 2\sigma_T\cos^2\theta\right] \qquad \text{(A-23)}$$

Drag of a Sphere

The expression for the drag force exerted on an element of area dA when both of its sides are exposed to the flow is (from Eq. A-23)

$$D = \tfrac{1}{2}\rho_i V^2 dA\left\{\frac{e^{-s^2\sin^2\theta}}{\sqrt{\pi}\, s}\left[2(2-\sigma_N)\sin^2\theta + 2\sigma_T\cos^2\theta\right] + \frac{\sigma_N}{s}\sqrt{\pi}\sin^2\theta\sqrt{\frac{T_w}{T_i}}\right.$$

$$\left. + \left[\operatorname{erf}(s\sin\theta)\right]\sin\theta\left[2(2-\sigma_N)\left(\sin^2\theta + \frac{1}{2s^2}\right) + 2\sigma_T\cos^2\theta\right]\right\} \qquad \text{(A-24)}$$

This expression can be integrated over the surface of the sphere to obtain the drag of a sphere. In general, if the surface of the body is a non-conducting material the temperature T_w will vary from one surface element to another. In the special case where the body is a perfect conductor, so that T_w is constant over the surface, Equation (A-24) may be integrated over all surface elements.

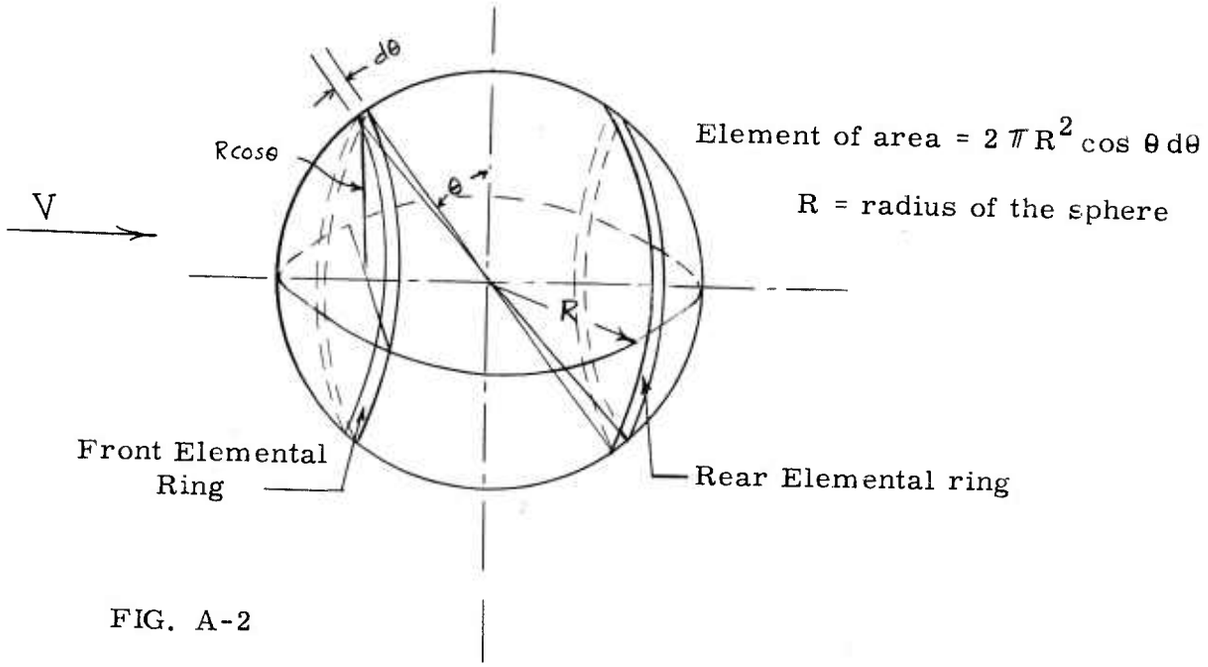

FIG. A-2

Thus

$$\frac{D}{\frac{1}{2}\rho_i V^2} = \int_0^{\pi/2} 2\pi R^2 \cos\theta \, d\theta \left\{ \frac{e^{-s^2\sin^2\theta}}{\sqrt{\pi}\, s} \left[2(2-\sigma_N)\sin^2\theta + 2\sigma_T \cos^2\theta \right] + \frac{\sigma_N}{s}\sqrt{\pi}\sin^2\theta \sqrt{\frac{T_w}{T_i}} \right.$$
$$\left. + \operatorname{erf}(s\sin\theta)\, \sin\theta \left[2(2-\sigma_N)\left(\sin^2\theta + \frac{1}{2s^2}\right) + 2\sigma_T\cos^2\theta \right] \right\}$$

$$= 2\pi R^2 \left\{ \frac{(2-\sigma_N+\sigma_T)(4s^4+4s^2-1)}{8s^4} \operatorname{erf} s + \frac{2-\sigma_N+\sigma_T}{2\sqrt{\pi}\, s^3}\left(\frac{1}{2}+s^2\right)e^{-s^2} \right.$$
$$\left. + \frac{\sigma_N}{3s}\sqrt{\pi}\sqrt{\frac{T_w}{T_i}} \right\}$$

The projected area of sphere = πR^2

$$\therefore \quad C_{D\,\text{sphere}} = \frac{2-\sigma_N+\sigma_T}{s^3}\left\{ \frac{4s^4+4s^2-1}{4s}\operatorname{erf} s + \frac{e^{-s^2}}{\sqrt{\pi}}\left(s^2+\frac{1}{2}\right) \right\} + \frac{2}{3}\frac{\sigma_N}{s}\sqrt{\pi}\sqrt{\frac{T_w}{T_i}} \qquad \text{(A-25)}$$

For diffuse reflection $\sigma_N = \sigma_T = 1$

$$C_{D\,\text{sphere}}\ \text{diffuse} = \frac{2}{s^3}\left\{ \frac{4s^4+4s^2-1}{4s}\operatorname{erf} s + \frac{e^{-s^2}}{\sqrt{\pi}}\left(s^2+\frac{1}{2}\right) + \frac{2}{3s}\sqrt{\pi}\sqrt{\frac{T_w}{T_i}} \right\} \qquad \text{(A-26)}$$

For specular reflection $\sigma_N = \sigma_T = 0$

$$C_{D\,\text{sphere}}\ \text{specular} = \frac{2}{s^3}\left\{ \frac{4s^4+4s^2-1}{4s}\operatorname{erf} s + \frac{e^{-s^2}}{\sqrt{\pi}}\left(s^2+\frac{1}{2}\right) \right\} \qquad \text{(A-27)}$$

Drag of a Cylinder Transverse to the Flow

Assuming again that the cylinder is a perfect conductor and hence T_w is constant over the whole surface the expression for the drag on an element dA given by the Equation (A. 24) can be integrated over the surface of the cylinder.

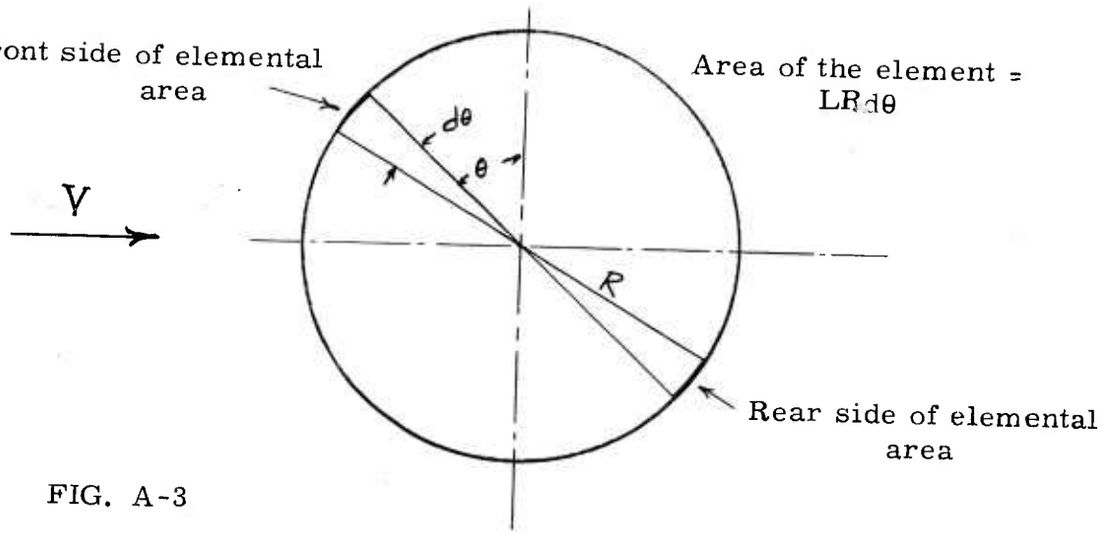

FIG. A-3

$$D_{cylinder} = \frac{\rho_i V^2}{2} L R \; 2 \int_0^{\pi/2} \left\{ \frac{e^{-s^2\sin^2\theta}}{\sqrt{\pi}\, s} \left[2(2-\sigma_N)\sin^2\theta + 2\sigma_T \cos^2\theta \right] + \frac{\sigma_N}{s} \sqrt{\pi} \sin^2\theta \sqrt{\frac{T_N}{T_i}} + \operatorname{erf}(s\sin\theta) \sin\theta \left[2(2-\sigma_N)\left(\sin^2\theta + \frac{1}{2s^2}\right) + 2\sigma_T \cos^2\theta \right] \right\} d\theta$$

The values of the integrals encountered are given in Ref. 14. The result is

$$D = \frac{1}{2}\rho_i V^2 2LR \left[\frac{\sigma_N}{4s} \sqrt{\frac{T_N}{T_i}}\, \pi^{3/2} + \frac{e^{-\frac{s^2}{2}} \sqrt{\pi}}{s} \left\{ (4 - 2\sigma_N + \sigma_T)\left(\frac{1}{2} + \frac{s^2}{3}\right) I_0\left(\frac{s^2}{2}\right) + (4 - 2\sigma_N + \sigma_T)\left(\frac{1}{6} + \frac{s^2}{3}\right) I_1\left(\frac{s^2}{2}\right) \right\} \right]$$

$$C_D = \frac{D}{\frac{1}{2}\rho_i V^2 2LR} \; ; \quad 2LR = \text{projected area of cylinder} \qquad \text{(A-28)}$$

where

$I_0\left(\frac{s^2}{2}\right)$ = modified Bessel function of first kind and zero order.

$I_1\left(\frac{s^2}{2}\right)$ = modified Bessel function of first kind and first order

For diffuse reflection $\sigma_N = \sigma_T = 1$

$$C_D \text{ diffuse} = \frac{\pi^{3/2}}{4s}\sqrt{\frac{T_N}{T_i}} + \frac{3e^{-\frac{s^2}{2}}\sqrt{\pi}}{s}\left[\left(\frac{1}{2}+\frac{s^2}{3}\right)I_0\left(\frac{s^2}{2}\right)+\left(\frac{1}{6}+\frac{s^2}{3}\right)I_1\left(\frac{s^2}{2}\right)\right] \quad (A-29)$$

For specular reflection $\sigma_N = \sigma_T = 0$

$$= \frac{4e^{-\frac{s^2}{2}}\cdot\sqrt{\pi}}{s}\left[\left(\frac{1}{2}+\frac{s^2}{3}\right)I_0\left(\frac{s^2}{2}\right)+\left(\frac{1}{6}+\frac{s^2}{3}\right)I_1\left(\frac{s^2}{2}\right)\right] \quad (A-30)$$

Energy Exhange

The aerodynamic forces on an element (in free molecule flow) due to the reflected stream of molecules depend on the wall temperature T_W. This value of T_W depends upon the efficiency of the energy transfer process that occurs between the solid surface and impinging stream and is described by the introduction of the thermal accommodation coefficient α (Eq. A-1)

$$\alpha = \frac{dE_i - dE_r}{dE_i - dE_W}$$

If dQ is the net convective heat transfer to the surface then

$$dQ = dE_i - dE_r$$

dE_i = incident energy, both translation and internal. α is assumed to be constant for both kinds of energy transfer

$$\therefore \quad dQ = \alpha(dE_i - dE_W)$$

Incident Energy on an Element of Area dA

The translational energy incident on the front side of an element in unit time is

$$\left(dE_{i_{tran}}\right)_{front} = \frac{1}{2}m\int_0^{\infty}\int_{-\infty}^{+\infty}\int_{-\infty}^{+\infty} n_i \xi^2 \xi_1 f(\xi_1,\xi_2,\xi_3)\, d\xi_1 d\xi_2 d\xi_3\, dA$$

$$= \frac{\rho_i(RT_i)^{3/2}}{\sqrt{2\pi}}\cdot\left\{e^{-s^2\sin^2\theta}\left(s^2+2\right)+\sqrt{\pi}\,s\sin\theta\left(1+\text{erf}.\, s\sin\theta\right)\left(s^2+\frac{5}{2}\right)\right\}dA$$

If the gas is monatomic then the total incident energy is given by the above expressions. If the gas is composed of diatomic molecules then each molecule carries an additional amount of energy called the internal energy. By the principle of equipartition of energy the amount of internal energy carried by each molecules is $(j/2)m\,RT_i$;

where j is the number of degrees of freedom of motion. For air at normal temperatures $j \cong 2$. j is related to the ratio of specific heats γ by the relation

$$j = \frac{5-3\gamma}{\gamma-1}$$

Therefore the interal energy of molecules striking the front surface is

$$\left(dE_{i\,int}\right)_{front} = \frac{5-3\gamma}{\gamma-1}\,\frac{m}{2}\,RT_i\,N_{i_{front}}\,dA \quad \text{where} \quad N_{i\,front} \text{ is number of molecules striking dA in unit time}$$

$$N_{i_{front}} = \frac{n_i\sqrt{2RT_i}}{2\sqrt{\pi}}\left\{e^{-s^2\sin^2\theta} + \sqrt{\pi}\,s\sin\theta\,(1+\mathrm{erf}\,s\sin\theta)\right\}$$

$$\therefore \left(dE_{i\,int}\right)_{front} = \frac{5-3\gamma}{\gamma-1}\,\frac{m}{2}(RT_i)^{3/2}\frac{n_i}{\sqrt{2\pi}}\,dA\left\{e^{-s^2\sin^2\theta} + \sqrt{\pi}\,s\sin\theta\,(1+\mathrm{erf}\,s\sin\theta)\right\}$$

Thus the total incident energy on front surface is

$$\left(dE_i\right)_{front} = \frac{\rho_i(RT_i)^{3/2}}{\sqrt{2\pi}}dA\left\{e^{-s^2\sin^2\theta}\left(s^2+2+\tfrac{j}{2}\right) + \sqrt{\pi}\,s\sin\theta\,(1+\mathrm{erf}\,s\sin\theta)\left(s^2+\tfrac{5}{2}+\tfrac{j}{2}\right)\right\} \qquad \text{(A-31)}$$

Similarly for the rear surface

$$\left(dE_i\right)_{rear} = \frac{\rho_i(RT_i)^{3/2}}{\sqrt{2\pi}}dA\left\{e^{-s^2\sin^2\theta}\left(s^2+2+\tfrac{j}{2}\right) - \sqrt{\pi}\,s\sin\theta\,(1-\mathrm{erf}\,s\sin\theta)\left(s^2+\tfrac{5}{2}+\tfrac{j}{2}\right)\right\} \qquad \text{(A-32)}$$

Energy carried by the Reflected Stream

The energy dE_W carried by the reflected stream of molecules when in Maxwellian equilibrium with the surface, can be calculated in a similar manner. For the front surface

$$\left(dE_{W\,trans}\right)_{front} = \frac{1}{2}m\int_{-\infty}^{0}\int_{-\infty}^{+\infty}\int_{-\infty}^{+\infty} n_{W_{front}}\,\bar{C}^2 C_1\,f(C_1,C_2,C_3)\,dC_1\,dC_2\,dC_3\;dA$$

$$= \frac{2\rho_{W_{front}}(RT_{W_{front}})^{3/2}}{\sqrt{2\pi}}dA = \frac{2\rho_i R^{3/2}}{\sqrt{2\pi}}\,T_{W_{front}}\,T_i^{1/2}\,dA\left(e^{-s^2\sin^2\theta} + \sqrt{\pi}\,s\sin\theta(1+\mathrm{erf}\,s\sin\theta)\right)$$

$$\left(dE_{W\,int}\right)_{front} = \frac{j}{2}\,m\,RT_{W_{front}}\,N_{W_{front}}\,dA$$

$$= \frac{j\rho_i R^{3/2}}{2\sqrt{2\pi}}\,T_{W_{front}}\,T_i^{1/2}\,dA\left\{e^{-s^2\sin^2\theta} + \sqrt{\pi}\,s\sin\theta\,(1+\mathrm{erf}\,s\sin\theta)\right\}$$

Thus the total energy = $dE_{w_{front}}(tran) + dE_{w_{front}}(int) = dE_{w_{front}}$

$$= \left(2+\frac{\dot{\delta}}{2}\right)\frac{\rho_i R^{3/2} T_{w_{front}} \sqrt{T_i}\, dA}{\sqrt{2\pi}}\left[e^{-s^2\sin^2\theta} + \sqrt{\pi}\, s\sin\theta\,(1+\mathrm{erf}\, s\sin\theta)\right] \quad (A-33)$$

Similarly, for the rear surface

$$(dE_w)_{rear} = \left(2+\frac{\dot{\delta}}{2}\right)\frac{\rho_i R^{3/2} T_{w_{rear}} T_i^{1/2} dA}{\sqrt{2\pi}}\left[e^{-s^2\sin^2\theta} - \sqrt{\pi}\, s\sin\theta\,(1-\mathrm{erf}\, s\sin\theta)\right] \quad (A-34)$$

For specular reflection $\alpha = 0$ and hence there is no energy transfer. If $\alpha \neq 0$ and if there is no heat transfer ($dQ=0$) then the element will reach a temperature known as recovery or equilibrium temperature. This value can be determined by equating the incident energy to the reflected energy.

The following expressions thus derived give the ratio of equilibrium temperature to incident (free-stream) temperature.

Front surface of the element

$$\frac{(T_{w_{equi}})_{frnt}}{T_i} = \frac{1}{(2+\dot{\delta}/2)}\left\{\frac{e^{-s^2\sin^2\theta}\left(s^2+2+\dot{\delta}/2\right)+\sqrt{\pi}\, s\sin\theta\,(1+\mathrm{erf}\, s\sin\theta)\left(s^2+\frac{5}{2}+\frac{\dot{\delta}}{2}\right)}{e^{-s^2\sin^2\theta}+\sqrt{\pi}\, s\sin\theta\,(1+\mathrm{erf}\, s\sin\theta)}\right\}$$

Rear Surface of the element

$$\frac{(T_{w_{equi}})_{rear}}{T_i} = \frac{1}{(2+\dot{\delta}/2)}\left\{\frac{e^{-s^2\sin^2\theta}\left(s^2+2+\dot{\delta}/2\right)-\sqrt{\pi}\, s\sin\theta\,(1-\mathrm{erf}\, s\sin\theta)\left(s^2+\frac{5}{2}+\frac{\dot{\delta}}{2}\right)}{e^{-s^2\sin^2\theta}-\sqrt{\pi}\, s\sin\theta\,(1-\mathrm{erf}\, s\sin\theta)}\right\}$$

Front and rear surfaces in perfect thermal contact

$$\frac{T_{w_{equil}}}{T_i} = \frac{1}{(2+\dot{\delta}/2)}\left\{\frac{e^{-s^2\sin^2\theta}\left(s^2+2+\dot{\delta}/2\right)+\sqrt{\pi}\, s\sin\theta\,\mathrm{erf}(s\sin\theta)\left(s^2+5/2+\frac{\dot{\delta}}{2}\right)}{e^{-s^2\sin^2\theta}+\sqrt{\pi}\, s\sin\theta\,\mathrm{erf}\, s\sin\theta}\right\}$$

Equilibrium Temperature of a Sphere

If T_w is constant over the entire surface area then the expressions for total incident and reflected energies on an element can be integrated to obtain the equilibrium temperature of a sphere.

Incident energy on an element dA in unit time is

$$\frac{2\rho_i (RT_i)^{3/2} dA}{\sqrt{2\pi}}\left\{e^{-s^2\sin^2\theta}\left(s^2+2+\frac{\dot{\delta}}{2}\right)+\sqrt{\pi}\, s\sin\theta\,(1+\mathrm{erf}\, s\sin\theta)\left(s^2+\frac{5}{2}+\frac{\dot{\delta}}{2}\right)\right\}$$

The elemental area chosen for integration is the same as that used in the drag force calculations (see Fig. A-2)

$dA = 2\pi r^2 \cos\theta \, d\theta$ (r = radius of the sphere)

$$(E_i)_{sphere} = \frac{2\rho_i (RT_i)^{3/2}}{\sqrt{2\pi}} 2\pi r^2 \int_0^{\pi/2} \left\{ \left(s^2 + 2 + \frac{j}{2}\right) e^{-s^2 \sin^2\theta} \cos\theta \, d\theta + \sqrt{\pi} s \left(s^2 + \frac{5}{2} + \frac{j}{2}\right) \sin\theta \, (1 + \text{erf}\, s \sin\theta) \cos\theta \, d\theta \right\}$$

$$= \frac{\rho_i (RT_i)^{3/2}}{\sqrt{2\pi}} 2\pi r^2 \left\{ e^{-s^2} \left[s^2 + \frac{5}{2} + \frac{j}{2} \right] + \sqrt{\pi}\, \text{erf}\, s \left[s^3 + s\left(3 + \frac{j}{2}\right) + \frac{1}{s}\left(\frac{3}{4} + \frac{j}{4}\right) \right] \right\}$$

$$(E_w)_{sphere} = \frac{2(2 + j/2)}{\sqrt{2\pi}} \rho_i R^{3/2} T_{weqv} T_i^{1/2} (2\pi r^2) \int_0^{\pi/2} \left\{ e^{-s^2 \sin^2\theta} \cos\theta \, d\theta + \sqrt{\pi}\, s \sin\theta \cos\theta \, \text{erf}\, s \sin\theta \, d\theta \right\}$$

$$= \frac{2(2 + j/2)}{\sqrt{2\pi}} \rho_i R^{3/2} T_{weqv} T_i^{1/2} (2\pi r^2) \left\{ \frac{e^{-s^2}}{2} + \frac{\sqrt{\pi}}{2} \text{erf}\, s \left(s + \frac{1}{2s}\right) \right\}$$

But $E_i = E_w$ for no net heat transfer (adiabatic model)

$$\therefore \frac{T_{weqv}}{T_i} = \frac{1}{2 + j/2} \left\{ \frac{e^{-s^2}\left(s^2 + \frac{5}{2} + \frac{j}{2}\right) + \sqrt{\pi}\, \text{erf}\, s \left[s^3 + s\left(3 + \frac{j}{2}\right) + \frac{1}{s}\left(\frac{3}{4} + \frac{j}{4}\right) \right]}{e^{-s^2} + \sqrt{\pi}\, \text{erf}\, s \left(s + \frac{1}{2s}\right)} \right\}$$

For a monatomic gas $j = 0$, for diatomic gas $\frac{j}{2} = 1$

Table VI gives the theoretically calculated values of equilibrium temperature and drag coefficient (due to incident and diffusely reflected molecules) for a sphere in free molecule flow

Equilibrium Temperature of a Cylinder Transverse to the Flow

The element of area chosen for integration is shown in Fig. A-3). T_w is assumed constant over the entire surface of the cylinder.

dA = L. r. dθ where r = rad. of the cylinder, L = length.

$$E_i = \frac{2\rho_i (RT_i)^{3/2}}{\sqrt{2\pi}} (L \cdot r) \left\{ 2 \int_0^{\pi/2} e^{-s^2 \sin^2\theta} \left(s^2 + 2 + j/2\right) d\theta + 2 \int_0^{\pi/2} \sqrt{\pi}\, s \sin\theta\, \mathrm{erf}\, s\sin\theta \left(s^2 + \frac{s}{2} + \frac{j}{2}\right) d\theta \right\}$$

$$= \frac{2\rho_i (RT_i)^{3/2}}{\sqrt{2\pi}} (L \cdot r) \left\{ \pi e^{-s^2/2} \left[I_0\left(\frac{s^2}{2}\right)\left(s^4 + s^2\left(\frac{7}{2} + \frac{j}{2}\right) + 2 + \frac{j}{2}\right) + I_1\left(\frac{s^2}{2}\right)\left(s^4 + \frac{5s^2}{2} + \frac{js^2}{2}\right) \right] \right.$$

$$E_w = \frac{2(2 + j/2)}{\sqrt{2\pi}} \rho_i R^{3/2} T_{WEQU} T_i^{1/2} (L \cdot r) \left\{ 2 \int_0^{\pi/2} e^{-s^2 \sin^2\theta} d\theta + 2 \int_0^{\pi/2} \sqrt{\pi}\, s \sin\theta\, \mathrm{erf}\, s \sin\theta\, d\theta \right.$$

$$= \frac{2(2 + j/2)}{\sqrt{2\pi}} \rho_i R^{3/2} T_{WEQU} T_i^{1/2} (L \cdot r) \left\{ \pi e^{-s^2/2} \left[I_0(s^2/2)(s^2 + 1) + I_1\left(\frac{s^2}{2}\right) s^2 \right] \right\}$$

$E_i = E_w$ for no net heat loss.

$$\frac{T_{WEQU}}{T_i} = \frac{1}{2 + j/2} \left\{ \frac{I_0\left(\frac{s^2}{2}\right)\left[s^4 + s^2\left(\frac{7}{2} + \frac{j}{2}\right) + 2 + j/2\right] + I_1\left(\frac{s^2}{2}\right)\left(s^4 + \frac{5s^2}{2} + \frac{js^2}{2}\right)}{I_0\left(\frac{s^2}{2}\right)(s^2 + 1) + I_1\left(\frac{s^2}{2}\right) s^2} \right\}$$

Table V gives the theoretically calculated values of equilibrium temperature and drag coefficient (due to incident and diffusely reflected molecules) for a cylinder in free molecule flow

TABLE I

SPHERE AND SUPPORT ROD SIZES

Sphere Diameter (in.)	Support Rod Dia. (in.)	Rod. Dia. / Sphere Dia.
0.4375	0.028	0.064
0.3435	0.020	0.058
0.280	0.016	0.057
0.1875	0.014	0.075
0.125	0.012	0.096
0.0936	0.010	0.107
0.0625	0.008	0.128

Note: Supports used for cross-stream and tailsting supported models were of the same size.

TABLE II

CYLINDER DRAG DATA

Mach No. = 2 00 Mean Free Path ≈ 0. 049

Cylinder Dia. (in.)	Knudsen No.	C_D
0. 180	0. 270	2 01
0. 1475	0. 33	2. 06
0. 134	0. 363	2. 13
0. 109	0. 446	2. 16
0. 0953	0. 510	2. 23
0. 072	0. 676	2. 35
0. 065	0. 749	2. 34
0. 0486	1. 00	2. 51
0. 049	1. 00	2. 49
0. 0348	1. 40	2. 61
0. 0285	1. 71	2. 84
0. 0203	2 37	2. 92
0. 0203	2. 40	2. 95
0. 016	3. 05	2. 96
0. 016	3. 04	3. 04
0. 014	3 48	3 03
0. 010	4. 87	3. 06
0. 010	4. 87	3. 01
0. 008	6. 08	3. 01

TABLE III

SPHERE DRAG DATA

(a) Cross-Stream Support

Test Mach Number = 2.02; Mean Free Path = 0.0493"

Sphere Dia. (in.)	Reynolds No.	Knudsen No.	Pan Force (milligrams) Gross	Tare	Net Force on Sphere (milligrams)	C_D
0.4375	27.78	0.113	778.0	258.5	141.0	1.94
0.3435	21.81	0 143	559.3	226.9	90.4	2.02
0.280	17.78	0.176	587.5	355.0	62.8	2 11
0.1875	11 90	0.263	289.2	172.5	31.8	2.38
0.1875	11.90	0.263	306.7	193.2	30.8	2.31
0.125	7.94	0.394	227.4	171.6	15.3	2.57
0.0936	5.94	0.527	208.1	174.6	9.1	2.73
0.0625	3.97	0.789	202.1	186.6	4.2	2.84

TABLE III (cont'd)

SPHERE DRAG DATA

(b) Tailsting Support

Test Mach Number = 2.02 Mean Free Path = 0.0493"

Sphere Dia. (in.)	Reynolds No.	Knudsen No.	Pan Force (milligrams) Gross	Tare	Net Force on Sphere (milligrams)	C_D
0.4375	27.78	0.113	547.3	46.3	137.1	1.88
0.3435	21.81	0.164	398.5	61.3	91.6	2.04
0.280	17.78	0.176	263.8	35.1	62.1	2.08
0.1875	11.90	0.263	172.0	58.5	31.1	2.32
0.125	7.94	0.394	121.9	66.1	15.3	2.57
0.0936	5.94	0.527	74.8	41.2	9.2	2.75
0.0625	3.97	0.789	73.4	56.5	4.6	3.11
0.0625	3.97	0.789	63.0	45.4	4.76	3.20

TABLE 4

RECOVERY TEMPERATURE OF CYLINDER MODELS.

Stagnation Temperature = 85°F. Mach No. = 2.00

Cylinder Dia. (in.)	Knudsen No.	Temp. of the Model °F
0.180	0.27	104.5
0.147	0.33	105.0
0.134	0.36	106.5
0.109	0.45	111 0
0.095	0.51	115 0
0.072	0.68	116.5
0.065	0.75	115 0
0.049	1.00	125.5
0.035	1.39	125.0
0.029	1.71	126.0
0.020	2.38	123.0
0.016	3.05	131.0
0.014	3.48	127.8
0.010	4.87	126.0

TABLE V

EQUILIBRIUM TEMPERATURE AND DRAG OF A TRANSVERSE CYLINDER IN FREE MOLECULE FLOW

S	speed ratio
T_w	temp. of the cylinder
T_i	free stream temp.
$(\ )_{mon}$	monatomic gas
$(\ )_{dia}$	diatomic gas
C_{D_i}	drag coefficient due to incident molecules
$(C_{D_r})_{mon}$	drag coefficient due to reflected molecules (monatomic gas)
$(C_{D_i})_{dia}$	drag coefficient due to reflected molecules (diatomic gas)
$C_D = C_{D_i} + C_{D_r}$	total drag coefficient

Values were computed assuming that $\sigma_N = \sigma_T = 1$ (complete diffuse reflection) and that there be no heat transfer from the cylinder. (i. e, the cylinder is at equilibrium temperature)

$$T_w = T_{w\,equil.}$$

S	$\left[\frac{T_{w\,equi}}{T_i}\right]_{mon}$	$\left[\frac{T_{w\,equi}}{T_i}\right]_{dia}$	C_{D_i}	$(C_{D_r})_{mon}$	$(C_{D_r})_{dia}$
0.1	1.007	1.005	26.65	13.97	13.95
0.2	1.030	1.020	13.63	7.063	7.029
0.3	1.066	1.044	9.060	4.791	4.741
0.4	1.116	1.077	6.909	3.676	3.612
0.5	1.178	1.118	5.643	3.021	2.944
0.6	1.250	1.167	4.818	2.594	2.506
0.7	1.334	1.222	4.246	2.297	2.199
0.8	1.426	1.284	3.829	2.078	1.972
0.9	1.528	1.352	3.516	1.912	1.799
1.0	1.639	1.426	3.274	1.782	1.662
1.1	1.757	1.505	3.084	1.678	1.553
1.2	1.885	1.590	2.932	1.593	1.463
1.3	2.020	1.680	2.809	1.522	1.388
1.4	2.165	1.776	2.707	1.463	1.325
1.5	2.318	1.878	2.623	1.413	1.272

TABLE V cont'd

S	$\left[\frac{T_{w\,equi}}{T_i}\right]_{mon}$	$\left[\frac{T_{w\,equi}}{T_i}\right]_{dia}$	C_{D_i}	$(C_{D_r})_{mon}$	$(C_{D_r})_{dia}$
1.6	2.479	1.986	2.553	1.370	1.226
1.7	2.650	2.100	2.494	1.333	1.187
1.8	2.830	2.220	2.443	1.301	1.152
1.9	3.019	2.346	2.400	1.273	1.122
2.0	3.218	2.479	2.362	1.249	1.096
2.1	3.426	2.617	2.330	1.227	1.072
2.2	3.644	2.763	2.301	1.208	1.052
2.3	3.871	2.914	2.276	1.191	1.033
2.4	4.108	3.072	2.255	1.176	1.017
2.5	4.355	3.237	2.235	1.162	1.002
2.6	4.611	3.408	2.218	1.150	0.988
2.7	4.878	3.585	2.202	1.139	0.976
2.8	5.154	3.769	2.188	1.129	0.965
2.9	5.440	3.960	2.176	1.12	0.955
3.0	5.736	4.157	2.164	1.111	0.946
3.1	6.042	4.361	2.154	1.106	0.938
3.2	6.358	4.572	2.145	1.097	0.930
3.3	6.684	4.789	2.136	1.091	0.923
3.4	7.019	5.013	2.128	1.085	0.917
3.5	7.365	5.243	2.121	1.079	0.911
3.6	7.720	5.480	2.115	1.076	0.905
3.7	8.086	5.724	2.109	1.070	0.900
3.8	8.461	5.974	2.103	1.066	0.895
3.9	8.847	6.231	2.098	1.062	0.891

TABLE VI

EQUILIBRIUM TEMPERATURE AND DRAG OF A SPHERE IN FREE MOLECULE FLOW

S	speed ratio
T_w	temp. of the sphere
T_i	free stream temp.
$(\ )_{mon}$	monatomic gas
$(\ )_{dia}$	diatomic gas
C_{D_i}	drag coefficient due to incident molecules
$(C_{D_r})_{mon}$	drag coefficient due to reflected molecules (monatomic gas)
$(C_{D_r})_{dia}$	drag coefficient due to reflected molecules (diatomic gas)
$C_D = C_{D_i} + C_{D_r}$	total drag coefficient

Values were computed assuming that $\sigma_N = \sigma_T = 1$ (complete diffuse reflection) and that there be no heat transfer from the sphere (i.e., the sphere is at equilibrium temperature).

$$T_w = T_{w\,\text{equilibrium}}$$

S	$\left(\frac{T_{w\,equi}}{T_i}\right)_{mon}$	$\left(\frac{T_{w\,equi}}{T_i}\right)_{dia}$	C_{D_i}	$(C_{D_r})_{mon}$	$(C_{D_r})_{dia}$
0.1	1.0066	1.0044	30.091	11.856	11.842
0.2	1.0265	1.0177	15.167	5.986	5.9602
0.3	1.0593	1.0395	10.210	4.0539	4.0159
0.4	1.1046	1.0697	7.7606	3.1047	3.0553
0.5	1.1617	1.1078	6.3137	2.5472	2.4874
0.6	1.2302	1.1535	5.3672	2.1843	2.1151
0.7	1.3094	1.2063	4.7059	1.9316	1.854
0.8	1.3988	1.2659	4.2222	1.7469	1.6619
0.9	1.4981	1.3321	3.8562	1.6070	1.5153
1.0	1.6068	1.4046	3.5721	1.4979	1.4004
1.1	1.7248	1.4832	3.3469	1.4108	1.3082
1.2	1.8519	1.5679	3.1656	1.3400	1.2330

TABLE VI cont'd

S	$\left(\frac{T_{w\,equi}}{T_i}\right)_{mon}$	$\left(\frac{T_{w\,equi}}{T_i}\right)_{dia}$	C_{D_i}	$(C_{D_r})_{mon}$	$(C_{D_r})_{dia}$
1.3	1.9879	1.6586	3.0174	1.2816	1.1706
1.4	2.1330	1.7553	2.8949	1.2327	1.1182
1.5	2.2870	1.8580	2.7925	1.1913	1.0738
1.6	2.4502	1.9668	2.7062	1.1560	1.0357
1.7	2.6224	2.0816	2.6328	1.1256	1.0028
1.8	2.8039	2.2026	2.5700	1.0992	0.9743
1.9	2.9946	2.3297	2.5158	1.0762	0.9693
2.0	3.1947	2.4631	2.4688	1.0560	0.9273
2.1	3.4042	2.6028	2.4278	1.0382	0.9078
2.2	3.6233	2.7488	2.3919	1.0224	0.8905
2.3	3.8519	2.9012	2.3602	1.0083	0.8751
2.4	4.0901	3.0601	2.3321	0.9957	0.8613
2.5	4.3380	3.2253	2.3072	0.9844	0.8489
2.6	4.5956	3.3970	2.2849	0.9743	0.8377
2.7	4.8629	3.5753	2.2649	0.9651	0.8275
2.8	5.40	3.760	2.2469	0.9568	0.8183
2.9	5.4269	3.9513	2.2307	0.9692	0.8099
3.0	5.7237	4.1491	2.2160	0.9623	0.8023
3.1	6.0303	4.354	2.2027	0.9360	0.7953
3.2	6.3467	4.5645	2.1905	0.9303	0.7889
3.3	6.6731	4.7820	2.1794	0.9250	0.7830
3.4	7.0093	5.0062	2.1693	0.9201	0.7776
3.5	7.3554	5.2369	2.1599	0.9156	0.7726
3.6	7.7114	5.4743	2.1513	0.9115	0.7680
3.7	8.0774	5.7183	2.1434	0.9077	0.7637
3.8	8.4533	5.9688	2.1361	0.9041	0.7597
3.9	8.8391	6.2261	2.1293	0.9008	0.7560
4.0	9.2348	6.4899	2.1230	.89771	0.7526
4.1	9.6406	6.7604	2.1172	0.8949	0.7494
4.2	10.0056	7.0375	2.1118	0.8922	0.7464
4.3	10.482	7.3212	2.1067	0.8897	0.7435
4.4	10.017	7.6116	2.1020	0.8873	0.7409
4.5	11.363	7.9086	2.0975	0.8852	0.7385
4.6	11.818	8.2123	2.0934	0.8831	0.7361
4.7	12.284	8.5226	2.0895	0.8812	0.7340
4.8	12.759	8.8396	2.0859	0.8793	0.7319
4.9	13.245	9.1632	2.0824	0.8776	0.7300
5.0	13.740	9.4935	2.0792	0.8760	0.7282

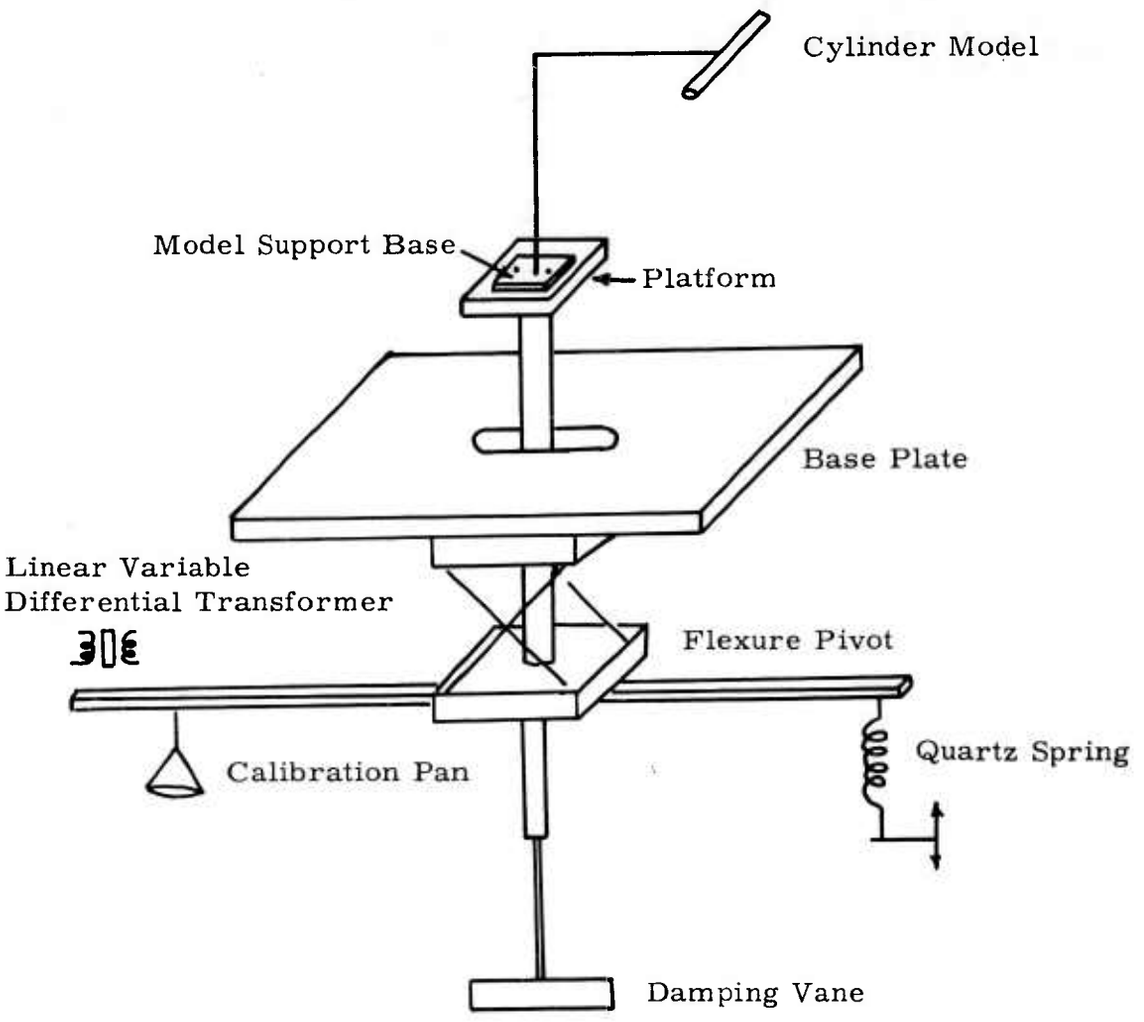

FIG. 1 SCHEMATIC DIAGRAM OF BALANCE

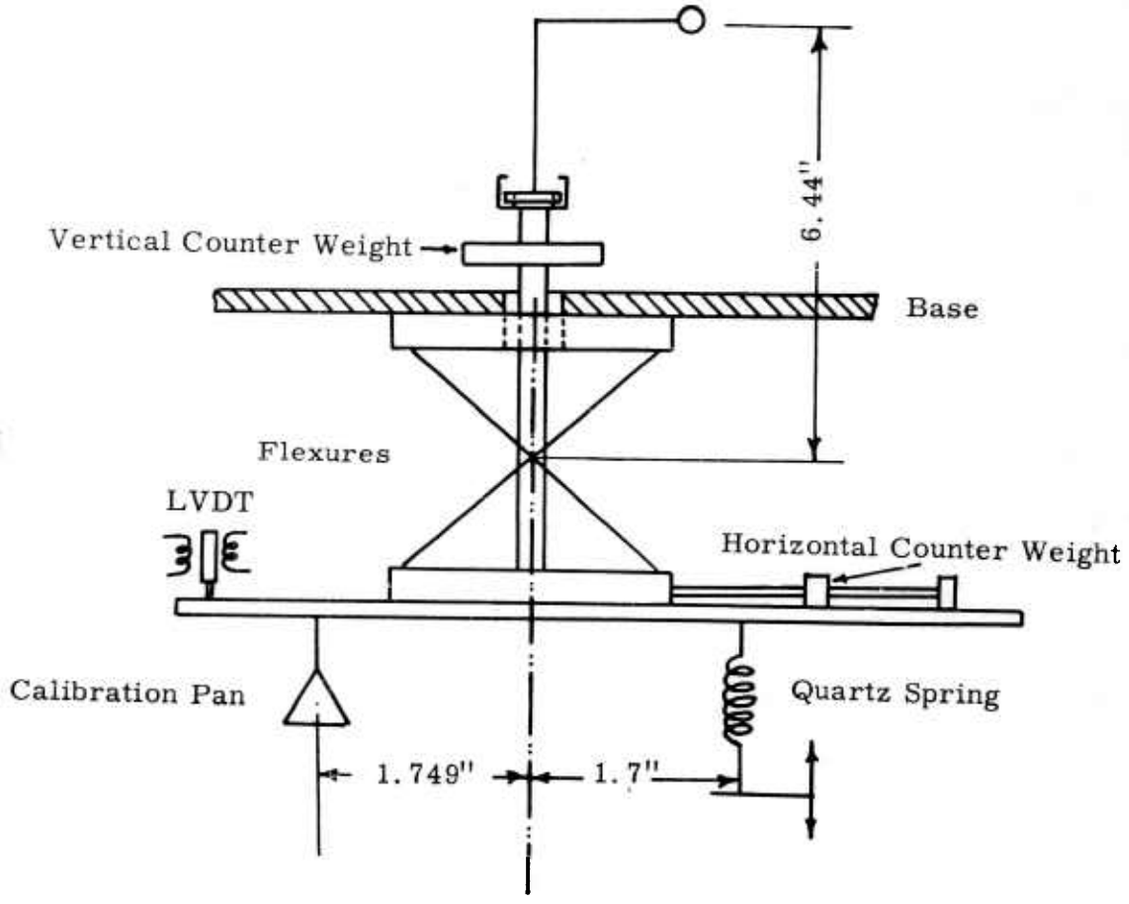

FIG. 2 SCHEMATIC OF BALANCE SHOWING LEVER ARM LENGTHS.

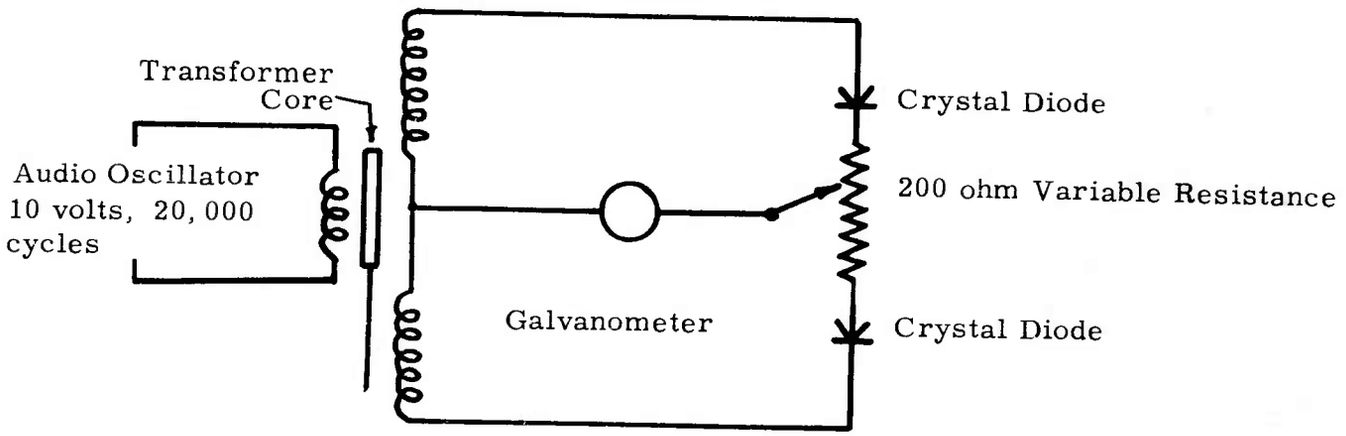

FIG. 3 WIRING DIAGRAM FOR LINEAR VARIABLE DIFFERENTIAL TRANSFORMER

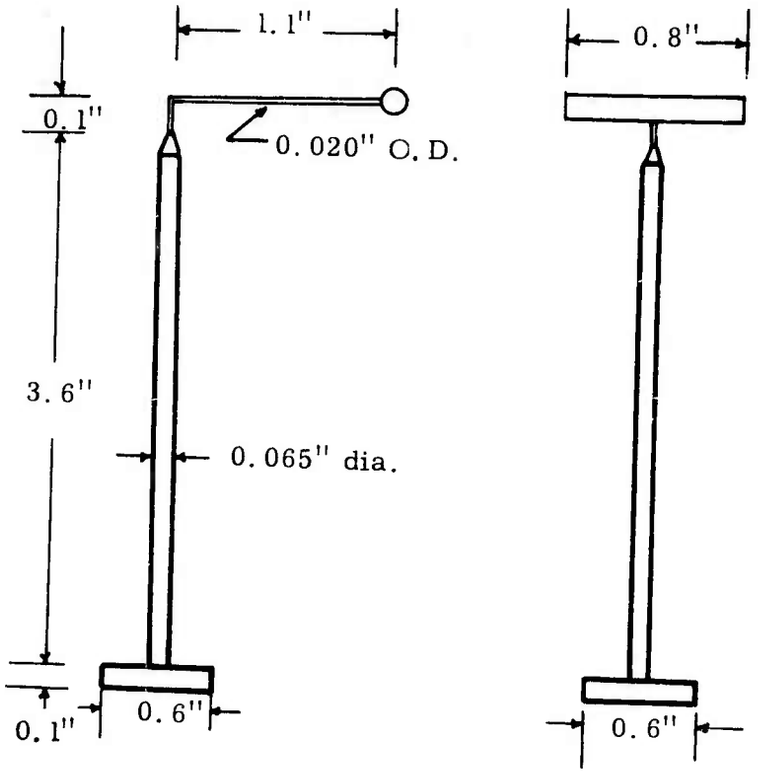

FIG. 4 DETAILS OF CYLINDER MODEL. MODEL AND SUPPORTING MOUNT MADE OUT OF STAINLESS STEEL HYPODERMIC TUBING. MODEL SILVER SOLDERED TO THE STING. DIAMETER OF THE MODEL VARIED FROM 0.008" to 0.180".

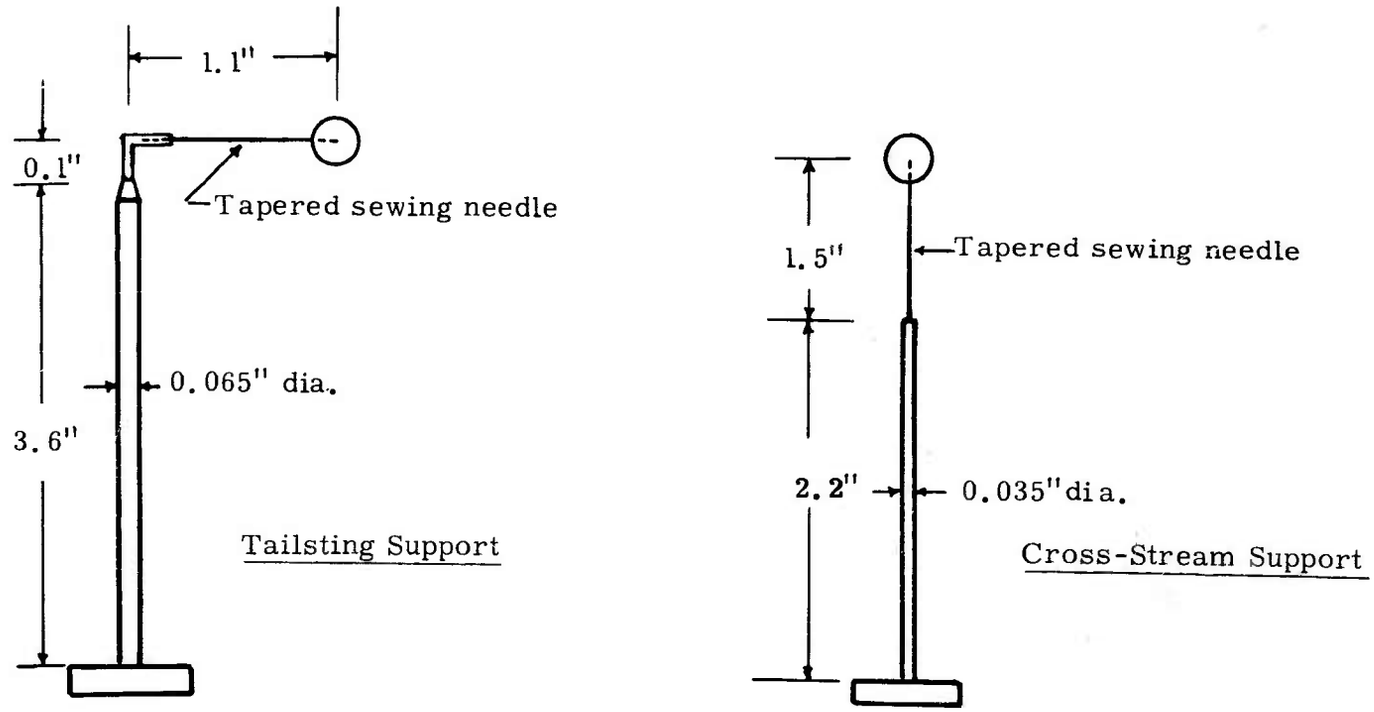

FIG. 5 DETAILS OF SPHERE MODELS. SPHERES PRESSED ON SEWING NEEDLE. DIAMETERS OF THE SPHERE VARIED FROM 0.0625" to 0.4375".

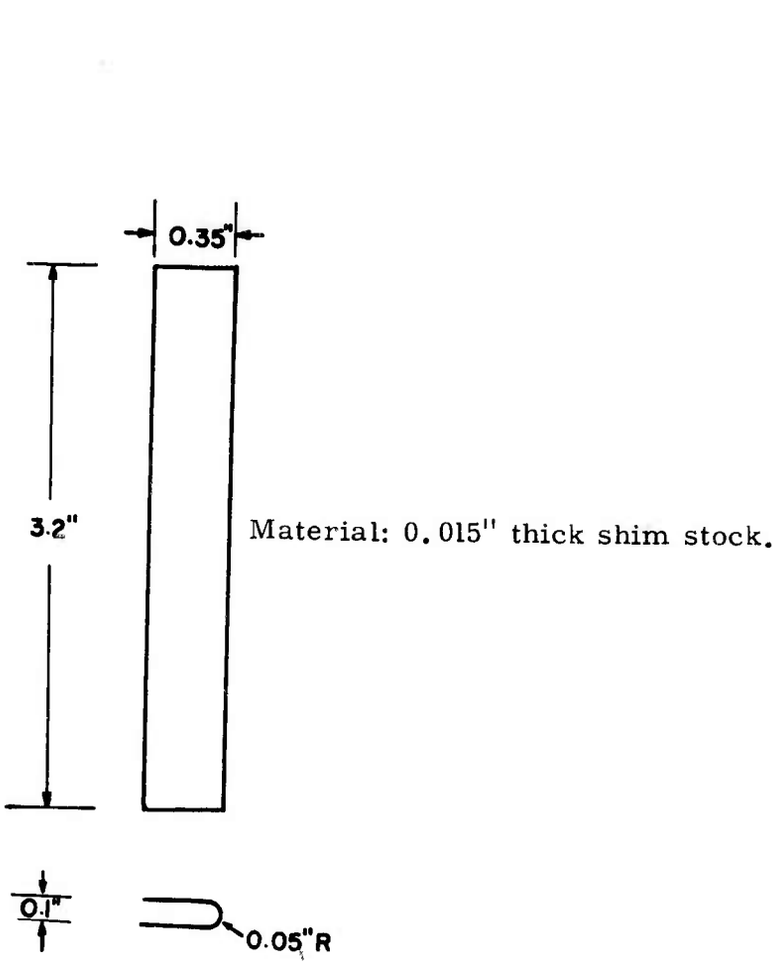

FIG. 6. DETAILS OF THE SHIELD.

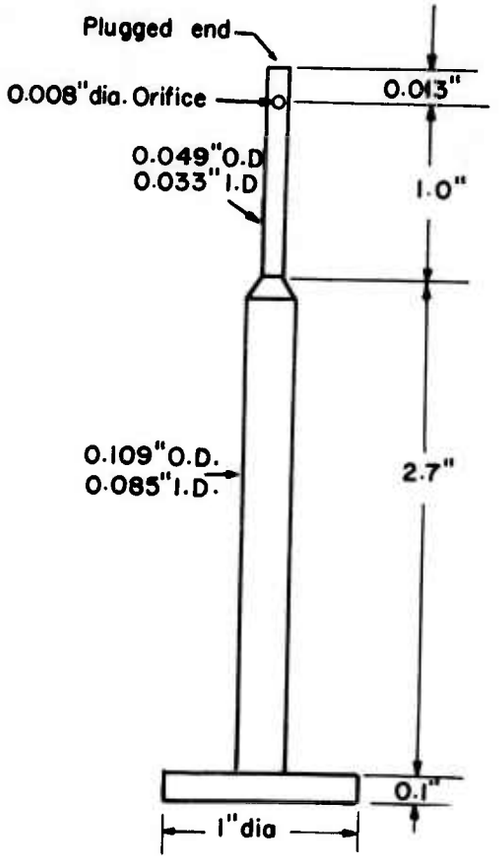

FIG. 7 GEOMETRY OF ORIFICE PROBE

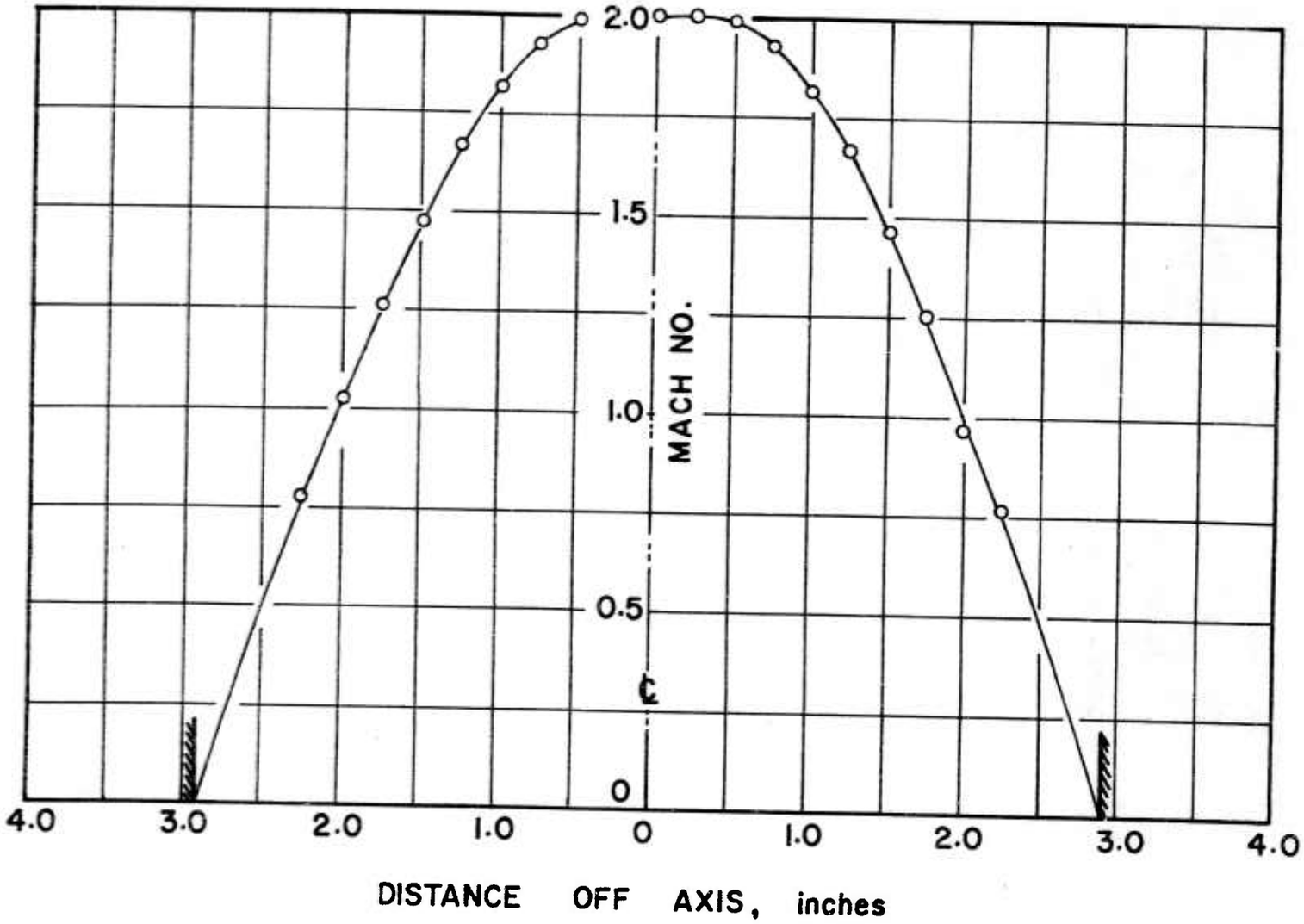

FIG. 8 MACH NUMBER PROFILE ACROSS THE PLANE $\frac{1}{4}$" FROM EXIT OF THE M = 2 NOZZLE AT DESIGN OPERATING CONDITIONS.

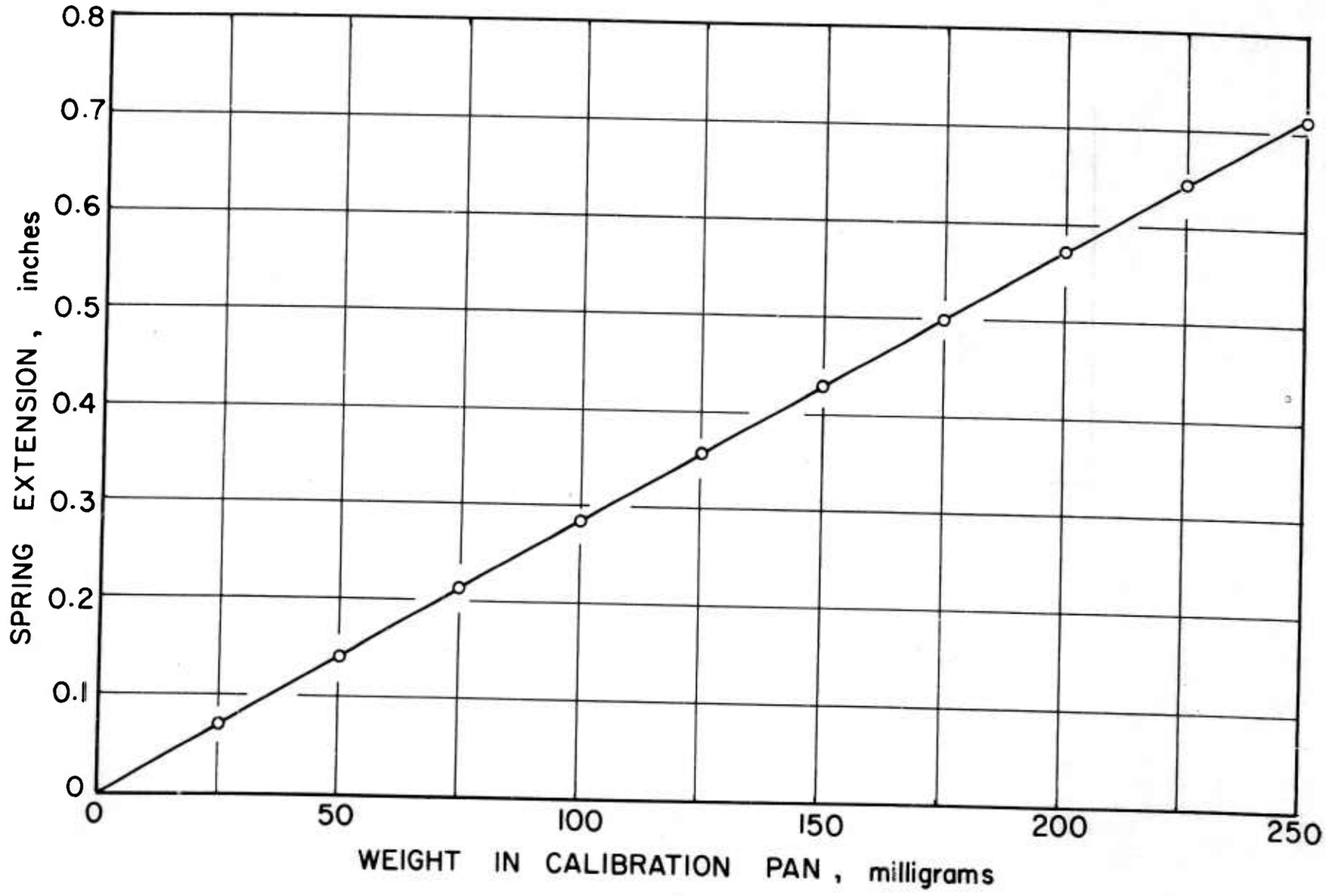

FIG. 9 TYPICAL CALIBRATION CURVE FOR DETERMINING THE SPRING CONSTANT OF THE QUARTZ SPRING.

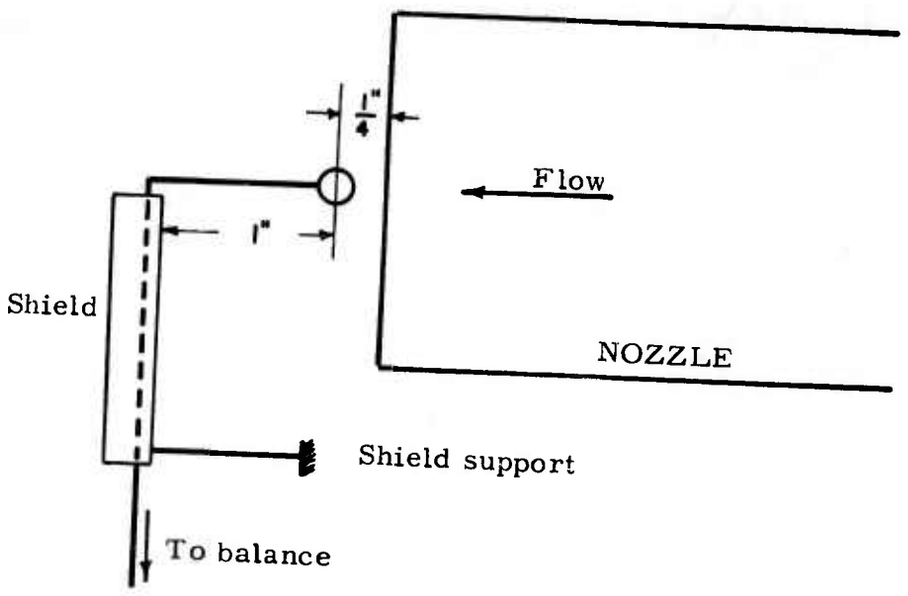

FIG. 10 POSITION OF THE SHIELD WITH RESPECT TO THE CYLINDER MODEL DURING RUN. SHIELD WAS USED TO COVER ONLY THE TRANSVERSE STING. (SIMILAR ARRANGEMENT USED FOR TAILSTING SUPPORTED SPHERE MODELS).

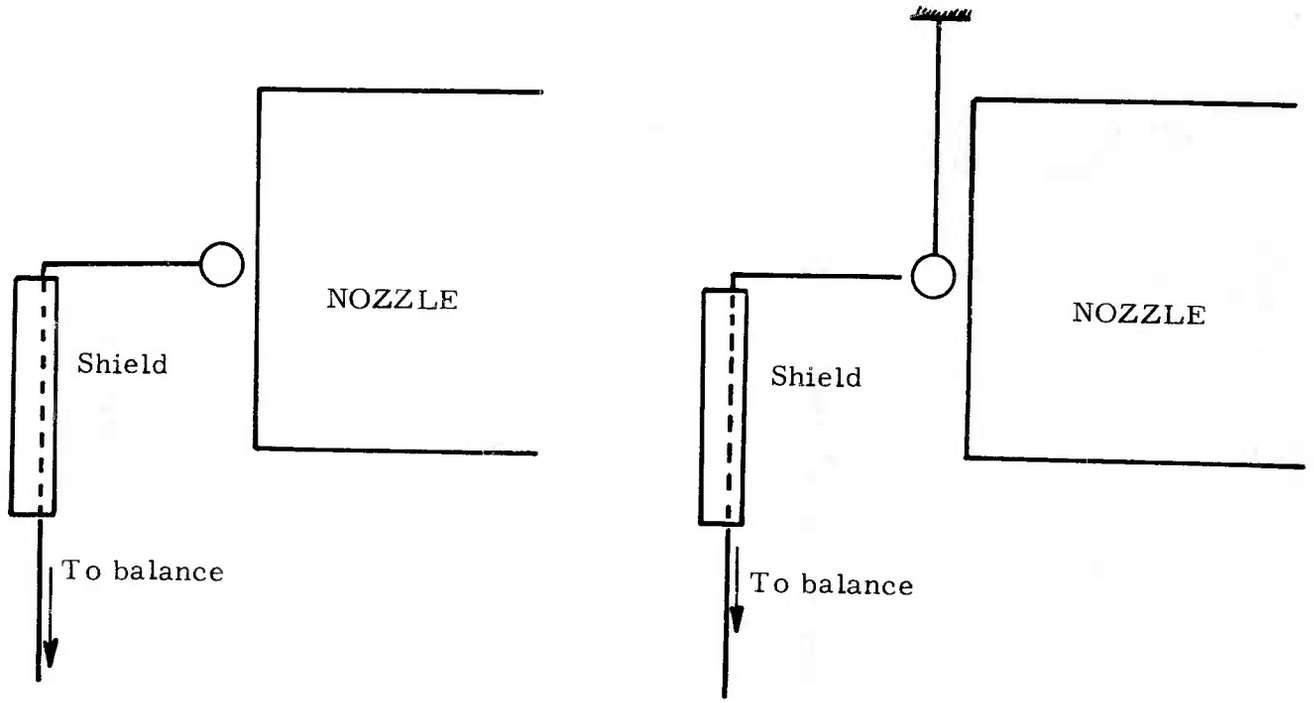

a) GROSS FORCE SET UP

b) TARE FORCE SET UP

FIG. 11 SKETCH OF SUPPORT FOR GROSS AND TARE FORCE MEASUREMENTS. SPHERE HELD BY A TAILSTING.

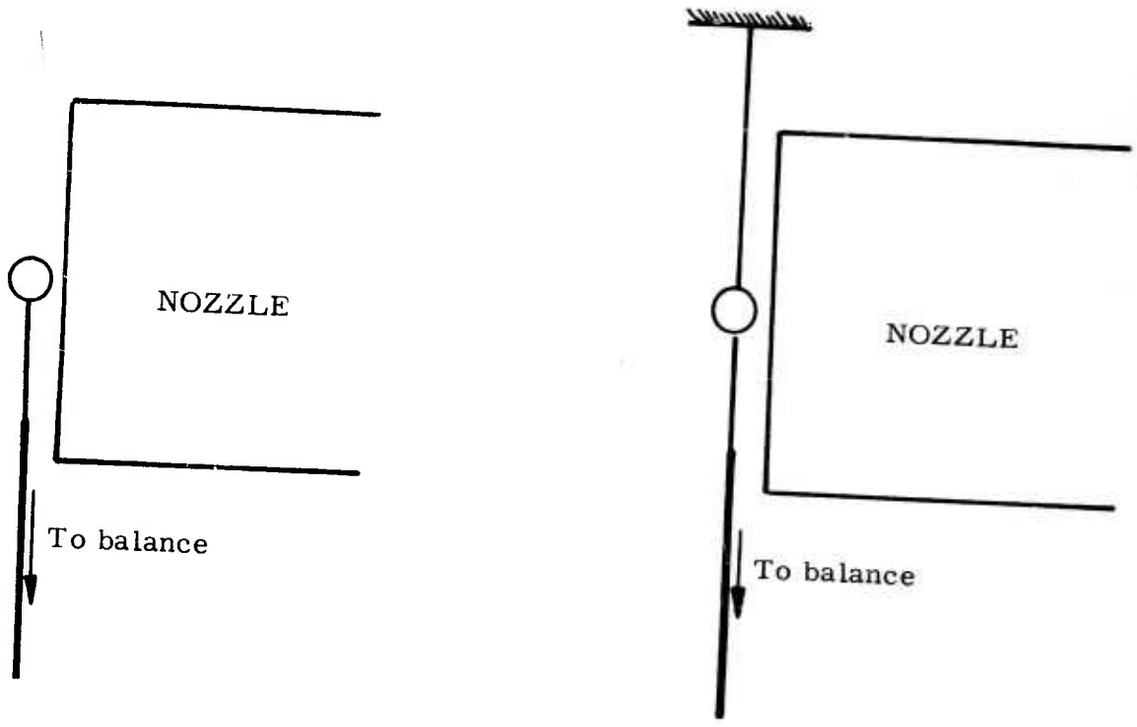

a) GROSS FORCE SET UP

b) TARE FORCE SET UP

FIG. 12 SKETCH OF SUPPORT FOR GROSS AND TARE FORCE MEASURMENTS. SPHERE HELD BY CROSS-STREAM SUPPORT

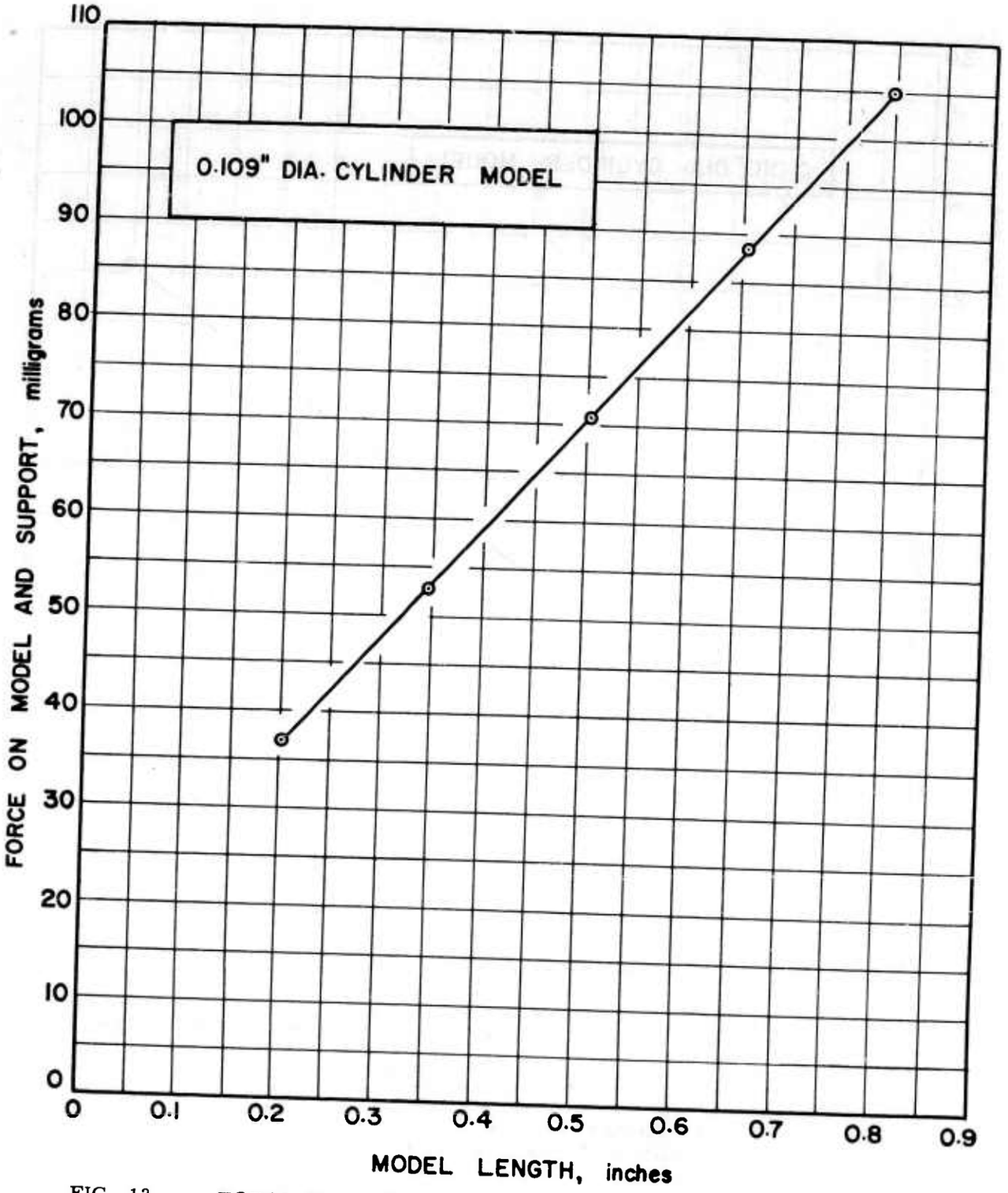

FIG. 13 TOTAL DRAG FORCE OF CYLINDRICAL MODEL AND SUPPORT AS A FUNCTION OF MODEL LENGTH.

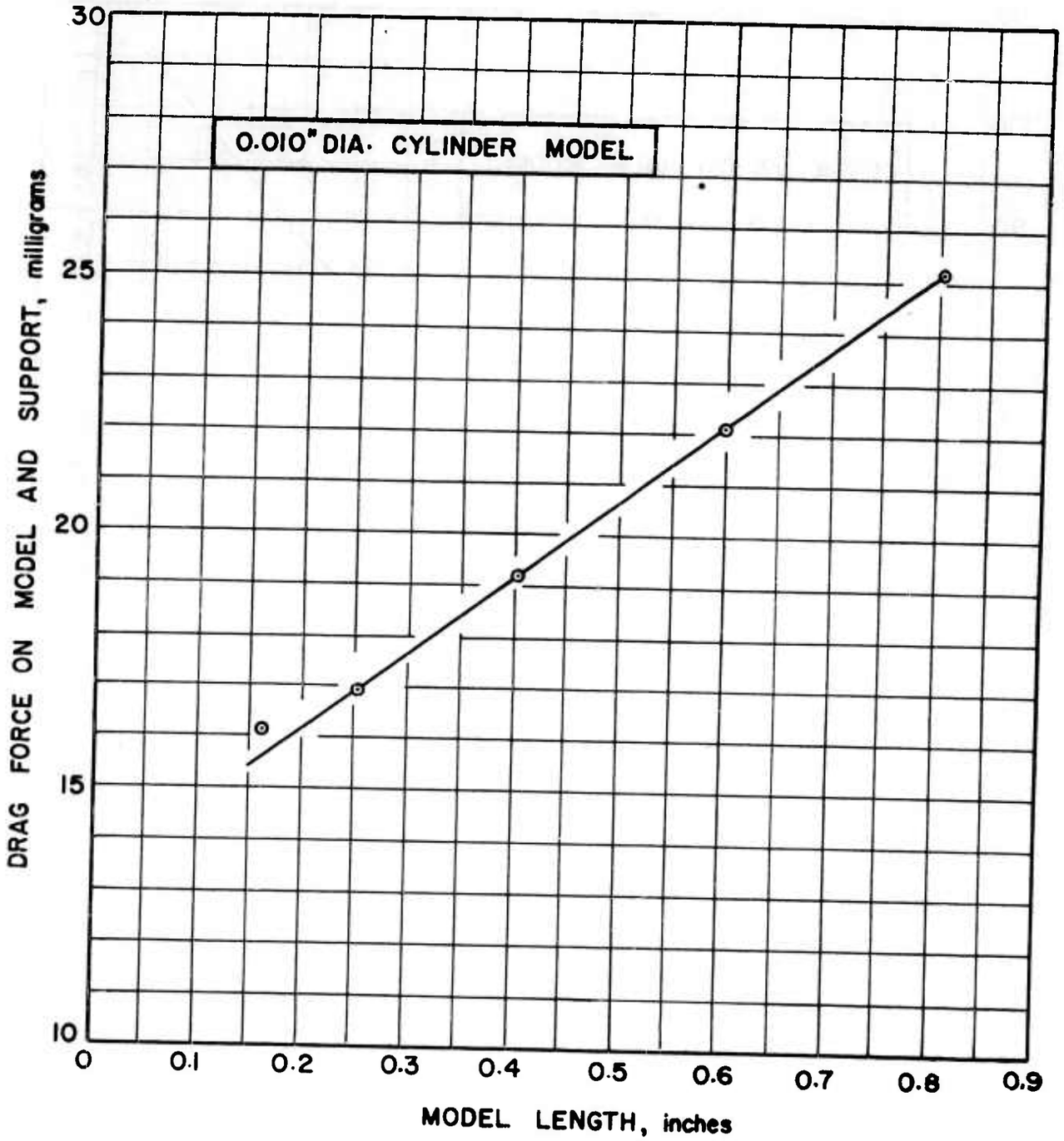

FIG. 14 TOTAL DRAG FORCE OF CYLINDRICAL MODEL AND SUPPORT AS A FUNCTION OF MODEL LENGTH.

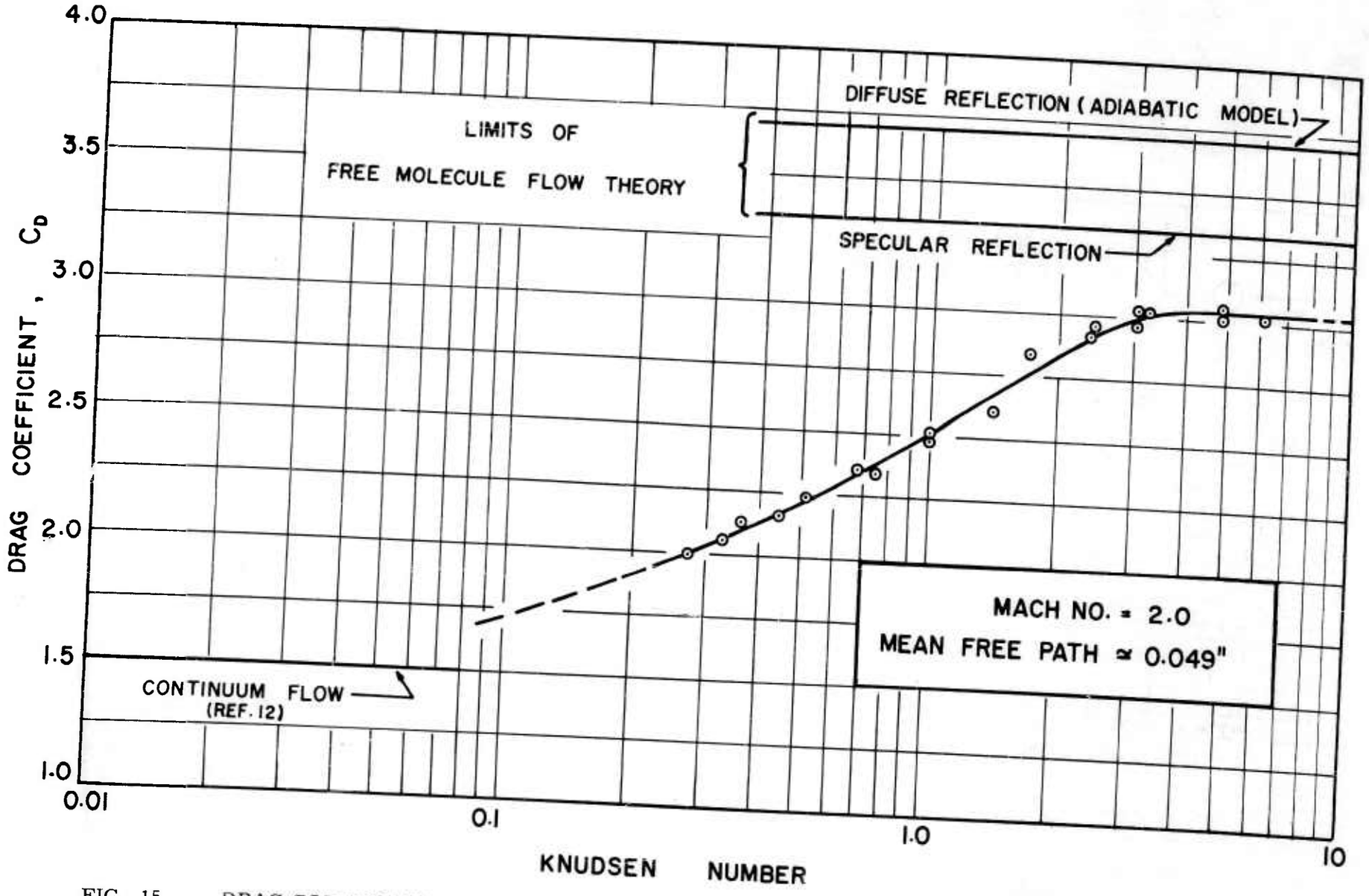

FIG. 15 DRAG COEFFICIENT OF RIGHT CIRCULAR CYLINDERS AS A FUNCTION OF KNUDSEN NUMBER (KNUDSEN NUMBER BASED ON CYLINDER DIAMETER).

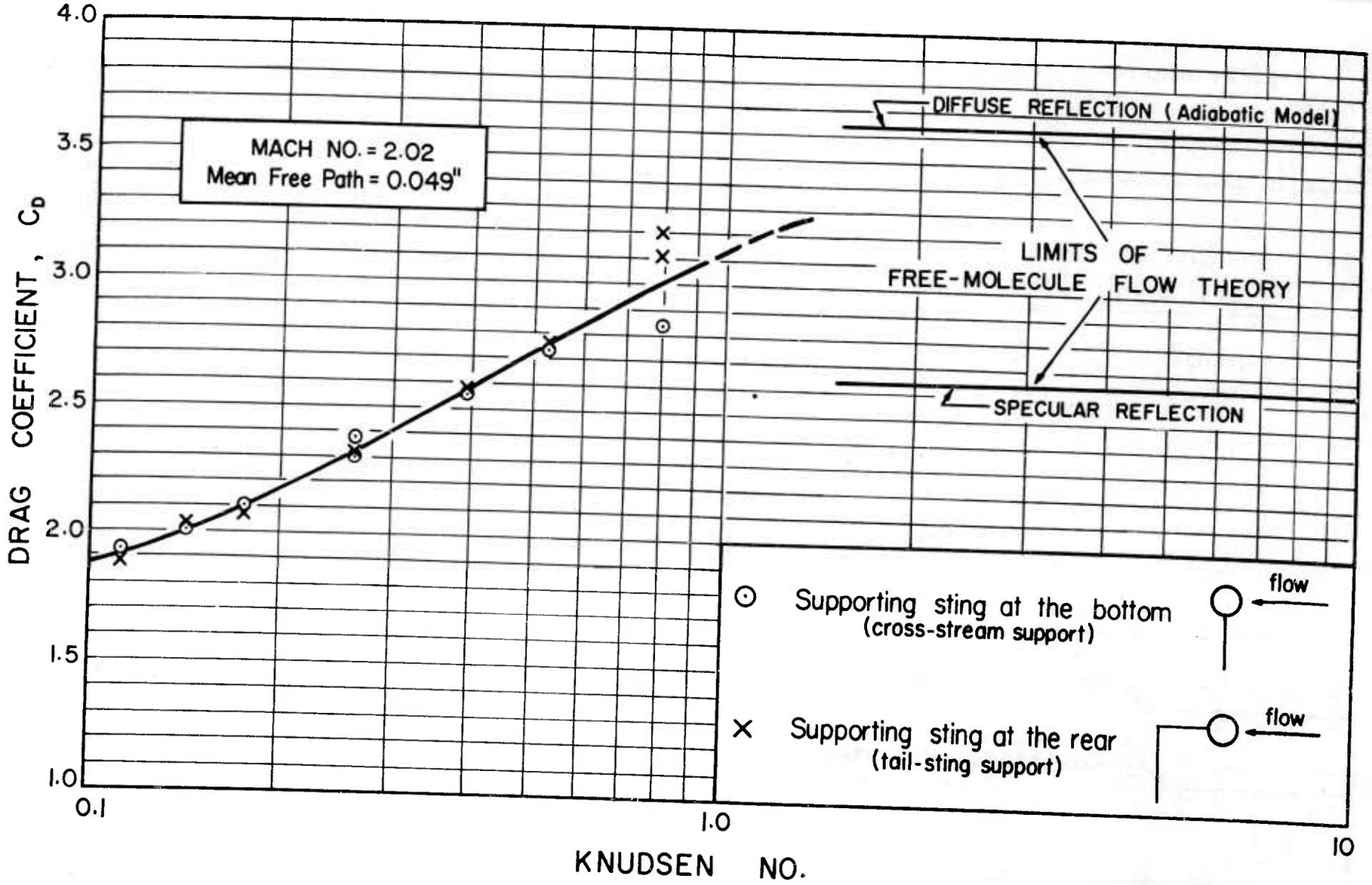

FIG. 16 DRAG COEFFICIENT OF SPHERES AS A FUNCTION OF KNUDSEN NUMBER (KNUDSEN NUMBER BASED ON SPHERE DIAMETER).

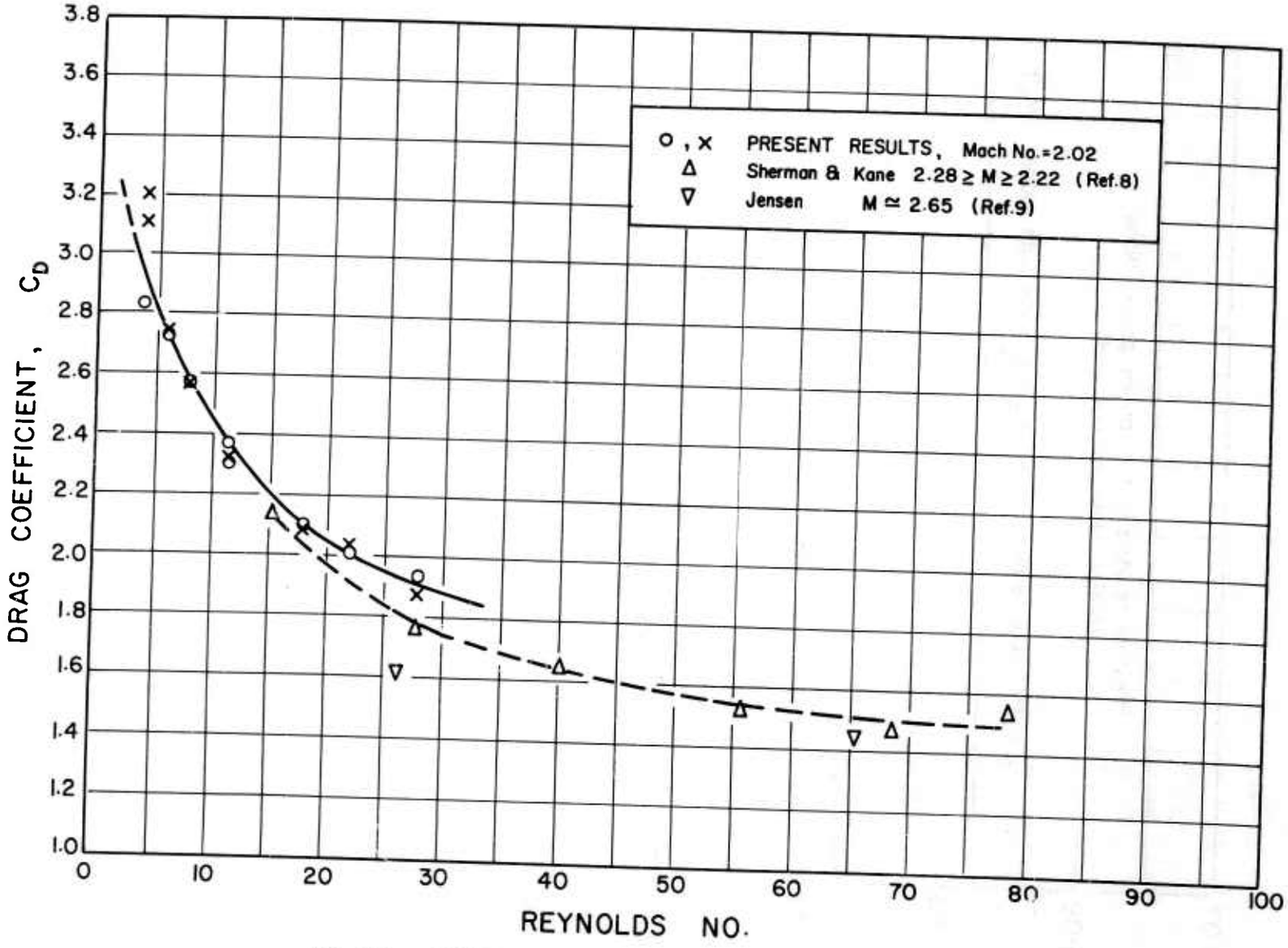

FIG. 17 DRAG COEFFICIENT OF A SPHERE AS A FUNCTION OF REYNOLDS NUMBER.

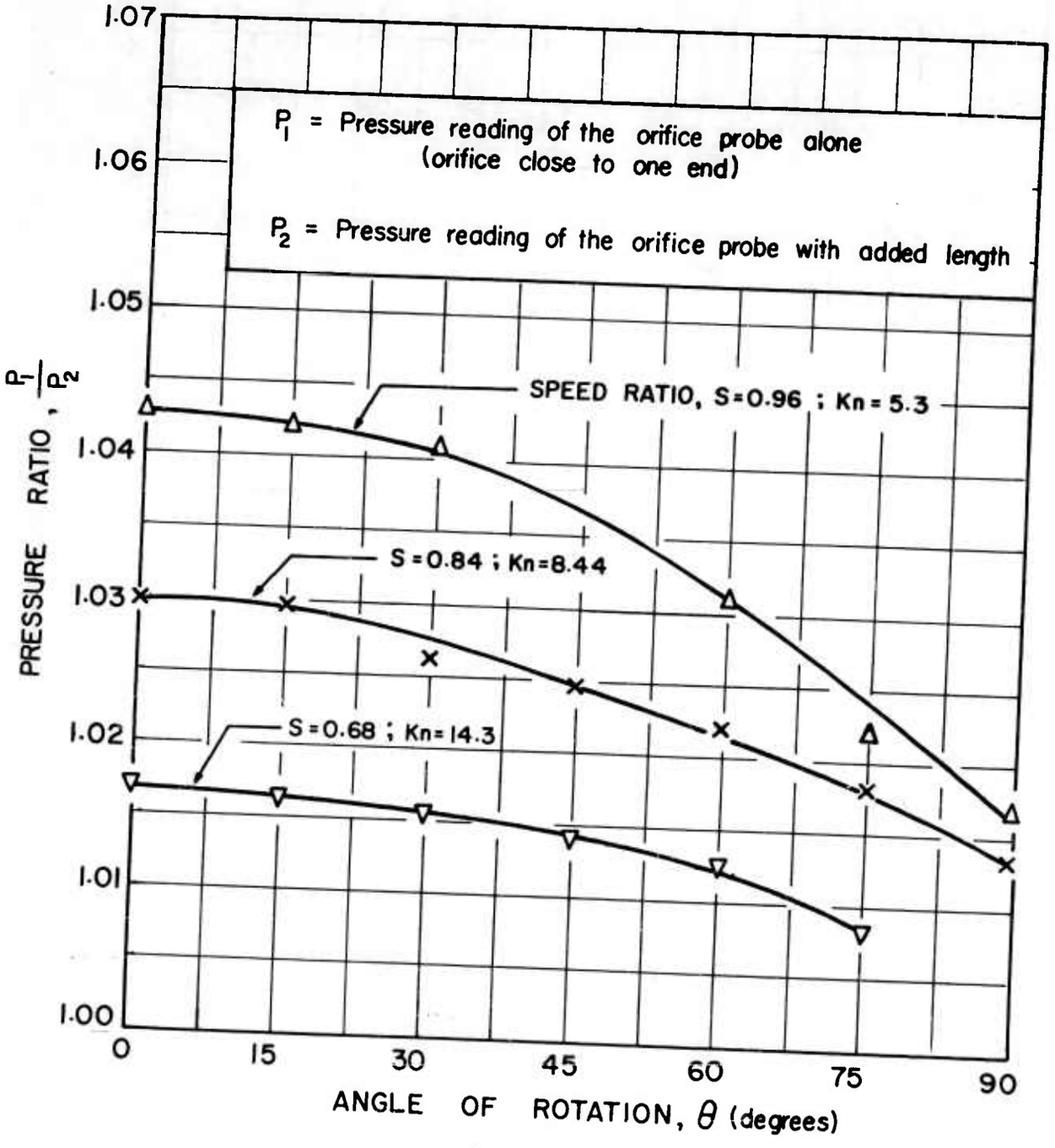

FIG. 18 RATIO OF PRESSURE READINGS WITH AND WITHOUT A DUMMY CYLINDER ON TOP OF THE PROBE OBTAINED BY ROTATING 0.049" DIAMETER ORIFICE PROBE IN SUBSONIC NOZZLE JET.

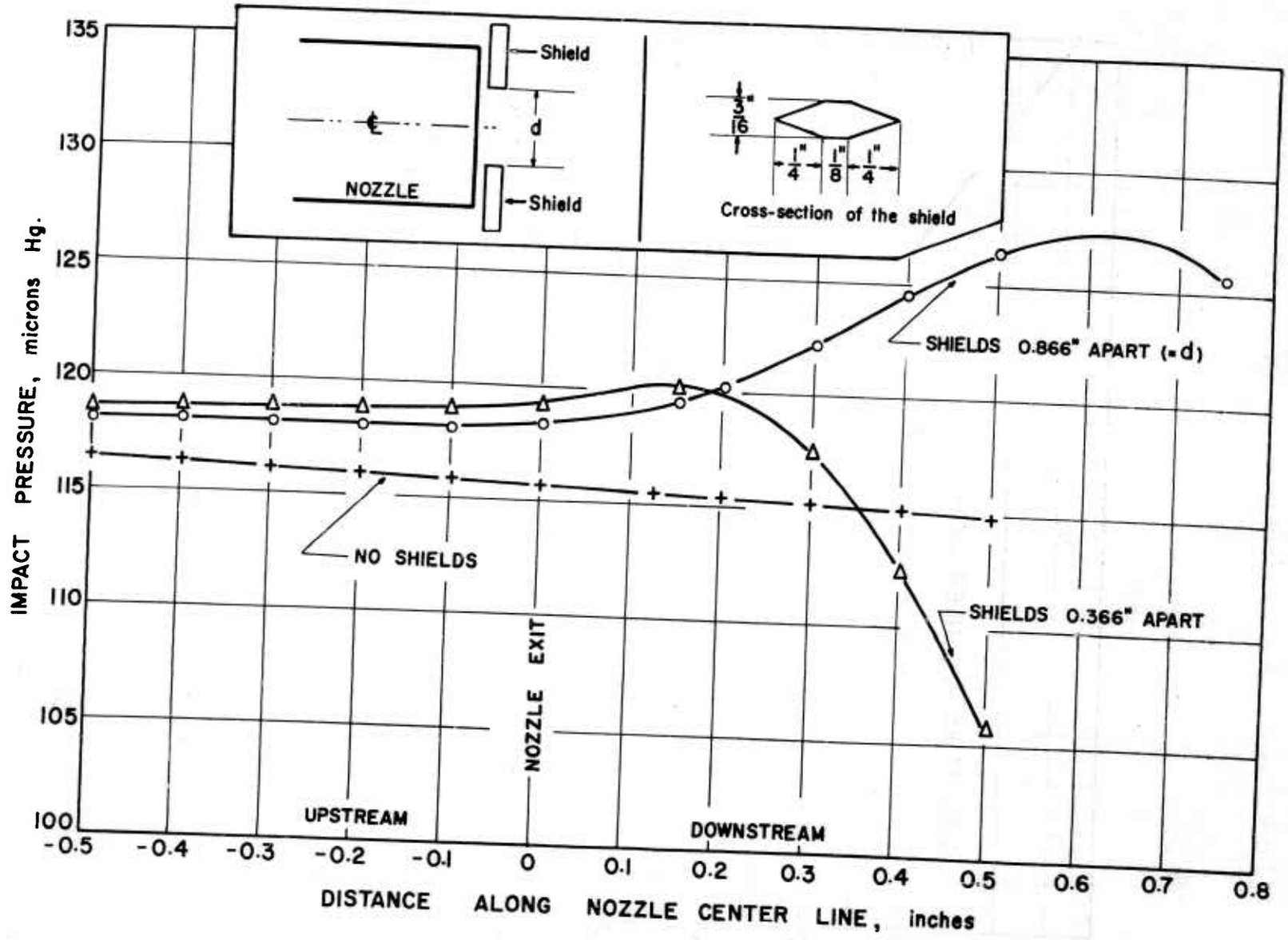

FIG. 19 IMPACT PROBE TRAVERSE ALONG THE CENTER LINE OF MACH 2 NOZZLE

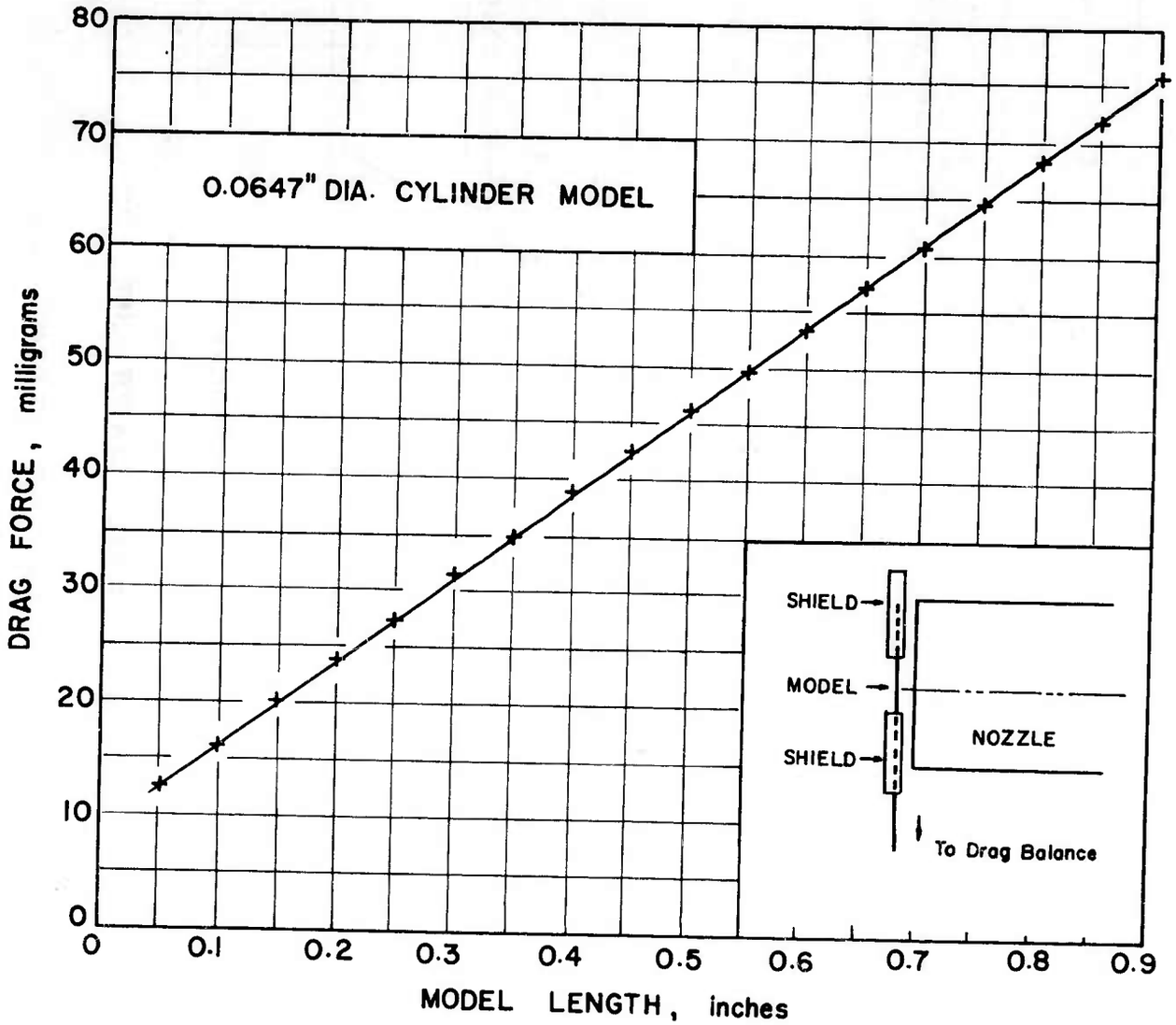

FIG. 20 DRAG FORCE OF A CYLINDER MODEL PLACED DOWNSTREAM OF THE SHIELDS AS A FUNCTION OF THE CYLINDER LENGTH.

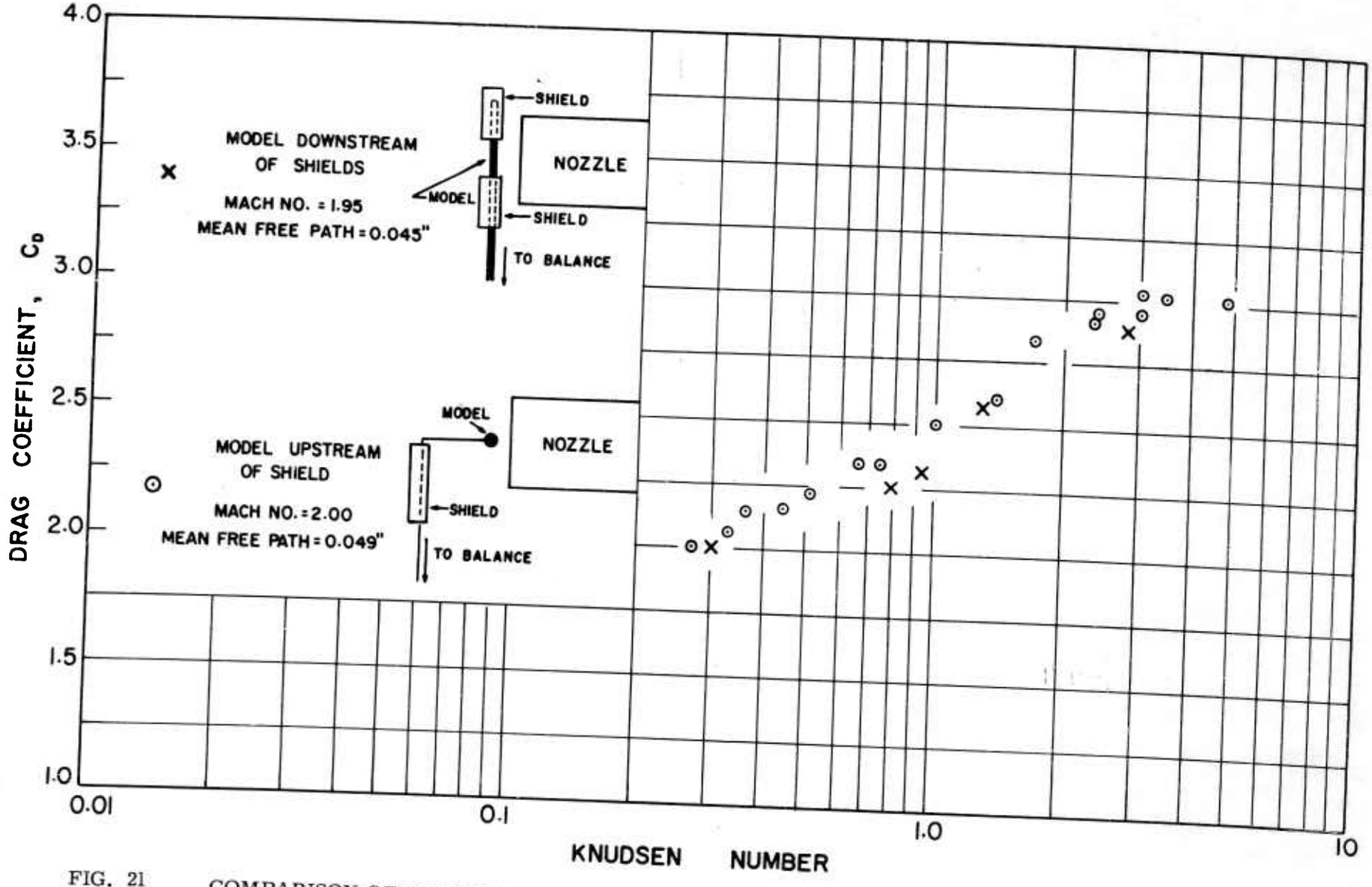

FIG. 21 COMPARISON OF THE DRAG COEFFICIENT OF CYLINDERS LOCATED RESPECTIVELY UPSTREAM AND DOWNSTREAM OF THE SHIELDS.

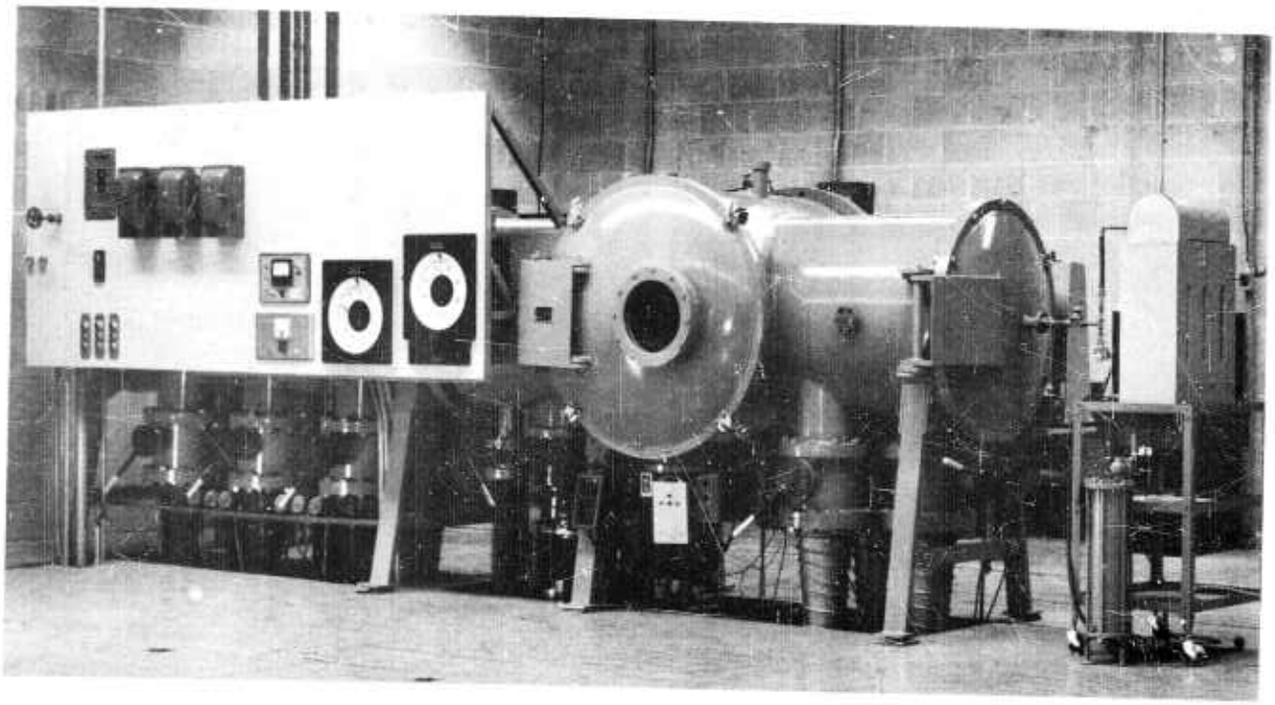

PLATE 1 UTIA LOW-DENSITY WIND TUNNEL

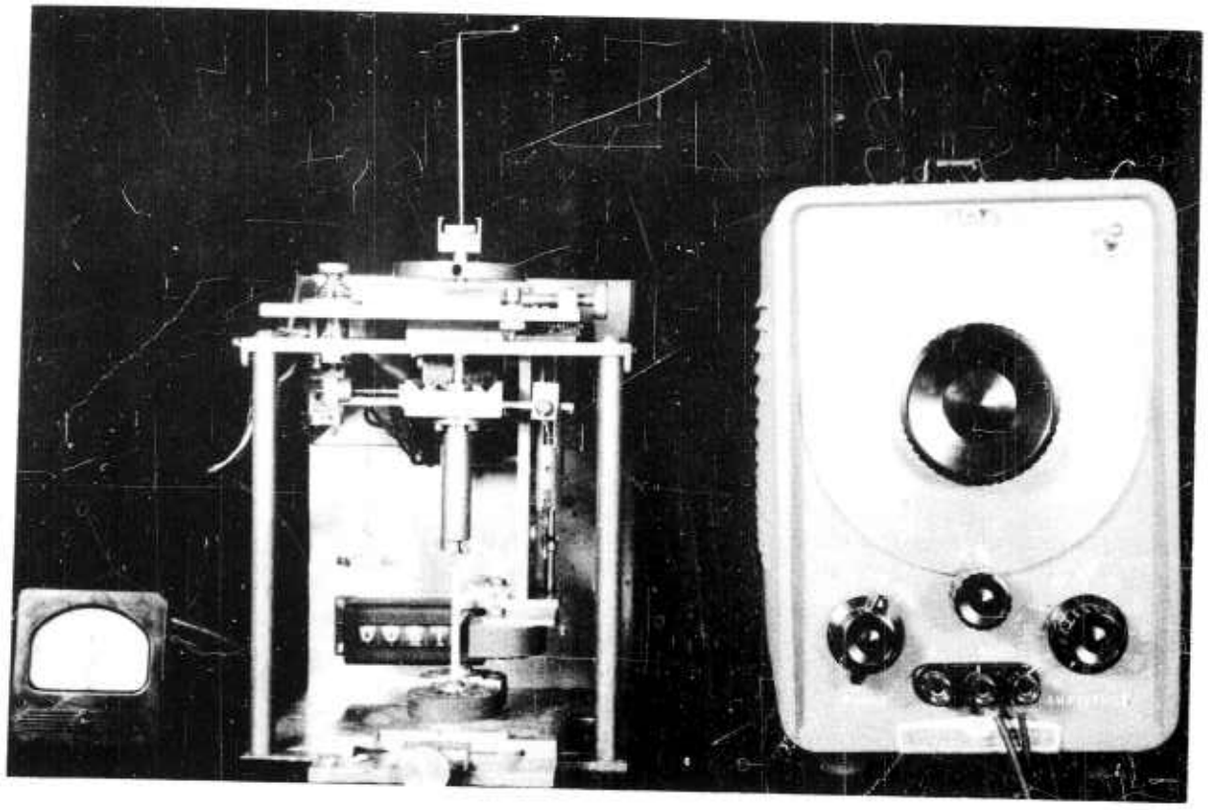

PLATE 2 DRAG BALANCE MECHANISM WITH GALVANOMETER AND OSCILLATOR POWER SUPPLY.

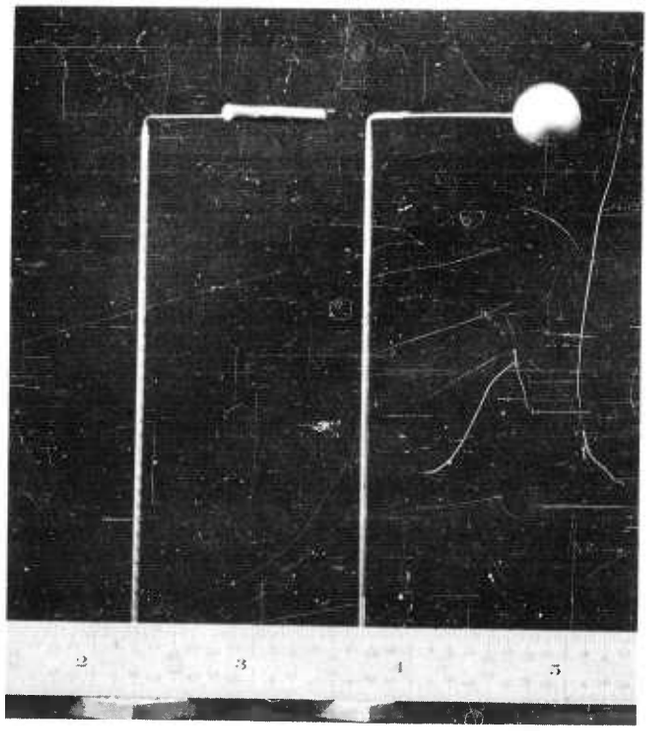

PLATE 3 TYPICAL CYLINDER AND SPHERE MODELS

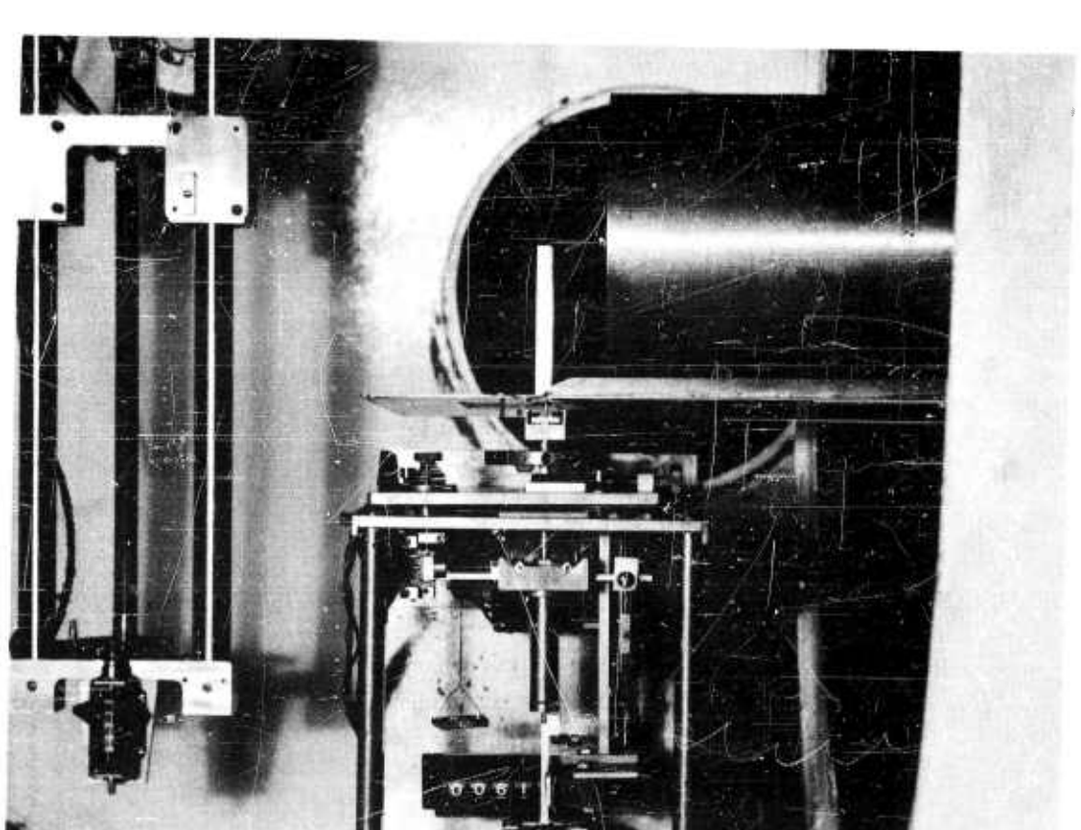

PLATE 4 TEST SECTION OF UTIA LOW-DENSITY WIND TUNNEL WITH MACH-2 NOZZLE INSTALLED. A CYLINDRICAL MODEL MOUNTED ON THE DRAG BALANCE IS PLACED IN THE CENTER OF THE FLOW. THE VERTICAL PORTION OF THE MOUNT IS SHIELDED. THE FLAT PLATE AT THE LOWER NOZZLE EDGE IS A BAFFLE, USED TO CUT DOWN THE CROSS FLOW IN THE BALANCE REGION.

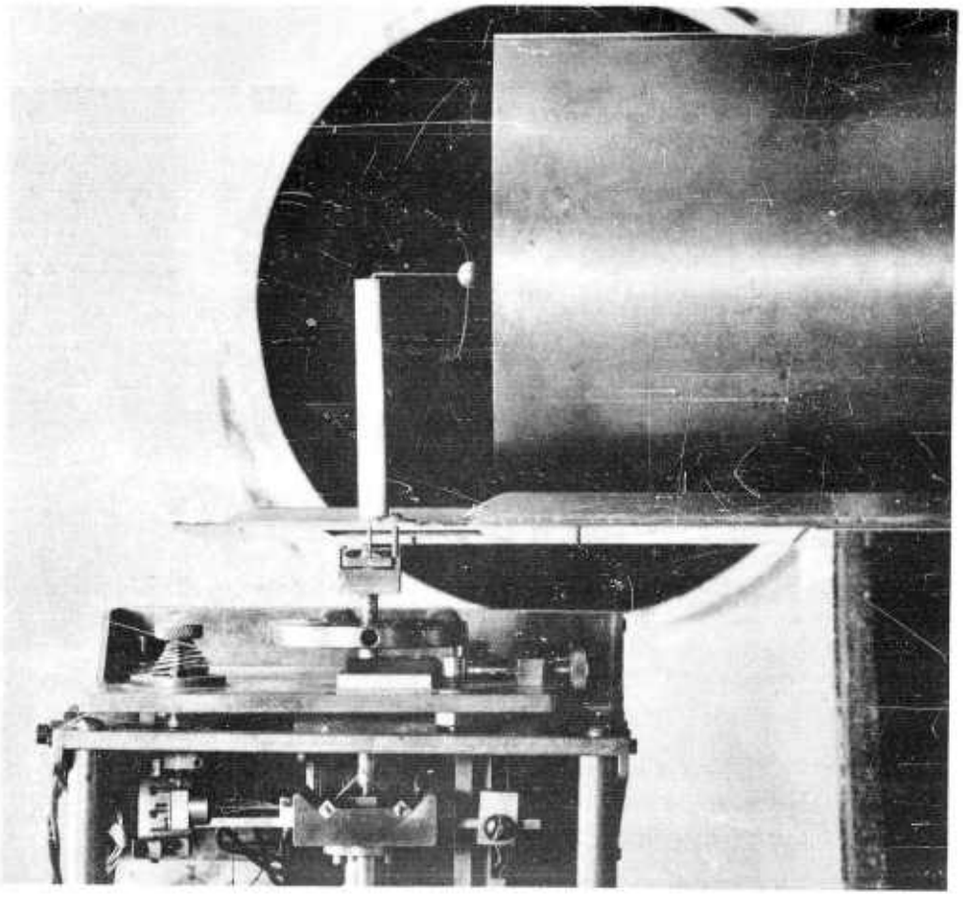

PLATE 5 ARRANGEMENT OF PLATE 4 WITH THE CYLINDRICAL MODEL REPLACED BY A SPHERICAL MODEL.

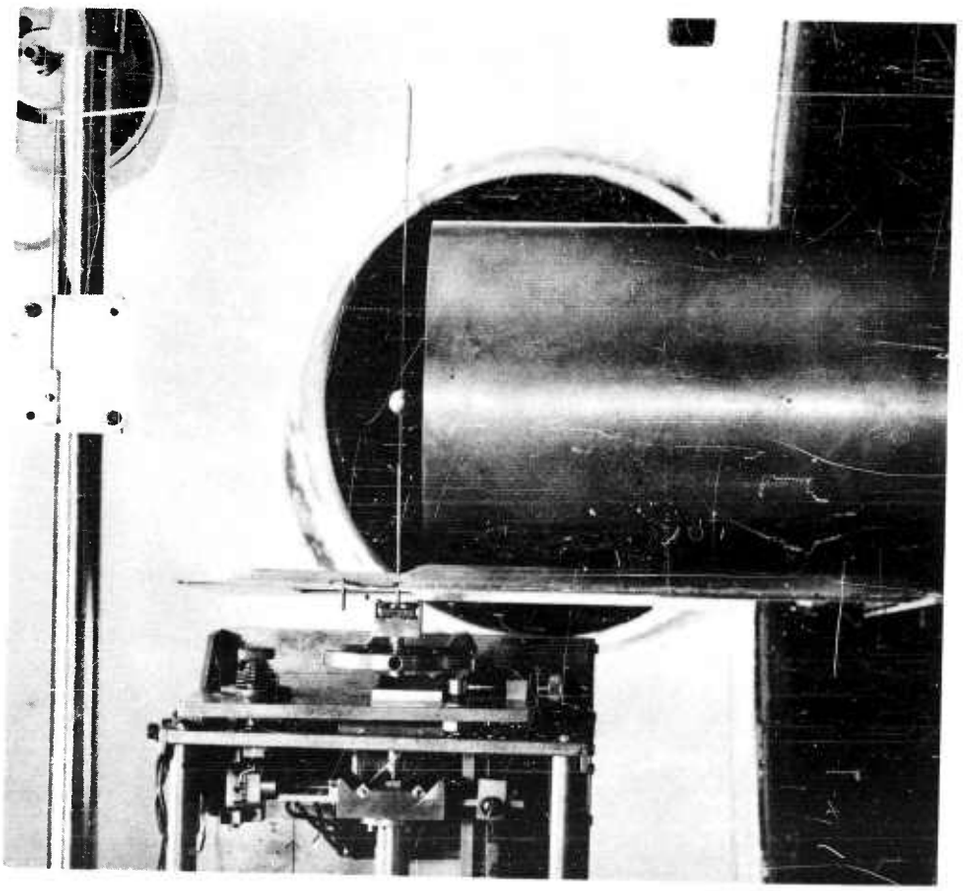

PLATE 6 A SPHERICAL MODEL MOUNTED ON A CROSS-STREAM SUPPORT FOR MEASURING THE TARE FORCE. THE SUPPORTS ARE NOT SHIELDED.

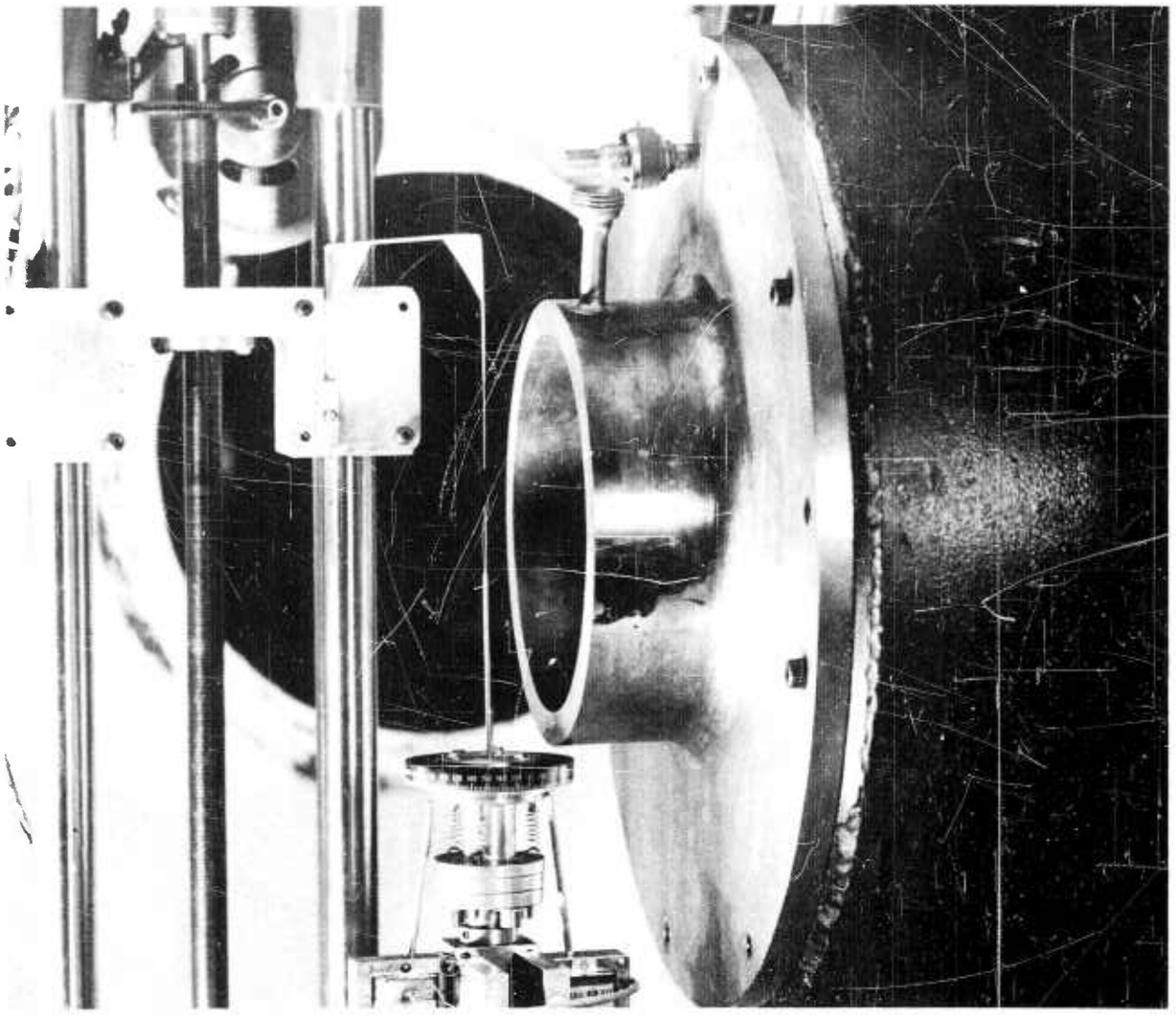

PLATE 7 ARRANGEMENT FOR DETERMINING THE EFFECT OF THE CYLINDER LENGTH ON A PRESSURE READING, USING A SUBSONIC NOZZLE. AN ORIFICE PROBE IS PLACED IN THE FLOW CENTER, AND A DUMMY CYLINDER ABOVE THE PROBE.

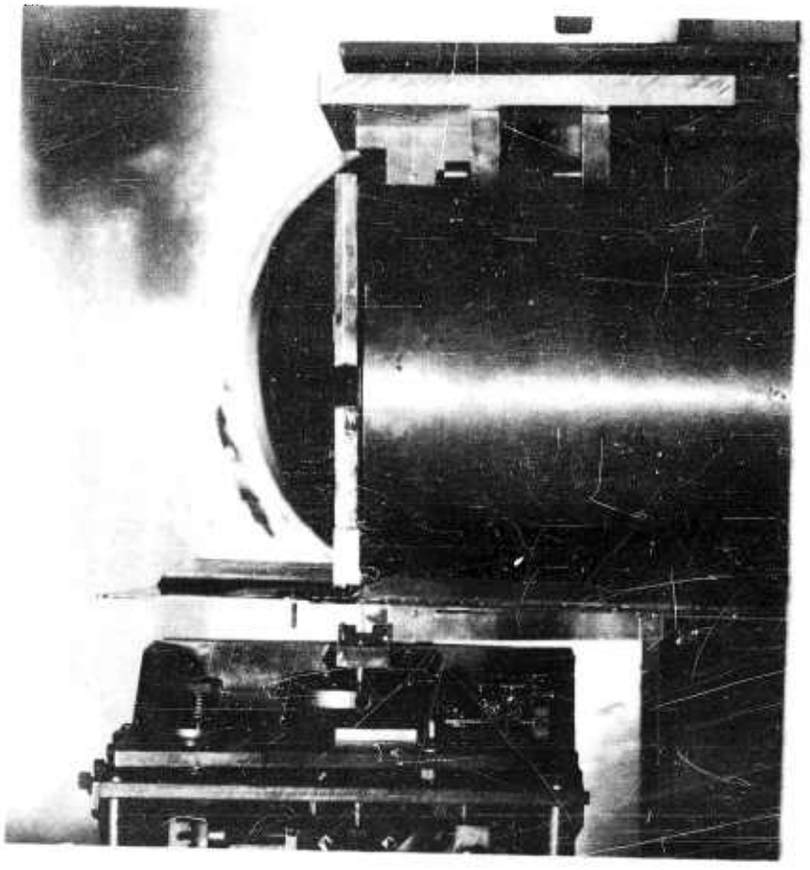

PLATE 8 A CYLINDRICAL MODEL. TWO MOVEABLE SHIELDS ARE MOUNTED UPSTREAM OF THE MODEL.

UTIA REPORT NO. 74

Institute of Aerophysics, University of Toronto

Drag Measurements on Circular Cylinders and Spheres in the Transition Regime at a Mach No. of 2

A. K. Sreekanth April, 1961 46 pages 29 figures 6 tables s

1. Transition Flow 2. Aerodynamic Drag

I. Sreekanth, A. K. II. UTIA Report No. 74

Measurements of the drag of circular cylinders placed transverse to the flow and spheres at a Mach number of 2 in air were obtained in the UTIA low density wind tunnel. The mean free path of the air in the test flow was 0.049" and the model sizes were such that Knudsen numbers in the range 0.2 to 6 for the cylinders and 0.1 to 0.8 for the spheres were covered.

Avoilable copies of this report ore limited. Return this cord to UTIA, if you require o copy.

UTIA REPORT NO. 74

Institute of Aerophysics, University of Toronto

Drag Measurements on Circular Cylinders and Spheres in the Transition Regime at a Mach No. of 2.

A. K. Sreekanth April, 1961 46 pages 29 figures 6 tables

1. Transition Flow 2. Aerodynamic Drag

I. Sreekanth, A. K. II. UTIA Report No. 74

Measurements of the drag of circular cylinders placed transverse to the flow and spheres at a Mach number of 2 in air were obtained in the UTIA low density wind tunnel. The mean free path of the air in the test flow was 0.049" and the model sizes were such that Knudsen numbers in the range 0.2 to 6 for the cylinders and 0.1 to 0.8 for the spheres were covered.

Available copies of this report ore limited. Return this cord to UTIA, if you require o copy.

UTIA REPORT NO. 74

Institute of Aerophysics, University of Toronto

Drag Measurements on Circular Cylinders and Spheres in the Transition Regime at a Mach No. of 2.

A. K. Sreekanth April, 1961 46 pages 29 figures 6 tables

1. Transition Flow 2. Aerodynamic Drag

I. Sreekanth, A. K. II. UTIA Report No. 74

Measurements of the drag of circular cylinders placed transverse to the flow and spheres at a Mach number of 2 in air were obtained in the UTIA low density wind tunnel. The mean free path of the air in the test flow was 0.049" and the model sizes were such that Knudsen numbers in the range 0.2 to 6 for the cylinders and 0.1 to 0.8 for the spheres were covered.

Available copies of this report are limited. Return this card to UTIA, if you require o copy.

UTIA REPORT NO. 74

Institute of Aerophysics, University of Toronto

Drag Measurements on Circular Cylinders and Spheres in the Transition Regime at a Mach No. of 2.

A. K. Sreekanth April, 1961 46 pages 29 figures 6 tables

1. Transition Flow 2. Aerodynamic Drag

I. Sreekanth, A. K. II. UTIA REPORT NO. 74

Measurements of the drag of circular cylinders placed transverse to the flow and spheres at a Mach number of 2 in air were obtained in the UTIA low density wind tunnel. The mean free path of the air in the test flow was 0.049" and the model sizes were such that Knudsen numbers in the range 0.2 to 6 for the cylinders and 0.1 to 0.8 for the spheres were covered.

Available copies of this report are limited. Return this card to UTIA, if you require o copy.